Response to Referees

We thank the referees for their comments. They have helped improve the clarity and quality of the manuscript. We have addressed each comment as follows: the original comments are shown in black, our responses are in blue, and corresponding changes to the manuscript are in *blue italics*. Any additional changes to the manuscript correct typographical errors and do not change the content.

Response to Referee #1

This study is very important to the community for recognizing the winter particulate nitrate pollution by heterogeneous reaction not only in surface layer but also above the canopy of the urban/suburban (similar results also obtained in Beijing based on tower measurements https://doi.org/10.5194/acp-18-10483-2018 which is worth to be cited in this paper).

The cited paper highlights both the importance of N_2O_5 particle nitrate formation aloft, as well as the insensitivity of particle nitrate formation in polluted regions to changes in $\gamma(N_2O_5)$ at sufficiently large values. Citations have been added to this paper accordingly.

Page 3, Line 10
Similarly, a box model analysis of tower and ground-based observations in Beijing, China also identified these processes as important contributors to surface-level particulate nitrate the following day (Wang et al., 2018).

Page 13, Line 22
Despite disagreement between the box model and parameterizations, the $\gamma(N_2O_5)$ values predicted by all three methods are large enough, in combination with the large measured aerosol SA, to fall within the range where models of nighttime chemistry are insensitive to variation in uptake efficiency (e.g. Macintyre and Evans, 2010; Riemer et al., 2003; Wang et al., 2018).

Section 3.3.1, I can understand what the authors want to present here, but I strongly suggest changing the PN2O5 to PNO3. for the convenience of readers who not so familiar with NO3 chemistry, otherwise it is hard to get the point of Eq. 6.

In order to maintain consistent terminology with previous studies (e.g. Bassandorj et al., 2017) and to help clarify this section, we have changed $P_{N_2O_5}$ to P_{NO_3} as the referee suggests. Please see our response to referee #2 for our full response related to this change.

The derived N2O5 uptake coefficient is high that previous two studies conducted by the same group though the iterative box model, if the N2O5 uptake efficiency is high enough and the production rate of particulate nitrate is only limited by the NO2 + O3, N2O5 concentration should be low, could the author provide more information about observed N2O5 concentration?

We have added a supplemental figure S6 showing the vertical distribution of N_2O_5, $ClNO_2$, $\gamma(N_2O_5)$, and $\phi(ClNO_2)$ during night flights over the SLV. We have also edited the following sentence in the main text to provide additional information about the N_2O_5 observations:

Page 13, Line 26
As further evidence of this limitation, the median lifetime of NO_2 with respect to O_3 ($\tau_{NO_2} = 1/(k_1[O_3])$) was 9-hours while the lifetime of N_2O_5 ($\tau_{N_2O_5} = 1/k_{N_2O_5}$) was just 14-minutes, resulting in low N_2O_5 mixing ratios (median = 0.03 ppbv) during the SLV pollution events (Figure S6).
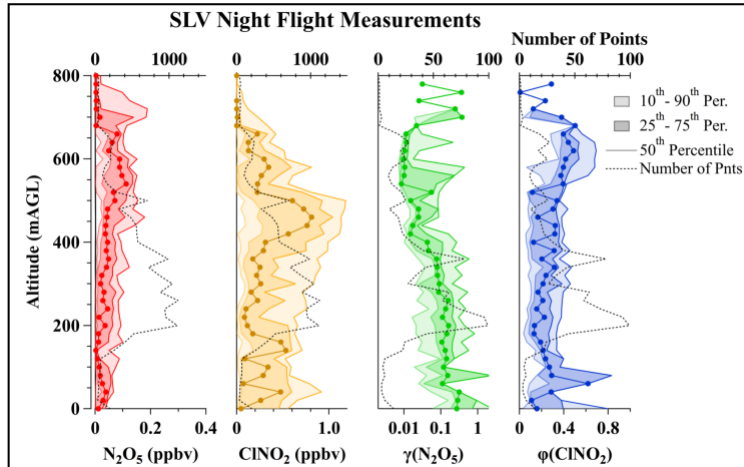
Supplemental Figure S6.

Figure S6. *Vertical profiles of N_2O_5, $ClNO_2$ (1-second measurements), and box-model derived $\gamma(N_2O_5)$ and $\phi(ClNO_2)$ values from all night flights over the SLV. In each panel, light shaded regions show the 10th-90th percentile ranges, dark shaded regions are the 25th-75th percentile ranges, and the solid lines are the 50th percentile. Dashed black lines show the number of points at each altitude.*

The label in Figure S2(b) is inconsistent with the description in the main text, where the median dry SA should be 151.9 ug m-3.

We have changed 151 to 151.9 and 353 to 353.1 to be consistent with Figure S2b.

Page 6, Line 7
For the 1031 10-second measurement periods with simultaneous values of $\gamma(N_2O_5)$ and $\phi(ClNO_2)$, the median dry aerosol SA was 151.9 $\mu m^2\ cm^{-3}$, which increased to 353.1 $\mu m^2\ cm^{-3}$ when accounting for hygroscopic growth (Figure S2b).

Page 8, line 7, missed a subscript the $(NH_4)_2SO_4$

Corrected

The production rate of particulate nitrate in Figure 6 and Figure 7 should be united in the main text as PNO3-. Figure 6b the unit of P(NO3-) and PM1.0 should be corrected.

We have changed the $P(NO_3^-)$ label in Figures 6 and 7 (see figure updates in our response to referee #2) to $P_{NO_3^-,max}$ to reflect and maintain consistency with the changes made in the text in response to referee #2. We also fixed a typo in its unit label. We have also updated PM_1 data in Figures 6 and 7 from units of ug sm^{-3} to display units of ug m^{-3} in order to maintain consistency with other parameters discussed here. This change impacts Figures 6b and 7 only, not the discussion or analyses.

SI, Section S2 PNO3- Calculation Details, repeated "in" (In in Section 3.3.1 of this analysis)

Corrected

Response to Referee #2

In the box model, does the loss rate of N2O5 have any impact on the O3 and NO2? If, hypothetically, N2O5 loss is set to zero, then the O3 and NO2 would evolve differently than if the loss is fast, correct? The model, by separating the O3 and NO2 optimization and the N2O5 and ClNO2 optimization seems to neglect this. Is this a concern? Is the robustness tested by then using the derived gamma_N2O5 and ClNO2 yields to ensure that O3 and NO2 profiles are unchanged?

The referee is correct that the loss rate of N_2O_5 will impact the evolution of O_3 and NO_2. Due to this dependence, the model does not completely separate the derivation of initial NO_2 and O_3 from the derivation of $k_{N_2O_5}$. Rather, once $k_{N_2O_5}$ has been derived, the model re-iterates both processes, re-calculating the initial O_3 and NO_2 concentrations with the updated $k_{N_2O_5}$ value, and then re-calculating $k_{N_2O_5}$. This entire process repeats until model predicted concentrations of O_3, NO_2, and N_2O_5 simultaneously reproduce the observed values. As k_{ClNO_2} does not impact the evolution of O_3, NO_2, or the total loss rate of N_2O_5 ($k_{N_2O_5}$), the third step derives k_{ClNO_2} by iteratively fitting to $ClNO_2$ observations. We have clarified the extent of the model iteration in the following text.

Page 5, Line 5
Briefly, the model forward-integrates the chemical mechanism (13 reactions, Table S1) starting 1.3 hours prior to sunset (see below), iteratively adjusting the initial concentrations of O3 and NO2, until the model-predicted concentrations are both within 0.5% of the aircraft observations. Holding these initial concentrations constant, the model next adjusts the total heterogeneous loss rate constant of N2O5 ($k_{N_2O_5}$) until the model output reproduces ambient nighttime observations of N2O5 to within 1%. As described in McDuffie et al. (2018b), the model iterates these steps, re-adjusting initial concentrations of O3 and NO2 and values of $k_{N_2O_5}$ until aircraft observations of NO2, O3, and N2O5 are simultaneously reproduced by the model. The final step holds these values constant while iteratively adjusting the production rate of ClNO2 (k_{ClNO_2}) until the modeled mixing ratios of ClNO2 are within 1% of the nighttime ClNO2 observations.

Fig. 6: For the night/day P(NO3) calculations, in panel a I find the legend descriptions to be a little confusing. Specifically, the meaning of "~ RL at night" confuses that this is daytime.

We have changed the label to:
"$P_{(NO_3^-,max)}$: *day only ~ nighttime RL*"
and have kept the original description in the Figure caption.

Fig. 6b: Is there a reason that the number of points at a given altitude is so different between NO2, O3, and PNO3 (and PM1)? Does this have to do with estimation of the surface area and differences in averaging time?

We appreciate the referee's attention to detail. In the original figure we had incorrectly plotted the NO_2 and O_3 data from all flights in the SLV, not just the data collected at night. We have updated the vertical profiles of these species in Figure 6b as shown below. As $P_{(NO_3^-,max)}$ is calculated using NO_2, O_3, temperature, and pressure, the number of $P_{(NO_3^-,max)}$ determinations is now equivalent to the number of NO_2 and O_3 measurements. The number of PM_1 measurements is lower due to the difference in measurement frequency of the AMS. We have now indicated this difference in the figure captions of Figure 6 and 7 (below). This error did not carry over to the analysis and does not impact the discussions in the main text or supplement. The vertical profiles in Figure 7 have also been checked and are correct. In addition, the PM_1 data in Figure 6b (and Figure 7) have been changed from units of ug sm^{-3} to ug m^{-3} in response to suggestions by referee #1.

Relevant changes to Figure 6 caption:
(b) Vertical profiles of O3, NO2, $P_{NO_3^-,max}$ (1-second data) and PM1 (10-second data) measured from the aircraft on all night flights over the SLV.
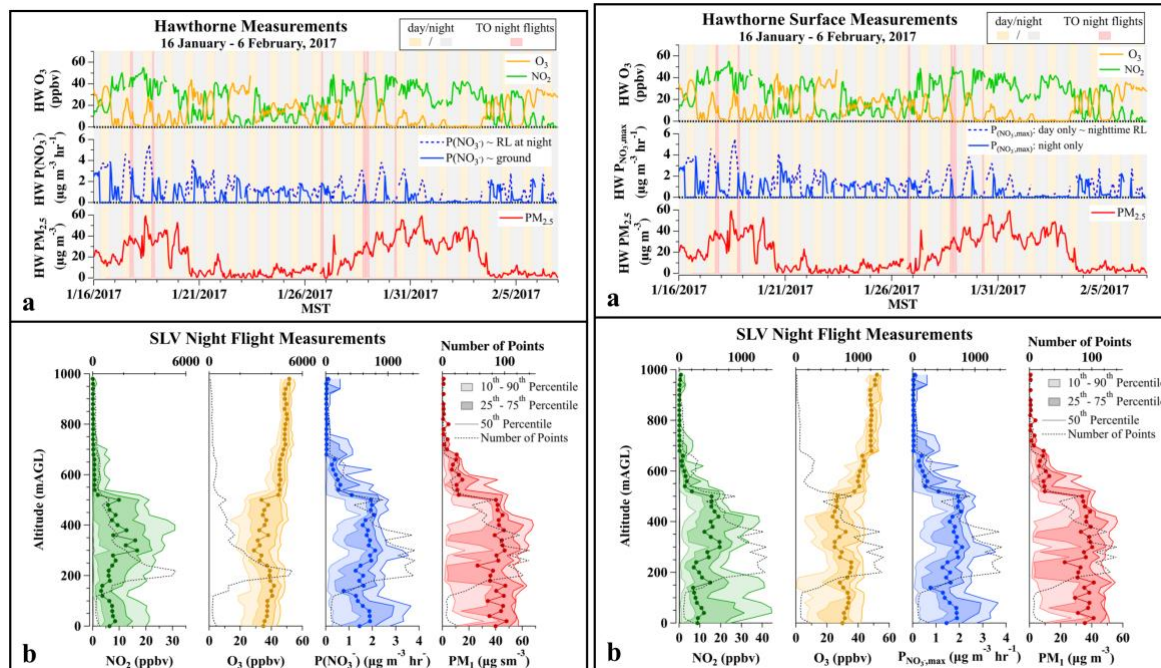
Relevant changes to Figure 7 caption:
Vertical Profiles of NO_2, O_3, $P_{NO_3^-,max}$ (1-second data), and PM_1 (10-second data) measured from the TO aircraft during 5 box patterns, flown over the SLV urban core between 21:20 and 00:30 MST on 28 and 29 January.

Figure 6
Original Version   Updated Version

Section 3.3.1: It seems like it would be a good idea to add a subscript (or some other indicator) of "max" to the P(NO3) values to make sure it is clear that these are the maximum. This is especially important for e.g. Fig. 6, where that context is not readily apparent.

We have changed $P_{NO_3^-}$ to $P_{NO_3^-,max}$ to help distinguish P_{NO_3} and $P_{NO_3^-}$, as well as remind the reader that $P_{NO_3^-,max}$ values are upper limit estimates for the production rate of particulate nitrate from N_2O_5 heterogeneous chemistry. We have also changed $P_{N_2O_5}$ to P_{NO_3} following the suggestion of referee #1. We have slightly changed the first paragraph is Section 3.3.1 as follows and changed the $P_{N_2O_5}$ and $P_{NO_3^-}$ terminology throughout the main text, supplement, and Figures 6 and 7.

Page 9, Line 8
An upper limit estimate of the instantaneous production rate of aerosol nitrate from heterogeneous N_2O_5 chemistry is defined here as $P_{NO_3^-,max}$. This rate can be calculated as two times the gas-phase production rate of the NO_3 radical (P_{NO_3}), given that reaction between NO_2 and O_3 (Eqs. (4) – (6)), rather than N_2O_5 uptake, is the rate limiting step for nitrate formation (discussed below). In Eq. (4), P_{NO_3} is calculated in units of molec. cm^{-3} s^{-1} but is typically reported in units of ppbv hr^{-1} as shown below. The reaction kinetics in Eq. (5) between NO_2 and O_3 are from the 2008 IUPAC recommendation (IUPAC, 2008) and $P_{NO_3^-,max}$ in Eq. (6) is calculated after P_{NO_3} has been converted to units of μg m^{-3} hr^{-1}, as detailed in Supplemental Section S2. This calculation estimates a maximum contribution of N_2O_5 heterogeneous chemistry to nitrate production as it assumes: 1) N_2O_5 is produced quantitatively from NO_3 (i.e. no competing reaction of NO_3 + VOC), 2) N_2O_5 is produced at the rate of NO_3 production (valid under cold conditions that shift the NO_3-N_2O_5 equilibrium to favor of N_2O_5), 3) N_2O_5 is efficiently taken up onto aerosol, and 4) aqueous-phase reactions form two molecules of HNO_3 for every molecule of N_2O_5 (i.e. $\phi(ClNO_2) = 0$).

$$P_{NO_3}[ppbv\ hr^{-1}] = \frac{k_4[O_3][NO_2]}{ND\ [molec.\ cm^{-3}]} * 3600\ [s\ hr^{-1}] * 1 \times 10^9\ [ppbv] \tag{1}$$

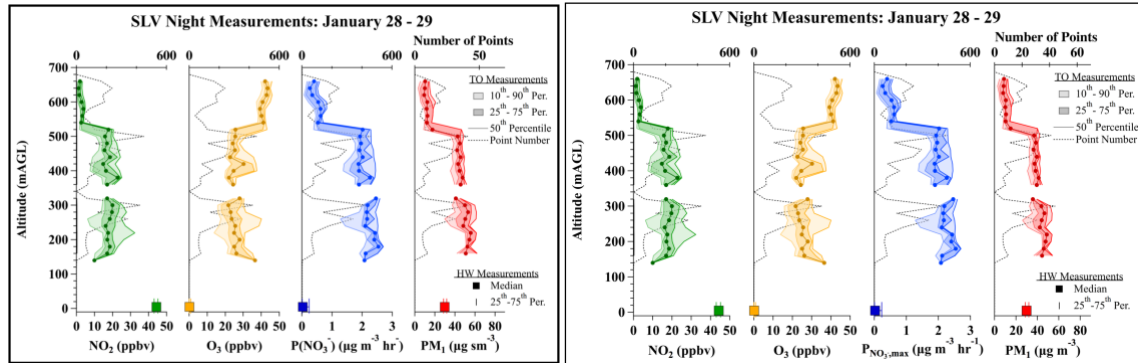$$k_4\ [cm^3\ molecule^{-1}\ s^{-1}] = 1.4 \times 10^{-13} e^{(-2470/T)} \tag{2}$$

$$P_{NO_3^-,max}[\mu g\ m^{-3}\ hr^{-1}] = 2 * (P_{NO_3}\ [\mu g\ m^{-3}\ hr^{-1}]) \tag{3}$$

Figure 6 changes – see above

Figure 7 changes
Original Version   Updated Version

P11/L33: Table S4 doesn't seem to address how uncertainties impact the ClNO2 yield, only net nitrate production. The paragraph, as written, sort of makes it seem like there is an implication of the ClNO2 yield being relatively insensitive to other uncertainties.

This paragraph discusses uncertainties in both $k_{N_2O_5}$ and k_{ClNO_2} that may lead to their respective over- and under-predictions. In Table S4, we have chosen to only show sensitivities of nitrate production (rather than γ(N₂O₅) and ϕ(ClNO₂) individually) because 1) uncertainties in nitrate production will be impacted by uncertainties in both $k_{N_2O_5}$ and k_{ClNO_2}, 2) nitrate production is the main focus of this study, and 3) our analysis shows that γ(N₂O₅) values are large enough that nitrate production will be largely be insensitive to changes in γ(N₂O₅). To highlight that the nitrate production sensitivities also include uncertainties in k_{ClNO_2}, we have re-phrased the last sentence in this paragraph as follows:

Page 11, Line 37
Overall, while the box model has a large number of uncertainties and assumptions, predictions of nocturnal nitrate production, which are subject to uncertainties in both $k_{N_2O_5}$ and k_{ClNO_2}, are not highly sensitive to sources other than dilution (discussed below, Table S4).

P12/Hygroscopic growth: Related, but not directly addressed, is that the time history of RH may matter. The authors use the RH at the point of measurement and, somehow, extrapolate this back in time in the model to give a minute-by-minute perspective on particle surface area. Historical fluctuations in RH could influence the point observations. Is there an attempt to account for variations in RH with time of day? Similarly, the authors seem to use a fixed dry SA, based on the intercept point. But if aerosol growth is occurring then the SA would evolve over time. What sort of uncertainty does this simplification bring in?

There are two separate issues relating to hygroscopic growth that we would like to clarify.

First is the possibility that we discuss on page 12 where an under-estimation of wet aerosol SA *at the time of measurement* is possible due to uncertainties in the hygroscopic growth curve at high RH. This would not impact the model derivation of $k_{N_2O_5}$ but would cause the $\gamma(N_2O_5)$ value from Eq. 1 to be too high.

The second issue that the referee raises is about the time-varying evolution of relative humidity and aerosol surface area between sunset and the time of measurement. Our box model assumes that sampled air parcels evolve over-night with constant temperature (i.e. constant reaction rate constants) and relative humidity (i.e. constant hygroscopic growth factor/wet SA). Therefore, the model-derived values ($k_{N_2O_5}$ and k_{ClNO_2}, $\gamma(N_2O_5)$ and $\phi(ClNO_2)$ by extension) are representative of the average conditions that lead to the observed concentrations of the model fit parameters, NO_2, O_3, N_2O_5, and $ClNO_2$. We agree that the history of RH and aerosol mass accumulation is important to consider and may result in a time-dependence of $k_{N_2O_5}$, that has been discussed previously in McDuffie et al., 2018b. As this time-dependence will not impact the potential under-estimation of calculated wet SA discussed on page 12, we have not made any changes to this section of the manuscript. Instead, we have added a brief discussion in the previous paragraph about the assumptions of constant T and SA. In addition, we have estimated the potential growth in aerosol surface area overnight using the model estimates of aerosol nitrate mass production. We have made no further changes as we have found that absolute nitrate production, the focus of this study, is not limited by $k_{N_2O_5}$ but by gas-phase oxidation rates.

The following changes have been made:

Page 5, Line 3
A zero-dimension chemical box model has been developed to simulate the nocturnal chemical evolution of an air parcel from sunset until the time of aircraft measurement (assuming constant temperature and relative humidity).

Page 6, Line 9
Additional uncertainties associated with hygroscopic growth and assumptions of constant SA are discussed below in Section 3.3.2.

Page 11, Line 33
Additional uncertainties in $k_{N_2O_5}$ and k_{ClNO_2} may arise from model assumptions of constant temperature and RH (i.e. rate constants and surface area) overnight. While model sensitivities to these uncertainties cannot be directly quantified, the percent growth in SA from nitrate accumulation is estimated to be less than the uncertainty in the dry SA measurement (34%). As modeled $k_{N_2O_5}$ values are also consistent with those derived from observations (discussed below), this source of uncertainty is not discussed further.

P12/L13: It should also be noted that the steady state approximation requires the surface area and temperature, not just NO2, O3, and N2O5.

Changed

Page 12, Line 19
The first method calculates $\gamma(N_2O_5)$ from observations of temperature, SA, NO_2, O_3, and N_2O_5, based on the steady state approximation ($\gamma(N_2O_5)_{ss}$), described by Brown et al. (2003) and defined in Supplemental Section S4.1.

P13/L33: It would be good if the authors commented here on the substantial variability in the derived values and, perhaps, the seeming bimodality (with a high production mode and a lower production mode).

We do not see a bimodality in Figure 9 (the nocturnal production rate of nitrate) and rather assume that the referee is referring to the two apparent modes in the N_2O_5 uptake coefficients in Figure 8. The source of these two $\gamma(N_2O_5)$ modes has not been investigated. Our analysis has shown that the production of aerosol nitrate (the focus of this study) is limited by the gas-phase oxidation of NO_2 (P_{NO_3}) rather than N_2O_5 uptake, so the difference in

these modes will have a limited impact on overnight nitrate production. We have, however, edited the following lines to 1) acknowledge the two $\gamma(N_2O_5)$ modes in Figure 8, 2) acknowledge the large variability in Figure 9, and 3) state that this variability in Figure 9 (nitrate production rates) is the result of the large variability in the observed nitrate radical production rates ($P_{NO_3,max}$) in Figure 6.

Page 10, Line 24
*For the SLV alone (N = 1030), the distribution in **Error! Reference source not found.** shows that $\gamma(N_2O_5)$ values ranged four orders of magnitude from 1×10^{-3} to > 1 with two modes centered near 0.01 and 0.08.*

Page 14, Line 5
***Error! Reference source not found.** shows the distribution of nightly nitrate production predicted by base case simulations (N = 1033), ranging from ~0 to 31 $\mu g\ m^{-3}$ nitrate night^{-1}, with a median of 9.9 $\mu g\ m^{-3}$ nitrate night^{-1}.*

Page 14, Line 17
As a result, the large variability in predicted nitrate production rates is reflective of the variability in the observed NO_3 radical production rates (Figure 6).

Page 14, Line 23
Estimating the impact of dilution by including a single first order dilution rate constant ($k_{dilution}$) of $1.3\times10^{-5}\ s^{-1}$ reduced the median nocturnal nitrate production rate by 42% to 5.7 $\mu g\ m^{-3}$ night^{-1} and resulted in a smaller range (~0 to 16 $\mu g\ m^{-3}$ night^{-1}) relative to base case simulations in Figure 9.

P14: The discussion of dilution/entrainment could be enhanced. The Womak paper was just published on 4/8, making it available. It seems that the authors here are arguing for an entrainment rate that is largely independent of time of day, except for the issue of changing height of the mixed layer. However, one might expect the entrainment rate to differ notably between the daytime and nighttime. It is unclear whether the authors are applying a daytime entrainment rate to the nighttime or really, in general, how entrainment is being accounted for. The origin of the 40% scaling factor is somewhat mysterious as well.

We have attempted to improve the clarity of the manuscript regarding the derivation and application of the $k_{dilution}$ term. To answer the referee's specific questions, Womack et al. 2019 derived a single $k_{dilution}$ value ($8 \times 10^{-6}\ s^{-1}$) to account for dilution (entrainment) in the boundary layer over the entire multi-day pollution build-up event. A single value was derived due to a lack of observational constraints relating to dilution. Though not directly detailed in the manuscript, Womack et al. increased this dilution (entrainment) rate constant by 40% ($1.3 \times 10^{-5}\ s^{-1}$) for their simulations of the nocturnal RL to account for the reduced volume of the RL relative to the total volume of the mixed boundary layer. While entrainment rates may vary between day and night conditions, the method of Womack et al. represents the single number that would best represent the average rate during this pollution episode. Therefore, we follow the same procedure and scale the boundary layer dilution rate constant from Womack et al. by 40% (8×10^{-6} /0.6) to estimate the role of dilution/mixing processes on nitrate produced overnight (~14 hours) in the RL during the same pollution event (e.g. Figure 9).

We had originally included a description of $k_{dilution}$ in supplemental section S1.4.1 but have added further details. It now reads:

Section S1.1.4
The dilution rate constant was derived by Womack et al. (2019) as the rate constant that, in combination with the derived surface albedo, allowed an observationally-constrained box model to best reproduce the build-up of total O_x (= NO_2 + O_3 + 1.5*(HNO_3 + pNO_3^-) + 3*N_2O_5 + $ClNO_2$ + PANs + OH + 2*alkyl nitrates) observed between 28 and 31 January, 2017 at the UU ground site. Womack et al. (2019) derived a $k_{dilution}$ value of $8\times10^{-6}\ s^{-1}$ for the boundary layer following this approach. Due to the reduced volume of the nocturnal RL relative to the boundary layer, this

rate constant was scaled up at night by 40% to maintain constant dilution over the entire pollution build-up period. The same approach was applied to our analysis, which resulted in a $k_{dilution}$ value of 1.3×10^{-5} s^{-1} for the RL. The box model-predicted nocturnal nitrate production rate was most sensitive to this parameter, with a 42.2% reduction in the median predicted rate when including an overnight dilution rate of 1.3×10^{-5} s^{-1}. Based on Figure S10 in Womack et al. (2019), the RL dilution rate constant could have reasonably ranged between 1.2 and 2.5×10^{-5} s^{-1} ($0.7 - 1.5 \times 10^{-5}$ s^{-1} / 0.6), depending on the surface albedo. Results incorporating this range of estimated dilution rate constants are discussed further in Section 3.3.3 of the main text and below in Figure S7.

The main text has been adjusted as follows:

Page 14, Line 25
As described in Womack et al. (2019) (and in Section S1.4.1), a single 1st-order dilution rate constant of 8×10^{-6} s^{-1} was derived for pollution event #4 in the SLV by fitting a box model to best reproduce the day-to-day build-up of observed $O_{x,total}$ between 28 January and 1 February at the UU ground site. In the model described by Womack et al. (2019), this rate constant was then scaled up by 40% when simulating the nocturnal RL in order to maintain constant dilution and account for the reduced volume relative to the mixed daytime boundary layer. While dilution / entrainment rates may vary day to night, the method of Womack et al. (2019) represents the single number that would best represent the average rate. The same procedure is followed here with a resulting $k_{dilution}$ value of 1.3×10^{-5} s^{-1}, which is ~60% lower than $k_{dilution}$ from the WINTER campaign, derived from observations of NO_y (= $NO + NO_2 + NO_3 + 2*N_2O_5 + ClNO_2 + RONO_2...$) overnight in a single RL air parcel over the eastern U.S. coast (McDuffie et al., 2018b).

See our response to the Pg 15/Ln 4 comment below for clarification on daytime dilution rate constant.

P15/L3: The difference between the L and M cases seems negligible, as is evident from Fig. 10. Why include both of these when they are so similar?

We have included both estimates because we wanted to test the entire range of possible dilution rate constants, determined by Womack et al., 2019. Even though the L and M dilution rate constant estimates are similar, we have decided to retain both, but have moved them to a new supplemental figure S7 and have updated the main text accordingly.

Page 15, Line 30
When considering the entire possible range of dilution rate constants from Womack et al. (2019), the median values from both cases were between 1.1 and 4.2 μg m^{-3} day^{-1}, as shown in Figure S7.

Figure S7.

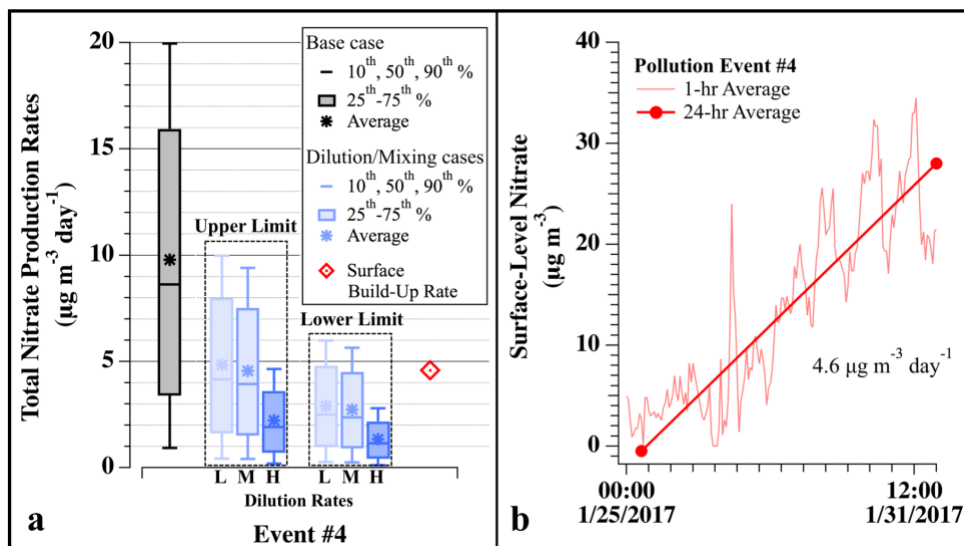*Figure S7. (a) For pollution event #4, comparison of model-predicted nocturnal nitrate production (μg m^{-3} day^{-1}) for base case simulations (gray), simulations with 24-hours of dilution (blue), and the average daily nitrate build-up observed at HW (red). Dilution cases are for simulations that incorporate nocturnal dilution rate constants of 1.2×10^{-5} (L), 1.3×10^{-5} (M), and 2.5×10^{-5} (H) s^{-1}, scaled by 60% during the day. Box and whisker plots show the $10^{th} - 90^{th}$ percentile distributions of each set. The red diamond shows the ground-based build-up rate, calculated from 24-hr averaged data at HW in panel b. Upper-limit values assume morning mixing between equivalent nitrate concentrations produced in the RL and NBL. Lower-limit values assume morning mixing with no nitrate production in the NBL (b) Observed concentrations and average daily build-up rate of nitrate aerosol mass (total mass * 0.58) at HW during event #4.*

P15/L4: Should the transition from nighttime to daytime also be accounted for? In other words, if most nitrate is formed aloft (as suggested) and the air in the RL is entrained to the surface starting at sunrise, then the nitrate in the RL will be distributed throughout the daytime mixed layer. Dilution from exchange with the FT will occur on top of this. However, that would also require accounting for the nitrate in the surface layer initially.

The referee is correct that morning mixing between the RL and nocturnal boundary layer (NBL) should have been included in addition to daytime dilution from free tropospheric entrainment. Since this box model predicts the amount of nocturnal nitrate produced in the RL only, we have incorporated the effect of morning mixing using two upper and lower limit case estimates. In both cases, the dilution associated with free tropospheric entrainment is treated the same way as originally described: a loss rate constant of $1.3x10^{-5}$ s^{-1} is applied overnight (~14 hours), reduced to $8x10^{-6}$ s^{-1} for the remaining 10 hours in the mixed boundary layer. We also assume instantaneous morning mixing following Womack et al., 2019. The time of mixing will not impact our estimates as we are only simulating nitrate loss processes after sunrise.

First, for the upper limit case, we assume that the amount of nitrate produced overnight in the RL is the same as in the NBL. This will result in the same nitrate concentration in the morning boundary layer after mixing as that produced overnight in the RL. This is an upper limit estimate because nitrate production in the NBL is expected to be smaller than production in the RL due to O_3 titration that reduces the NO_2 oxidation rate in the NBL. In confirmation, Womack et al., 2019 found that nitrate production in the NBL was lower than in the RL (Womack et al., Figure S6). This upper limit case represents the maximum amount of nocturnally-produced nitrate that would be observed at the ground when considering the effects of 24-hour dilution. This is also the same as the dilution case that we had originally included.

Second, the lower limit case assumes that no nitrate is produced in the NBL overnight (consistent with Jan. 31 and Feb 1st in Figure S6 of Womack et al., 2019). In this case, modeled morning nitrate concentrations are diluted by 40% to account for mixing between the NBL (40%) and RL (60%) volumes. Daytime entrainment then follows as described above.

While there are uncertainties, these two cases better capture the possible range of nocturnal nitrate observed at the surface for an improved comparison with surface observations. In addition, we have added

supplemental figure S7 (see response to previous comment) to show the upper and lower limit case results for the entire range of dilution rate constants that was derived by Womack et al., 2019 (1.2-2.5x10^{-5} s^{-1}).

To account for these two cases, the following updates have been made to the main text and Figure 10.

Abstract:
Lastly, additional model simulations suggest nocturnal N_2O_5 uptake produces between 2.4 and 3.9 μg m^{-3} of nitrate per day when considering the possible effects of dilution. This nocturnal production is sufficient to account for 52 - 86% of the daily observed surface-level build-up of aerosol nitrate, though accurate quantification is dependent on modeled dilution, mixing processes, and photochemistry.

Page 15, Line 11
*   Comparing modeled RL chemical nitrate production to the observed ground-based accumulation rate can provide an estimate for the fractional contribution of N_2O_5 uptake to total particulate nitrate production in the SLV. Direct comparison is difficult, however, as the 24-hour ground-based accumulation rate includes contributions from photochemistry and nocturnal formation in the RL and nocturnal boundary layer (NBL), and is impacted by dilution and mixing processes. For example, the amount of nocturnally produced nitrate at the surface will depend on mixing between the NBL and RL during morning boundary layer expansion (**Error! Reference source not found.**). In Figure 10a, the median base case prediction without dilution or mixing (gray, 8.6 μg m^{-3} night^{-1}) was nearly twice as large as the 24-hour average accumulation rate observed at the surface during the same event (4.6 μg m^{-3} night^{-1}, red) Therefore, to more directly compare box model predictions and ground-based observations, Figure 10a also shows the results from two simulations that include upper- and lower-limit estimates of loss from nocturnal and daytime dilution. For both scenarios, the nighttime (0-14 hours) $k_{dilution}$ value of 1.3×10^{-5} s^{-1} (blue) was applied to all modeled species as described above. At sunrise, morning mixing between the NBL (taken as 40% by volume) and RL (taken as 60% by volume) was then estimated using the assumed volume ratio between the two layers and assuming either equivalent nocturnal nitrate production in both layers (upper limit) or no production in the NBL (lower limit). Nocturnal production in the NBL is expected to be suppressed relative to the RL due to O_3 titration (e.g. Figure 6 and Figure S6 in Womack et al. (2019)), making the assumption of equivalence an upper limit estimate to nocturnally-produced nitrate at the surface after morning mixing. The upper limit case required no reduction of the model-predicted nitrate concentrations at sunrise (e.g. Figure 9), whereas these concentrations were instantaneously reduced by 40% for the lower limit case. To account for daytime dilution in the remaining ~10 hours, morning concentrations for both cases were further diluted with the daytime boundary dilution rate constant from Womack et al. (2019) (8×10^{-6} s^{-1}), described above and in Section S1.4.1. For a single 24-hour period, this resulted in a net median of 2.4 to 3.9 μg m^{-3} nitrate produced from nocturnal heterogeneous N_2O_5 uptake for the lower and upper-limit cases, respectively. When considering the entire possible range of dilution rate constants from Womack et al. (2019), the median values from both cases were between 1.1 and 4.2 μg m^{-3} day^{-1}, as shown in Figure S7.*
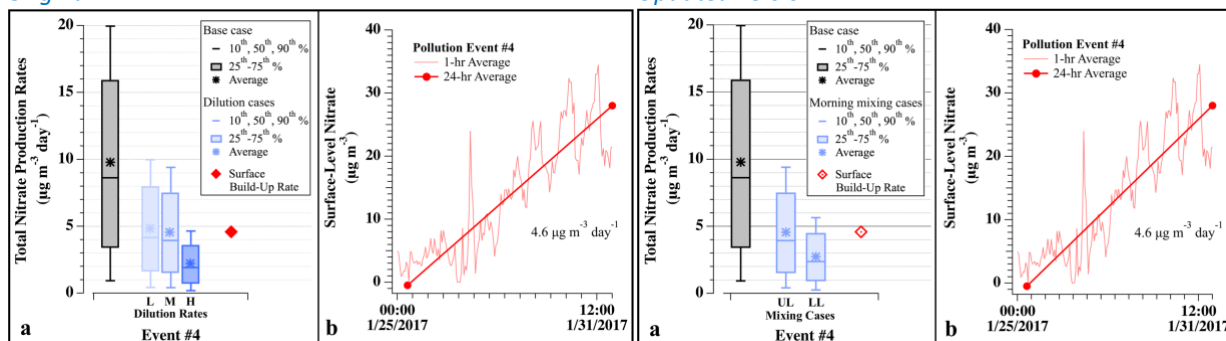
Page 16, Line 1
Therefore, while results in Figure 10a (including dilution) predict a median nocturnal fractional contribution of 52 - 86% (ranging between 24 and 91% (Figure S7)), confirmation and further quantification of this result will require additional, vertically resolved measurements of aerosol composition, gas-phase precursors, and physical parameters, as well as more sophisticated modeling of these multi-day pollution accumulation events with 3D-chemical transport models.

Page 17, Line 1
When considering the possible effects of 24-hour dilution, model simulations predicted a reduced median of 2.4 - 3.9 μg m^{-3} nitrate day^{-1}, corresponding to 52 - 86% (median) of the net aerosol nitrate accumulation that was observed at a SLV ground site.

Figure 10 Updates
Original   *Updated version*

*Figure 1. (a) For pollution event #4, comparison of model-predicted nocturnal nitrate production (μg m^{-3} day^{-1}) for base case simulations (gray), simulations with 24-hours of dilution (blue), and the average daily nitrate build-up observed at HW (red). Dilution cases are for simulations that incorporate nocturnal dilution rate constants of 1.2×10^{-5} (L), 1.3×10^{-5} (M), and 2.5×10^{-5} (H) s^{-1}, scaled by 60% during the day. Box and whisker plots show the 10th – 90th percentile distributions of each set. Upper-limit (UL) values assume morning mixing between equivalent nitrate concentrations produced in the RL and NBL. Lower-limit (LL) values assume morning mixing with no nitrate production in the NBL The red diamond shows the ground-based build-up rate, calculated from 24-hr averaged data at HW in panel b. (b) Observed concentrations and average daily build-up rate of nitrate aerosol mass (total mass * 0.58) at HW during event #4.*

P15/L9: I have some difficulty with the framing here. The authors start by saying that nocturnal chemistry and largely explain the nitrate accumulation at the surface. But then they go on to say that Womack (who looked at the same events) concluded that photochemical production is quite important too. Notably, while Pusede et al. (2016) implicated nocturnal nitrate production as very important, they did not discount daytime production to the extent suggested here and Prabhakar et al. (2017), building on Pusede et al. (2016), concluded that daytime production plays an important role. I suggest that the authors consider revising the first sentence and how they frame the discussion here. They have only considered nighttime formation and thus their ultimate conclusions regarding the contributions of daytime processes are limited.

We had intended to state that our results suggested that most of the 24-hour nitrate accumulation could be accounted for, not that there was no role of photochemistry. In light of the additional dilution included for morning mixing (discussed above) and these comments, we have made the following changes to this paragraph. We have also changed sentences throughout the text for the same effect.

Page 15, Line 32
Comparison of modeled rates to the observed surface build-up of 4.6 μg m^{-3} day^{-1} suggests that on average, nitrate produced from heterogenous chemistry can account for at least 50% of the nitrate accumulation observed at the surface. This result is qualitatively consistent with an observational analysis by Pusede et al. (2016), who determined that nocturnal heterogeneous chemistry was the main source of regional aerosol nitrate during wintertime pollution events in the San Joaquin Valley. The lower limit estimate, however, is also similar to a box model analysis of this same event by Womack et al. (2019) who found roughly equal contributions between photochemical and nocturnal nitrate production pathways, highlighting that photochemical nitrate production is also occurring during these events. Therefore, while results in Figure 10a (including dilution) predict a median nocturnal fractional contribution of 52 - 86% (ranging between 24 and 91% (Figure S7)), confirmation and further quantification of this result will require additional, vertically resolved measurements of aerosol composition, gas-phase precursors, and physical parameters, as well as more sophisticated modeling of these multi-day pollution accumulation events with 3D-chemical transport models.

Page 15, Line 12
Direct comparison is difficult, however, as the 24-hour ground-based accumulation rate includes contributions from photochemistry and nocturnal formation in the RL and nocturnal boundary layer (NBL), and is impacted by dilution and mixing processes.

Abstract
Lastly, additional model simulations suggest nocturnal N_2O_5 uptake produces between 2.4 and 3.9 $\mu g\ m^{-3}$ of nitrate per day when considering the possible effects of dilution. This nocturnal production is sufficient to account for 52 - 86% of the daily observed surface-level build-up of aerosol nitrate, though accurate quantification is dependent on modeled dilution, mixing processes, and photochemistry.

A minor grammar question: should it be "in the SLV" or "in SLV". I would have thought the former, as the SLV is not a city but a region (like the western US, which the authors refer to with a "the").

We agree and have made this change throughout the main text and supplement.

P13/L5: "empirically-based" should just be "empirical."

Changed

On the contribution of nocturnal heterogeneous reactive nitrogen chemistry to particulate matter formation during wintertime pollution events in Northern Utah

Erin E. McDuffie[1,2,3ξ], Caroline Womack[1,2], Dorothy L. Fibiger[1,2†], William P. Dube[1,2], Alessandro Franchin[1,2], Ann Middlebrook[1], Lexie Goldberger[4‡], Ben H. Lee[4], Joel A. Thornton[4], Alexander Moravek[5], Jennifer Murphy[5], Munkhbayar Baasandorj[6§], Steven S. Brown[1,3]

[1]Chemical Sciences Division, National Oceanic and Atmospheric Administration, Boulder, CO, USA
[2]Cooperative Institute for Research in Environmental Sciences, University of Colorado, Boulder, CO, USA
[3]Department of Chemistry, University of Colorado, Boulder, CO, USA
[4]Department of Atmospheric Science, University of Washington, Seattle, WA, USA
[5]Department of Chemistry, University of Toronto, Toronto, Canada
[6]Department of Atmospheric Sciences, University of Utah, Salt Lake City, UT, USA

[ξ]Now at: Department of Physics and Atmospheric Science, Dalhousie University, Halifax, NS, Canada
[†]Now at: California Air Resources Board, Sacramento, CA, USA
[‡]Now at: ARM Aerial Facility, Pacific Northwest National Laboratory, Richland, WA, USA
[§]Now at: Chevron Corporation, Houston, TX, USA

Correspondence to: Steven S. Brown (steven.s.brown@noaa.gov)

Abstract. Mountain basins in Northern Utah, including the Salt Lake Valley (SLV), suffer from wintertime air pollution events associated with stagnant atmospheric conditions. During these events, fine particulate matter concentrations ($PM_{2.5}$) can exceed national ambient air quality standards. Previous studies in the SLV have found that $PM_{2.5}$ is primarily composed of ammonium nitrate (NH_4NO_3), formed from the condensation of gas-phase ammonia (NH_3) and nitric acid (HNO_3). Additional studies in several western basins, including the SLV, have suggested that production of HNO_3 from nocturnal heterogeneous N_2O_5 uptake is the dominant source of NH_4NO_3 during winter. The rate of this process, however, remains poorly quantified, in part due to limited vertical measurements above the surface, where this chemistry is most active. The 2017 Utah Winter Fine Particulate Study (UWFPS) provided the first aircraft measurements of detailed chemical composition during wintertime pollution events in the SLV. Coupled with ground-based observations, analysis of day and nighttime research flights confirm that $PM_{2.5}$ during wintertime pollution events is principally composed of NH_4NO_3, limited by HNO_3. Here, observations and box-model analyses assess the contribution of N_2O_5 uptake to nitrate aerosol during pollution events using the NO_3^- production rate, N_2O_5 heterogeneous uptake coefficient ($\gamma(N_2O_5)$), and production yield of $ClNO_2$ ($\phi(ClNO_2)$), which had medians of 1.6 $\mu g\ m^{-3}\ hr^{-1}$, 0.076, and 0.220, respectively. While fit values of $\gamma(N_2O_5)$ may be biased high by a potential under-measurement in aerosol surface area, other fit quantities are unaffected. Lastly, additional model simulations suggest nocturnal N_2O_5 uptake produces between 2.4 and 3.9 $\mu g\ m^{-3}$ of nitrate per day when considering the possible effects of dilution. This nocturnal production is sufficient to account for 52 - 86% of the daily observed surface-level build-up of aerosol nitrate, though accurate quantification is dependent on modeled dilution, mixing processes, and photochemistry.

1 Introduction

Over 80% of Utah's population lives in counties that experience periods of elevated fine particulate matter ($PM_{2.5}$ < 2.5 μm in diameter) during the winter season (U.S. Census Bureau, 2018; Whiteman et al., 2014). In these counties, the highest levels have been limited to three northern valleys along the Wasatch Mountains, shown in Figure 1 (north to south: Cache Valley (Logan Non-attainment area (NAA)), Salt Lake Valley (Salt Lake NAA), and Utah Valley (Provo NAA)). These valleys were designated by the U.S. EPA as "Moderate" non-attainment areas (NAA) in December 2009, with the Salt Lake and Provo areas reclassified from moderate to "Serious" in May 2017 (Utah Department of Environmental Quality). Elevated $PM_{2.5}$ concentrations in these regions impact public health and are associated with increases in emergency room visits for asthma (Beard et al., 2012). Short-term exposure to $PM_{2.5}$ has also been shown to increase the chance of triggering acute ischemic heart disease events by 4.5-6% per 10 μg m^{-3} in sensitive populations living in the Wasatch region (Pope et al., 2006; Pope et al., 2015).

Elevated wintertime $PM_{2.5}$ concentrations in these valleys typically correspond to multi-day events of high atmospheric stability (e.g. Whiteman et al., 2014; Silcox et al., 2012; Gillies et al., 2010; Wang et al., 2012; Green et al., 2015; Silva et al., 2007; Baasandorj et al., 2017), associated with large, synoptic-scale high-pressure systems that transit from west to east, simultaneously impacting multiple basins across the intermountain western U.S. (e.g. Reeves and Stensrud, 2009). Warm temperatures aloft cause boundary layer stratification that reduces mixing and traps cold air and emissions near the surface, illustrated in Figure 2 and discussed further below. These events, termed persistent cold air pools (PCAPs), typically mix-out after 1-5 days but have been observed to persist for as long as 18 days (Whiteman et al., 2014). Similar meteorological patterns have been linked to wintertime $PM_{2.5}$ accumulation in basins across the western U.S. (e.g. Chen et al., 2012; Green et al., 2015). During past PCAP and pollution events in Utah, data from ground-based measurements in the Salt Lake Valley (SLV) have reported day to day build-up rates of total $PM_{2.5}$ mass in the range of ~6-10 μg m^{-3} day^{-1} (Baasandorj et al., 2017; Silcox et al., 2012; Whiteman et al., 2014) before plateauing after ~ 6 days into an event (Baasandorj et al., 2017). Average 24-hour concentrations reported during PCAP events between 2001 and 2016 have been as large as 40-80 μg m^{-3} in Salt Lake (Baasandorj et al., 2017; Silcox et al., 2012) and Utah Valleys (Malek et al., 2006), and up to 132.5 μg m^{-3} in Logan, Utah (Cache Valley) (Malek et al., 2006).

Previous ground-based studies have identified ammonium nitrate (NH_4NO_3) as the main component of $PM_{2.5}$ (70 - 80% by mass) during PCAP events in all three Northern Utah Valleys (Silva et al., 2007; Hansen et al., 2010; Kuprov et al., 2014; Kelly et al., 2013; Long et al., 2003; Long et al., 2005a; Long et al., 2005b; Baasandorj et al., 2017). Ammonium nitrate formation is thermodynamically favorable under cold wintertime conditions from the equilibrium between gas-phase ammonia (NH_3) and nitric acid (HNO_3), shown in Reaction (R1) in Figure 2 (e.g. Kuprov et al., 2014; Nowak et al., 2012; Mozurkewich, 1993). $PM_{2.5}$ mitigation strategies that are based on control of these gas-phase species are expected to be more effective if the limiting reagent and its sources can be identified. Both model- and observationally-informed ground-based analyses have suggested that NH_4NO_3 formation in Cache and Salt Lake Valleys is limited by the production of HNO_3 (Kuprov et al., 2014; Mangelson et al., 1997; Martin, 2006; Utah Division of Air Quality, 2014c, b, a; Franchin et al., 2018), though uncertainties remain in how this limitation may be impacted by temporal and spatial variations.

While NH_3 is directly emitted from agricultural sources, industrial processes, waste disposal, and automobile emissions (Behera et al., 2013; Livingston et al., 2009), HNO_3 forms chemically in the atmosphere from the oxidation of NO_x (=NO + NO_2), which in turn arises mainly from combustion emissions. There are two mechanisms by which this formation occurs, illustrated by reactions (R2 - R6) in Figure 2. The first is through daytime NO_2 oxidation by the hydroxyl radical (OH) (Figure 2, R2) and the second is through the nocturnal heterogeneous uptake of dinitrogen pentoxide (N_2O_5) (R6), which itself is a product of nocturnal

2

NO_x oxidation (R3 – R5). The former is relatively more important during the summer (Brown et al., 2004) whereas the latter, the focus of this study, may be relatively more important in winter (e.g. Wagner et al., 2013) due to reduced OH concentrations, colder temperatures that favor N_2O_5 in its equilibrium with NO_3 (R5), and longer nights that allow more time for nocturnal reactions to occur. The nocturnal heterogeneous production of HNO_3 is also expected to be largest in the residual layer (RL), due to the near surface accumulation of NO, which titrates O_3 (R3) and reacts with NO_3 (R7), the precursor to N_2O_5 (e.g. Brown and Stutz, 2012).

The role of this nocturnal reactive nitrogen chemistry in the formation of $PM_{2.5}$ has been considered in previous wintertime studies, though nocturnal, vertically-resolved measurements have been relatively limited. Previous studies using ground and tower-based observations, as well as mid-morning aircraft vertical profiles have identified heterogeneous chemistry and subsequent morning transport from aloft as a major source of surface-level NH_4NO_3 in California's San Joaquin Valley (e.g. Brown et al., 2006; Prabhakar et al., 2017; Pusede et al., 2016; Watson and Chow, 2002). Similarly, a box model analysis of tower and ground-based observations in Beijing, China also identified these processes as important contributors to surface-level particulate nitrate the following day (Wang et al., 2018). In Northern Utah specifically, nocturnal heterogeneous chemistry has been considered a source for $PM_{2.5}$ (Baasandorj et al., 2017; Kuprov et al., 2014), though vertically resolved measurements have been limited to ground-based observations at different elevations along the Wasatch Mountains (Baasandorj et al., 2017). In an analysis of ground-based HNO_3 and $PM_{2.5}$ observations in the SLV, Kuprov et al. (2014) suggested that daytime HNO_3 formation was dominant over the contribution from nocturnal heterogeneous chemistry. Baasandorj et al. (2017), however, noted that ground-based measurements in this region may not capture the extent of heterogeneous chemistry aloft in the RL, which is expected to be distinct from the surface composition (e.g. Brown et al., 2007; Brown and Stutz, 2012; Stutz et al., 2004). Therefore, vertical gradients in NO_x and oxidants could promote efficient HNO_3 and NH_4NO_3 formation aloft, which could contribute to enhanced surface-level $PM_{2.5}$ concentrations the following day. Regardless of altitude, the absolute contribution at all altitudes will depend on 1) the rate of NO_3 and N_2O_5 production, 2) the efficiency of N_2O_5 uptake onto aerosol ($\gamma(N_2O_5)$) and 3) the heterogeneous production yield of HNO_3 relative to $ClNO_2$ ($\phi(ClNO_2)$) (Osthoff et al., 2008; Behnke et al., 1997). Net accumulation of NH_4NO_3 at the surface, however, also depends on mixing and dilution associated with growth of the convective boundary layer and mixing of the RL down to the surface the following day. Quantification of these processes is key in designing effective mitigation strategies for Utah's wintertime air pollution and requires vertically resolved observations of chemical composition at night.

In this study, we present results from the Utah Winter Fine Particulate Study (UWFPS), which consisted of aircraft and ground-based observations throughout Cache, Salt Lake, and Utah Valleys during January and February 2017. This analysis focuses on data from 16 aircraft flights (5 at night) during two pollution events between 16 January and 1 February 2017. These flights were carried out in the SLV, the most populated of the three Utah Non-Attainment Areas. The first section presents an overview of $PM_{2.5}$ during winter 2016-2017. In the second section, ambient mixing ratios of total (gas and particle-phase) oxidized and reduced nitrogen are used to identify the limiting reagent to NH_4NO_3 aerosol formation, as well as its spatial and temporal trends. The final section presents upper-limit NH_4NO_3 production rate estimates and results from an observationally-fit chemical box model to calculate $\gamma(N_2O_5)$, $\phi(ClNO_2)$, and an estimated contribution of nocturnal heterogeneous chemistry to NH_4NO_3 formation in the SLV. The contribution of nocturnal production relative to photochemically-driven NO_2 oxidation will have consequences for the development of effective mitigation strategies as day and nighttime production processes may have different sensitivities to NO_x emissions and VOC radical sources (Pusede et al., 2016; Womack et al., 2019), such that net sensitivities will be determined by the dominant formation mechanism.

Deleted: (Wang et al., 2018b)

Deleted: N

Deleted: also

Deleted: as

Deleted: in northern Utah

Formatted: Not Superscript/ Subscript

Deleted: -level NH_4NO_3

Deleted: during

Deleted: a

Deleted: component

Deleted: A

Deleted: is presented in the first section

Deleted: A

Deleted: shown in the second section to

Deleted: assess

Deleted: from aircraft observations

Deleted: that is fit to observations

2 Methods

2.1 UWFPS Campaign Overview and Instrumentation

The UWFPS campaign included both aircraft and ground-based measurements throughout the Salt Lake, Cache, and Utah Valleys during January and February 2017 (Figure 1). A total of 23 research flights were conducted during both day and night with the NOAA Twin Otter (TO) aircraft. The TO was equipped with aerosol and gas-phase instrumentation (summarized in Table 1) to probe the regional sources and formation mechanisms of $PM_{2.5}$. While flights were conducted over three valleys, the focus of this analysis will be on the more densely populated SLV, with relevant flight tracks highlighted in the right panel of Figure 1.

Briefly, the TO payload included gas-phase measurements of NO_x, NO_2, NO_y, and O_3 (1 Hz sample frequency) from a NOAA Cavity Ring Down Spectrometer (NOxCaRD) (Wild et al., 2014), NH_3 (1 Hz sample frequency) measurements from an Aerodyne mid infrared absorption instrument (QC-TIDLAS) from the University of Toronto (Ellis et al., 2010), and N_2O_5, HNO_3, and $ClNO_2$ (1 Hz sample frequency) measured with an iodide Time-of-Flight Chemical Ionization Mass Spectrometer (I$^-$TOF-CIMS) from the University of Washington (Lee et al., 2014; Lee et al., 2018). Accuracies for NO_x, NO_2, and O_3 were 5% and 12% for NO_y. with stated detection limits of 60 pptv (2σ) (Wagner et al., 2011; Wild et al., 2014) in the boundary layer. Gas-phase NH_3 was measured with a detection limit of 450 pptv (1s 3σ), as described in further detail by Moravek et al. (2019). Accuracy and detection limits for N_2O_5, $ClNO_2$, and HNO_3 were similar to those reported from the same instrument deployed during the Wintertime INvestigation of Transport, Emissions, and Reactivity (WINTER) campaign ($\leq$ 0.6 pptv (1s 1σ), 30%) (Lee et al., 2018). Non-refractory sub-micron aerosol composition (sampled every ~ 10 s) was measured with the NOAA Aerosol Mass Spectrometer (AMS) (Bahreini et al., 2009; Middlebrook et al., 2012) and aerosol size (sample every ~ 3 s) with a commercial Ultra-High Sensitivity Aerosol Spectrometer (UHSAS) (Brock et al., 2011). Average detection limits for AMS aerosol composition were 0.04, 0.09, 0.33, 0.03, and 0.07 μg sm^{-3} (sm^{-3} refers to m^3 under standard conditions (1 atm and 273.15 K)) for particulate nitrate, ammonium, organics, sulfate, and chloride, respectively. Uncertainties were ~20% for all species (Franchin et al., 2018). Ambient temperature and pressure (1 Hz sample frequency) were measured with a commercial (Avantech) meteorological probe. The accuracy of the commercial UHSAS instrument was also expected to be similar to that used during WINTER (dry surface area density: ~34%).

Additional ground-based measurements used in this analysis include hourly $PM_{2.5}$, NO_2, O_3, and temperature from the Utah Department of Air Quality (UDAQ) instrumentation at the Hawthorne (HW) monitoring site (Figure 1). Total $PM_{2.5}$ mass was measured with a Thermo Scientific 1405-DF Dichotomous Ambient Air Monitor, NO_2 with a Teledyne API T200U Chemiluminescence detector, and O_3 with a Teledyne API T400 UV absorption spectrometer, all in accordance with EPA guidelines (Environmental Protection Agency, 2018). Select volatile organic compounds (VOCs) were also measured at the University of Utah (UU) ground site by a Proton-Transfer Reaction Mass Spectrometer. Further information about the UWFPS campaign and aircraft and ground-based instrumentation can be found in additional publications (Franchin et al., 2018; UWFPS Science Team, 2018; Womack et al., 2019; Moravek et al., 2019).

4

2.2 Box Model

2.2.1 Description

A zero-dimension chemical box model has been developed to simulate the nocturnal chemical evolution of an air parcel from sunset until the time of aircraft measurement (assuming constant temperature and relative humidity). Extensive model details have

5   been previously discussed in McDuffie et al. (2018b). Briefly, the model forward-integrates the chemical mechanism (13 reactions, Table S1) starting 1.3 hours prior to sunset (see below), iteratively adjusting the initial concentrations of O_3 and NO_2, until the model-predicted concentrations are both within 0.5% of the aircraft observations. Holding these initial concentrations constant, the model next adjusts the total heterogeneous loss rate constant of N_2O_5 ($k_{N_2O_5}$) until the model output reproduces ambient nighttime observations of N_2O_5 to within 1%. As described in McDuffie et al. (2018b), the model iterates these steps, re-adjusting initial

10   concentrations of O_3 and NO_2 and values of $k_{N_2O_5}$ until aircraft observations of NO_2, O_3, and N_2O_5 are simultaneously reproduced by the model. The final step holds these values constant while iteratively adjusting the production rate of $ClNO_2$ (k_{ClNO_2}) until the modeled mixing ratios of $ClNO_2$ are within 1% of the nighttime $ClNO_2$ observations. The N_2O_5 uptake coefficients ($\gamma(N_2O_5)$) and $ClNO_2$ production yields ($\phi(ClNO_2)$) are then calculated following Eqs. (1) and (2), where c is the mean molecular speed and SA is the ambient wet PM_1 surface area density (described below). The model repeats this entire process every 10 seconds for all

15   flights conducted at night, as determined by time and aircraft GPS altitude.

$$\gamma(N_2O_5) = \frac{4 * k_{N_2O_5}}{c * SA} \tag{1}$$

$$\varphi(ClNO_2) = \frac{k_{ClNO_2}}{k_{N_2O_5}} \tag{2}$$

Holding the derived $k_{N_2O_5}$ and k_{ClNO_2} values constant, the model can further simulate the total nitrate produced overnight by forward-integrating the model until the time of sunrise, as shown for a representative SLV point in Figure 3. Here, total nitrate

20   (gas + particulate-phase) is represented as HNO_3 only, as this model does not include aerosol thermodynamics that partition nitrate between the gas and particle phases. Modeled gas-phase HNO_3 is assumed to partition to the particle phase with 100% efficiency, following observations presented in Franchin et al. (2018) that show > 90% of total nitrate is in the particle phase during wintertime pollution events in the SLV. As modeled nitrate is initialized with a concentration of 0 μg m^{-3}, concentrations predicted at sunrise represent the total amount of nitrate produced from nocturnal chemistry over the course of a single night (i.e. nocturnal nitrate

25   production rate). These base case values assume no overnight loss from dilution and constant values of $\gamma(N_2O_5)$ and $\phi(ClNO_2)$, as discussed further in Section 3.3.3.

2.2.2 Model Simplifications and Uncertainties

For the UWFPS campaign, the box model was run in a similar manner to that described previously in McDuffie et al. (2018b), for nocturnal aircraft observations collected in the RL over the eastern U.S. coast during the 2015 WINTER campaign. Due to more

30   limited instrumentation during UWFPS than WINTER, a larger number of box model assumptions and simplifications were required, which are summarized below.

5

Deleted: of both are

Deleted: and production rate constant of $ClNO_2$ (k_{ClNO_2})

Deleted: simultaneously

Deleted: and $ClNO_2$

Deleted: Figure 3

Deleted: , therefore

First, the wet SA density for the base case simulations was calculated by applying a hygroscopic growth curve as a function of RH (Figure S2) to the dry PM_1 SA measured by the UHSAS (details in Section S1.3). The growth curve was derived with the Extended-AIM Aerosol Thermodynamic Model (Wexler and Clegg, 2002), assuming pure NH_4NO_3 particles. Alternatively, estimating the growth factor from AMS organic measurements and estimates of aerosol organic density and

5 hygroscopicity constant (κ_{Org}) (described in S1.3, (Jimenez et al., 2009; Mei et al., 2013; Cerully et al., 2015; e.g. Kuwata et al., 2012; Brock et al., 2016; Shingler et al., 2016)), resulted in only a ~3% change in the total wet SA for night flights during UWFPS (Figure S2a). For the 1031 10-second measurement periods with simultaneous values of $\gamma(N_2O_5)$ and $\phi(ClNO_2)$, the median dry aerosol SA was 151.9 μm^2 cm^{-3}, which increased to 353.1 μm^2 cm^{-3} when accounting for hygroscopic growth (Figure S2b). Additional uncertainties associated with hygroscopic growth and assumptions of constant SA are discussed below in Section 3.3.2.

10 Second, loss of the nitrate radical (NO_3) from its reaction with volatile organic compounds (VOCs) was assumed to occur with a single first-order rate constant (k_{NO_3}), calculated for each flight from a combination of historical ground-based VOC measurements and select VOC measurements from a PTR-MS at the UU site (see Supplemental Section S1.2 for details; Atkinson and Arey (2003)). At night, NO_3 serves as one of the primary tropospheric oxidants for VOCs and can react with RO_2 and HO_2 radicals to contribute to nocturnal NO_x recycling (Vaughan et al., 2006). In this analysis, NO_3-VOC reactions were lumped and

15 treated as a net NO_x sink with values of the first order loss rate constant, k_{NO_3}, ranging from 1.5×10^{-3} - 9.5×10^{-3} s^{-1} (NO_3 lifetime ~100 – 1000 s). These rate constants are slightly larger than average values measured during the WINTER campaign (1.3×10^{-4} to 4.6×10^{-4} s^{-1}) (McDuffie et al., 2018b) and within the range previously reported (3×10^{-5} to 1×10^{-2} s^{-1}) during winter 2012 at a ground site in Colorado (Wagner et al., 2013). Additional NO_x-regeneration from reactions of NO_3 with HO_2 and RO_2 radicals were not included in this analysis due to a lack of radical measurements. An under-prediction in k_{NO_3} from these uncertainties would cause

20 both an over-prediction in the loss rate constant of N_2O_5, as well as the subsequent production of nitrate. While uncertainties in k_{NO_3} can lead to large model uncertainties during summertime conditions (e.g. Phillips et al., 2016), NO_3-VOC reactivity is largely reduced during the winter season as a result of lower biogenic emissions and colder temperatures that favor N_2O_5 in its equilibrium with NO_3. Sensitivity studies discussed below showed 0.2% changes in the median model-predicted nocturnal nitrate production rate associated with ± 50% changes in k_{NO_3} (Table S4). The possibility of varying VOC reactivity with time was also investigated

25 (Section S1.4.5) but resulted in a minimal (<0.1%) impact on nitrate production results presented below. The potential for other rate constants to vary with time may additionally lead to increased variability in the results presented in Section 3.3.

Third are uncertainties in assumptions regarding the start time and duration of each simulation. All simulations were initialized at 1.3 hours prior to sunset, assuming no initial concentration of N_2O_5 or $ClNO_2$. The pre-sunset time of 1.3 hours was derived for the WINTER campaign, based on the time when predicted daytime N_2O_5 concentrations (described in Section S1.4.4

30 and Brown et al. (2005)) diverged from ambient observations when approaching sunset. This value was not recalculated for UWFPS simulations as daytime N_2O_5 calculations require measurements of j(NO_3) photolysis rates, which were not available during UWFPS. The median nocturnal nitrate production rate, however, changed by <0.3% when this pre-sunset time was varied between 0 and 2 hours. Photolysis rates during this time were also calculated from those measured during the WINTER campaign (Section S1.4.3; Shetter and Müller (1999)). While WINTER photolysis rates may have been larger than those during Utah PCAP

35 events, the median modeled nocturnal nitrate production rate showed a small sensitivity (< 2.8%) to ± 40% changes in these values (Section S1.4.3). Additional uncertainties in air age (i.e. simulation start time and duration), however, may still serve to over-

Deleted: aerosol SA

Deleted: and only impact the $\gamma(N_2O_5)$ values reported here (not the nitrate production rates) as $k_{N_2O_5}$ and k_{ClNO_2} are independent of the aerosol SA.

Deleted: ,

Deleted: s

Deleted: measured

predict N_2O_5 loss rates and nocturnal nitrate based on previous sensitivity studies (McDuffie et al., 2018b). A combination of these assumptions will lead to a greater uncertainty in model results near sunset, as discussed in Section 3.3.2.

Fourth, air parcel mixing and deposition of gas-phase nitric acid were not included in base case simulations. Additional simulations, described in Section S1.4.2, included deposition using a first order nitric acid loss constant of 2.6×10^{-6} s^{-1}, calculated from a boundary layer height of 800 m, deposition velocity of 2.7 cm s^{-1} (Zhang et al., 2012), and gas/particle nitrate fraction of 8% from Franchin et al. (2018). The median nocturnal nitrate production rate increased by < 8% when this depositional loss of HNO_3 was included. In contrast, modeled nitrate production was most sensitive (-42.2% reduction) to the addition of a 1st order loss processes, meant to simulate air parcel dilution and O_3 entrainment from vertical mixing between the RL and free troposphere (Table S4). Based on a previous analysis by Womack et al. (2019), the dilution rate constant here was estimated to be 1.3×10^{-5} s^{-1} in the RL, with a possible range of $1.2\text{-}2.5\times10^{-5}$ s^{-1} (described in Section S1.4.1). Results from simulations that include dilution are discussed further in the final section.

Finally, the absolute uncertainty associated with each individual nocturnal nitrate production rate was calculated from the quadrature addition of the uncertainties associated with sensitivity tests described above and in Section S1.4, as well as uncertainties in the NO_2, O_3, N_2O_5, and $ClNO_2$ measurements used as model fit parameters (< 6% for all tests). Production rates derived from model fits to observations, as well as the absolute uncertainties associated with all 17 sensitivity tests are shown as a time series in Figure S3, with dilution contributing 92% of the total uncertainty (light blue in Figure S3), on average. Both the base case results (black dots) and those from simulations including the effects of air parcel dilution are discussed in Section 3.3.3.

3 Results and Discussions

3.1 PM$_{2.5}$ in Salt Lake Valley – Winter 2017

To provide an overview of wintertime pollution events in the SLV, Figure 4 shows a time series of total PM$_{2.5}$ mass (1-hour and 24-hour averages) measured at the UDAQ Hawthorne (HW) site (Figure 1) from 1 December 2016 to 22 February 2017. Additional time series of ground-based PM$_{2.5}$ measurements for all three Utah NAAs are provided in Franchin et al. (2018). The SLV data in Figure 4 show four pollution events that exceeded the NAAQS during the 2016-2017 winter. Calculated from 24-hour measurements, the four largest pollution events during December 2016 and January 2017 had daily PM$_{2.5}$ build-up rates that ranged from $3.7 - 15.6$ μg m^{-3} day^{-1} (see Figure 4), encompassing the daily rates reported previously in the same valley (Whiteman et al., 2014; Silcox et al., 2012; Baasandorj et al., 2017). The last two major pollution events (10 - 22 January (Event #3) and 25 January - 5 February (Event #4)) overlapped with the flights during UWFPS, shown by the gray shading in Figure 4. Average non-refractory (NR) PM$_1$ aerosol mass fractions measured during these periods by the TO AMS showed that the aerosol was primarily composed of NH_4NO_3 (Figure 4, pie charts). The sum of NO_3^- and NH_4^+ contributed to 76.6% and 74.0% of the total PM$_1$ mass measured during the last two pollution episodes (74% average (Franchin et al., 2018)), which agree with previous ground-based observations (e.g. Baasandorj et al., 2017) of past seasons. Nitrate alone contributed to an average 57% and 58% of the total aerosol mass during pollution episodes #3 and #4, respectively. During the relatively clean period sampled between 8 and 12 February 2017, the combined NH_4^+ + NO_3^- fraction decreased to an average of 57%, with a larger relative contribution from aerosol organics. The remaining analyses here will focus on aircraft flights during the two late January pollution events (#3 and #4) to evaluate the contribution of nocturnal RL heterogeneous nitrogen chemistry to observed surface-level nitrate during pollution events.

7

3.2 Limiting and Excess Reagents for NH$_4$NO$_3$ Aerosol

As NH$_4$NO$_3$ was the principle component of PM$_{2.5}$ during pollution events in the SLV (Figure 4), the contribution from heterogeneous reactive nitrogen processes is dependent on whether NH$_4$NO$_3$ formation is limited by the availability of gas-phase NH$_3$ or HNO$_3$. Under ambient conditions, gas-phase NH$_3$ and HNO$_3$ are assumed to be in a thermodynamic equilibrium with their

5   particulate equivalents (NO$_3^-$(p) and NH$_4^+$(p)). The limiting reagent can therefore be inferred from the ratio of total oxidized (HNO$_3$(g) + NO$_3^-$(p)) to total reduced nitrogen (NH$_x$ = NH$_3$(g) + NH$_4^+$(p)), shown in Eq (3). This ratio does not account for other aerosol components such as (NH$_4$)$_2$SO$_4$, NH$_4$HSO$_4$, and NH$_4$Cl, but should generally represent the NH$_4$NO$_3$ aerosol system when particulate concentrations of sulfate and inorganic chloride are low, as was observed during UWFPS 2017 (Figure 4 and Franchin et al. (2018)). A nitrogen ratio greater than 1 indicates that oxidized nitrogen is in excess and NH$_4$NO$_3$ particle formation is limited

10   by the presence of NH$_3$. Conversely, a ratio smaller than 1 indicates that formation is limited by the presence of HNO$_3$, which itself is limited by the oxidation rate of NO$_x$. In a HNO$_3$-limited system, NH$_4$NO$_3$ formation will be sensitive to changes in HNO$_3$ concentrations resulting from both day and nighttime NO$_x$ oxidation processes. Daytime NO$_x$ oxidation rates during winter will depend on specific conditions but are generally slower, such that nighttime oxidation may play a dominant role (e.g. Wood et al., 2005; Kenagy et al., 2018).

15

$$NRatio = \frac{HNO_3(g) + NO_3^-(p)}{NH_3(g) + NH_4^+(p)} \tag{3}$$

A time series of nitrogen ratios in the SLV between 17 January and 1 February is shown in Figure 5a, calculated from 10s averaged (AMS frequency) measurements of gas and particle-phase compounds aboard the TO aircraft. Figure 5a shows that NH$_4$NO$_3$ particle formation in the SLV during pollution episodes was largely limited by HNO$_3$ (median ratio 0.77), but highly variable (range of 0.1 -1.9) and time dependent, with the frequency of NH$_3$-limited conditions increasing throughout both late

20   January pollution events. The color scale in Figure 5a and the vertical profiles of average and 10-90th percentile nitrogen ratios in Figure 5b further show that the lowest nitrogen ratios corresponded to the lowest altitudes. This evidence of HNO$_3$-limitation near the ground is consistent with all previous ground-based observations that show exclusive HNO$_3$-limitation in the SLV (Kelly et al., 2013; Utah Division of Air Quality, 2014c). The increased frequency of NH$_3$-limited points throughout both pollution episodes (Figure 5a), however, is opposite the trend predicted by Baasandorj et al. (2017), who suggested that observed surface-level oxidant

25   depletion should lead to more HNO$_3$-limited conditions over time. Events of NH$_3$-limitation (excess HNO$_3$) during 2017, however, only occurred at the highest altitudes (panel b) and their increasing frequency with time (panel a) is consistent with these events reflecting negative NH$_3$ gradients away from the surface and/or the production of HNO$_3$ aloft from nocturnal N$_2$O$_5$ chemistry. The rate of HNO$_3$ production from nocturnal heterogeneous chemistry is expected to be maximized at higher altitudes, removed from NO emissions and O$_3$ titration at the surface (Figure 2). Results here are also consistent with aerosol thermodynamic modeling

30   studies by Franchin et al. (2018) who found that simulations of total PM$_1$ mass during UWFPS flights over the SLV were proportionally sensitive to 50% reductions in total nitrate. Additional simulations by Franchin et al. (2018), however, also showed near 50% PM$_1$ reductions with 50% reductions in total ammonium (NH$_3$+NH$_4^+$), indicating that 50% ammonium reductions may be enough to shift the SLV from the HNO$_3$ to NH$_3$-limited regime. This is consistent with nitrogen ratios in Figure 5 approaching and exceeding values of 1.

8

Deleted: Figure 4

Formatted: Subscript

Deleted: Figure 4

Deleted: Figure 5

Deleted: Figure 5

Deleted: ese results

Deleted: are

Deleted: Figure 5

Deleted: resulted in

Deleted: (Franchin et al., 2018)

Deleted: ,

3.3 Nitrate Production via Heterogeneous Reactive Nitrogen Chemistry

The absolute amount of nitrate chemically produced from heterogeneous chemistry will depend on the production rate of the nitrate radical and gas-phase N_2O_5 (Section 3.3.1), N_2O_5 aerosol uptake efficiency (Section 3.3.2), and yields of $ClNO_2$ and HNO_3 (Section 3.3.2), which are quantified below. The final section (Section 3.3.3) presents forward-integrated box model simulations to further quantify the nocturnal nitrate production rate and estimate the contribution of this chemistry to NH_4NO_3 formation during January 2017 in the SLV.

3.3.1 Maximum Instantaneous Nitrate Production Rates

An upper limit estimate of the instantaneous production rate of aerosol nitrate from heterogeneous N_2O_5 chemistry is defined here as $P_{NO_3^-,max}$. This rate can be calculated as two times the gas-phase production rate of the NO_3 radical (P_{NO_3}), given that reaction between NO_2 and O_3 (Eqs. (4) – (6)), rather than N_2O_5 uptake, is the rate limiting step for nitrate formation (discussed below). In Eq. (4), P_{NO_3} is calculated in units of molec. cm^{-3} s^{-1} but is typically reported in units of ppbv hr^{-1} as shown below. The reaction kinetics in Eq. (5) between NO_2 and O_3 are from the 2008 IUPAC recommendation (IUPAC, 2008) and $P_{NO_3^-,max}$ in Eq. (6) is calculated after P_{NO_3} has been converted to units of µg m^{-3} hr^{-1}, as detailed in Supplemental Section S2. This calculation estimates a maximum contribution of N_2O_5 heterogeneous chemistry to nitrate production as it assumes: 1) N_2O_5 is produced quantitatively from NO_3 (i.e. no competing reaction of NO_3 + VOC), 2) N_2O_5 is produced at the rate of NO_3 production (valid under cold conditions that shift the NO_3-N_2O_5 equilibrium to favor of N_2O_5), 3) N_2O_5 is efficiently taken up onto aerosol, and 4) aqueous-phase reactions form two molecules of HNO_3 for every molecule of N_2O_5 (i.e. $\phi(ClNO_2) = 0$).

$$P_{NO_3}[\text{ppbv hr}^{-1}] = \frac{k_4[O_3][NO_2]}{ND\,[\text{molec. cm}^{-3}]} * 3600\,[\text{s hr}^{-1}] * 1 \times 10^9\,[\text{ppbv}] \tag{4}$$

$$k_4\,[\text{cm}^3\,\text{molecule}^{-1}\,\text{s}^{-1}] = 1.4 \times 10^{-13} e^{(-2470/T)} \tag{5}$$

$$P_{NO_3^-,max}[\text{µg m}^{-3}\,\text{hr}^{-1}] = 2 * (P_{NO_3}\,[\text{µg m}^{-3}\,\text{hr}^{-1}]) \tag{6}$$

The value of $P_{NO_3^-,max}$ is expected to vary with altitude due to boundary layer dynamics and surface NO_x emissions that can deplete O_3 at night near the surface, as described previously in Baasandorj et al. (2017). The time series in Figure 6a illustrates that the O_3 measured at HW was frequently absent at night during the 3rd and 4th pollution events in January 2017. As surface-level O_3 was titrated overnight, ground-site data cannot provide direct information about $P_{NO_3^-,max}$ aloft in the RL. In the absence of vertical observations during pollution events in 2016, a previous analysis by Baasandorj et al. (2017) used late afternoon measurements at the HW ground site to predict NO_3 production rates (P_{NO_3}) in the RL that varied from 0 up to ~ 2 ppbv hr^{-1} (~ 0 – 5 µg m^{-3} hr^{-1}), but with values frequently < 1 ppbv hr^{-1}. These values correspond to instantaneous nitrate production rates ($P_{NO_3^-,max}$) of ~ 0 – 10 µg m^{-3} hr^{-1}, with typical values closer to 5 µg m^{-3} hr^{-1}. Late afternoon estimates from the same site during 2017 (dashed lines in Figure 6, from Eq. (6)), suggest smaller $P_{NO_3^-,max}$ rates in 2017 than in 2016, with values between 1 and 5 µg m^{-3} hr^{-1} during UWFPS pollution events (Figure 6a).

The bottom panels of Figure 6b show the binned, vertical profiles of median, 25th, and 75th percentile instantaneous $P_{NO_3^-,max}$ values, along with aircraft observations of O_3, NO_2, and PM_1 for all UWFPS night flights (red shaded regions in Figure 6a). The vertical profiles show a relatively uniform distribution of $P_{NO_3^-,max}$ with altitude through the lowest 600 m. The dashed

9

black lines also show that the number of points in each altitude bin was weighted toward the 100-500 m altitude range. The median instantaneous $P_{NO_3^-,max}$ value in this polluted layer (0-600 mAGL) was 1.6 µg m^{-3} hr^{-1} (N = 21666). This value is at the low range of estimates of 1.6 - 5 µg m^{-3} hr^{-1} that are predicted from late afternoon ground-based observations on each flight day (dashed line in the middle panel of Figure 6a), following the method of Baasandorj et al. (2017).

5   Vertical profiles in Figure 6b do not show evidence for a reduction in $P_{NO_3^-,max}$ or O$_3$ near the surface, as is expected for O$_3$ titration near the ground level (shown in panel a). The distribution in panel b, however, is affected by the location of the missed approaches / landings in the SLV (Salt Lake International and South Valley Regional airfields), which are further from the urban center of Salt Lake City than the HW ground site (see Figure 1). Vertical profiles to the surface over urban Salt Lake City were not possible due to a lack of airfields for missed approaches. Instead, the SLV flights often executed box patterns over the eastern

10   Salt Lake basin at several altitudes. Figure 7 shows the vertical distribution of $P_{NO_3^-,max}$ values from these boxes on January 28 - 29 between 21:20 – 00:30 local time, compared to $P_{NO_3^-,max}$ measured at surface level during the same interval. At 300 and 500 m AGL, the median (and interquartile range) $P_{NO_3^-,max}$ was 2.2 (2.1 to 2.4) and 1.9 (1.8 to 2.1) µg m^{-3} hr^{-1}, while at 650 m, slightly above the most concentrated pollution layer, it was 0.5 (0.3 to 0.7) µg m^{-3} hr^{-1}. The median value at the HW ground site, directly below the aircraft, was 0.02 (0.01 to 0.2) µg m^{-3}. These plots demonstrate that $P_{NO_3^-,max}$ is typically low or zero at night near the

15   surface within the urban area of Salt Lake City, but large within the RL. Away from the urban area, the vertical distributions of $P_{NO_3^-,max}$ are also likely more uniform (Figure 6b) due to the lack of O$_3$ titration within the nocturnal boundary layer. In the final section below, nightly integration of these instantaneous $P_{NO_3^-,max}$ values are compared to box model predictions of total nitrate.

3.3.2 Modeled Uptake Coefficients and Production Yields

Both the aerosol uptake efficiency of N$_2$O$_5$ (γ(N$_2$O$_5$)) and the production yield of ClNO$_2$ (ϕ(ClNO$_2$)) are highly variable, dependent

20   on aerosol composition, and can impact the absolute amount of nitrate formed from nocturnal heterogeneous nitrogen chemistry. The nighttime formation of nitrate, however, is only limited by these processes when N$_2$O$_5$ uptake is inefficient and is instead limited by the oxidation rate of NO$_2$ (R1) (discussed above) at sufficiently large values of γ(N$_2$O$_5$).

As described in Section 2.2, an iterative box model was fit to observations of NO$_2$, O$_3$, N$_2$O$_5$, and ClNO$_2$ to quantify γ(N$_2$O$_5$) and ϕ(ClNO$_2$) during pollution events. For the SLV alone (N = 1030), the distribution in Figure 8 shows that γ(N$_2$O$_5$)

25   values ranged four orders of magnitude from 1 ×10^{-3} to > 1 with two modes centered near 0.01 and 0.08. Values approaching or exceeding 1 are unphysical and suggest artifacts in the γ(N$_2$O$_5$) determinations for UWFPS (see below), at least for the largest values. Values of ϕ(ClNO$_2$) encompassed the entire possible range of 0 to 1 (Figure 8). The medians for this subset were 0.076 and 0.220 for γ(N$_2$O$_5$) and ϕ(ClNO$_2$), respectively. For all UWFPS flights between 16 January and 1 February 2017, the median γ(N$_2$O$_5$) and ϕ(ClNO$_2$) values in the RL (N = 2195) were 0.049 and 0.256, respectively, derived from box-model fits to observations. These

30   values are compared to multiple derivation methods further below.

Compared to previous studies, the median γ(N$_2$O$_5$) over the SLV was twice as large as the mode derived with a similar model using data from the Nitrogen, Aerosol Composition, and Halogens on a Tall Tower (NACHTT) campaign near Denver, Colorado in winter 2011 (Wagner et al., 2013). Similarly, the median was over 5 times larger than the median calculated using the same model from the 2015 WINTER campaign (McDuffie et al., 2018b). The largest values during UWFPS exceeded those from

35   both WINTER and NACHTT studies, while the smallest values were also larger than either of the respective minimums. The two most common suppression mechanisms that lead to reductions in γ(N$_2$O$_5$) are associated with the presence of organic material and

Deleted: Figure 7

Deleted: Figure 8

Deleted: .

10

nitrate in the aerosol phase. Insoluble aerosol organics have been shown to suppress N_2O_5 uptake in previous laboratory studies (e.g. Griffiths et al., 2009; Thornton et al., 2003; McNeill et al., 2006; Thornton and Abbatt, 2005; Cosman et al., 2008; Badger et al., 2006; Folkers et al., 2003) and large organic mass fractions have been associated with $\gamma(N_2O_5)$ reductions in past field studies (Bertram et al., 2009; McDuffie et al., 2018b). The average dry mass fraction of aerosol organics (i.e. organic mass / total dry aerosol mass) during the SLV pollution events was less than half of the average during the WINTER campaign (~18% vs 40%) and 40% lower than the average during NACHTT (27%, (Wagner et al., 2013)). Aerosol nitrate can also suppress uptake as soluble nitrate facilitates the reformation of gas-phase N_2O_5 (Bertram and Thornton, 2009; Griffiths et al., 2009), and nitrate mass fractions have been negativly correlated with $\gamma(N_2O_5)$ in previous field-studies (Wagner et al., 2013; Morgan et al., 2015; Riedel et al., 2012; Bertram et al., 2009; McDuffie et al., 2018b). The presence of sufficient aerosol water, however, can offset this nitrate suppression by promoting N_2O_5 aqueous solvation and reaction (e.g. Bertram and Thornton, 2009; Griffiths et al., 2009; Mentel et al., 1999; Wahner et al., 1998), resulting in increases in $\gamma(N_2O_5)$ with the ratio of water to nitrate (McDuffie et al., 2018b). The average dry mass fraction of aerosol nitrate was much larger during UWFPS (60%) than during NACHTT (30%, Wagner et al. (2013)) or WINTER (15%, McDuffie et al. (2018b)). High humidity conditions during UWFPS (77% average RH during pollution events) resulted in average aerosol water mass fractions (i.e. water mass / aerosol dry mass + water mass) near 70%, as calculated with an aerosol thermodynamic model, described in Franchin et al. (2018). This higher RH likely contributed to efficient N_2O_5 uptake during UWFPS despite the presence of aerosol nitrate. In fact, the largest 25% of UWFPS $\gamma(N_2O_5)$ values exceed the largest value (0.175) that has been reported from recent field studies (Figure 4 in McDuffie et al. (2018b)).

The median $\phi(ClNO_2)$ value of 0.220 during the SLV pollution events was 4 times larger than during the NACHTT campaign (Riedel et al., 2013; Wagner et al., 2013), but within a factor of 2 larger than the median derived during WINTER over the U.S. east coast (McDuffie et al., 2018a). The SLV median was also similar to medians reported from previous ground-based studies across North America (Mielke et al., 2016; Mielke et al., 2011; Mielke et al., 2013; Wagner et al., 2012; Thornton et al., 2010). Heterogeneous $ClNO_2$ production requires aerosol chloride (R6) (e.g. Behnke et al., 1997) and though a consistent geographic pattern in $\phi(ClNO_2)$ has not emerged from past studies (Figure 2 in McDuffie et al. (2018a)), heterogeneous chemistry in the vicinity of the Great Salt Lake appears to produce $ClNO_2$ with the same efficiency as comparable measurements near North American ocean coastlines. $ClNO_2$ production yields, however, remain smaller than those predicted based on measured aerosol composition, as discussed below.

While large $\gamma(N_2O_5)$ and moderate $\phi(ClNO_2)$ values indicate efficient nitrate production from heterogeneous chemistry during UWFPS, these values may be upper and lower limits, respectively. As discussed in Section 2.1, limited observations of VOC and photolysis rates, as well as uncertainties in air age, and dilution may cause the $k_{N_2O_5}$ and k_{ClNO_2} values (and subsequent $\gamma(N_2O_5)$ and $\phi(ClNO_2)$) to be over- and under-predicted, respectively. This is more likely near sunset where the model has an increased sensitivity to assumptions in simulation start time (McDuffie et al., 2018b). Uncertainties in gas-phase measurements may also contribute to uncertainties in the model predictions, though the level of uncertainty associated with these parameters is small (Table S4). Additional uncertainties in $k_{N_2O_5}$ and k_{ClNO_2} may arise from model assumptions of constant temperature and RH (i.e. rate constants and surface area) overnight. While model sensitivities to these uncertainties cannot be directly quantified, the percent growth in SA from nitrate accumulation is estimated to be less than the uncertainty in the dry SA measurement (34%). As modeled $k_{N_2O_5}$ values are also consistent with those derived from observations (discussed below), this source of uncertainty is not discussed further. Overall, while the box model has a large number of uncertainties and assumptions, predictions of nocturnal

11

Deleted: that observed

Moved (insertion) [1]

Deleted: -derived

Deleted: values of

Deleted: As summarized in Table S4, the box model

nitrate production, which are subject to uncertainties in both $k_{N_2O_5}$ and k_{ClNO_2}, are not highly sensitive to sources other than dilution (discussed below, Table S4).

Independent of the model fits of $k_{N_2O_5}$ and k_{ClNO_2}, unphysically large γ(N₂O₅) values (> 0.1 in Figure 8) may alternatively be an artifact arising from under-measurement of ambient aerosol SA. Low aerosol SA would bias high the γ(N₂O₅) calculation in

5 Eq. (1) without influencing the model derivations of $k_{N_2O_5}$ and k_{ClNO_2}. In this study, wet aerosol SA was calculated as described above by applying a relative humidity-dependent growth factor curve to the measured dry PM₁ SA. Despite large concentrations of total dry SA (Figure S2), an under-prediction in the wet SA could arise from uncertainties in the hygroscopic growth curve or additional unmeasured SA from large particles (> 1 μm). Both factors would be exacerbated by the high humidity conditions encountered during UWFPS since large, hydrated particles would not be sampled efficiently by the aerosol inlet and hygroscopic

10 growth curves are highly uncertain above ~ 95% RH (corresponding to 6.7% of the SLV data). A third possible cause of under-measured SA is the presence of fog under high humidity conditions. Fog is well known to promote rapid heterogeneous processes (Lelieveld and Crutzen, 1990), and is associated with surface areas that can be orders of magnitude larger than accumulation mode aerosol. For example, fog has been demonstrated to lead to rapid N₂O₅ loss at a ground site in Hong Kong, during November - December 2013 (Brown et al., 2016). It is therefore possible that unmeasured SA under high humidity conditions could bias the

15 calculated γ(N₂O₅) values high relative to values reported in previous literature. Any bias caused by aerosol SA, however, would not impact the model-derived $k_{N_2O_5}$ and k_{ClNO_2} values that are used to calculate nocturnal nitrate production rates in the final analysis below.

To further evaluate the UWFPS γ(N₂O₅) and ϕ(ClNO₂) values, box model determinations are compared to two other derivation methods in Figures 8 and S5. The first method calculates γ(N₂O₅) from observations of temperature, SA, NO₂, O₃, and

20 N₂O₅, based on the steady state approximation (γ(N₂O₅)ₛₛ), described by Brown et al. (2003) and defined in Supplemental Section S4.1. This method shows excellent agreement with box model results (Figure 8 and S5). The steady state method has been shown in previous analyses to over-predict γ(N₂O₅) values under cold, high NOₓ conditions, but only if the first order rate constants for NO₃ and N₂O₅ loss (k_{NO_3} and $k_{N_2O_5}$) are modest (Brown et al., 2003). Both the steady state and box model γ(N₂O₅) values are consistent with a rapid first order loss constant of N₂O₅ (median $k_{N_2O_5}$ = 1.1×10⁻³ s⁻¹), suggesting the steady state approach is valid

25 for SLV conditions. The corresponding median lifetime (1/$k_{N_2O_5}$) of 14 minutes is, for example, much shorter than the lifetimes of 2-18 hours calculated from a previous steady state analysis of aircraft measurements over Texas in fall 2006 (Brown et al., 2009). Nevertheless, the color scale in Figure S5 shows that the largest γ(N₂O₅) values (≥ 0.1) were exclusively derived for air sampled within 3 hours of sunset (4.3 hr simulation time), where previous analysis has shown the steady state approximation to be least reliable. As Figure S5 shows large values of γ(N₂O₅) from both the box model and the steady state analysis during this time,

30 there may be a common bias between the methods if these values are indeed too large.

The second method calculates both γ(N₂O₅) and ϕ(ClNO₂) using laboratory-derived parameterizations from Bertram and Thornton (2009) (BT09), based on aerosol volume-to-surface area ratio, N₂O₅ solubility (Fried et al., 1994), aerosol molarities of water, nitrate, and chloride (calculated as described in Section S4.2), and laboratory-derived reaction rate constant ratios. Further details of each parameterization are provided in Supplemental Section S4.2. These parameterizations have had mixed success in

35 reproducing previous field-derived values (e.g. Bertram et al., 2009; Riedel et al., 2012; McDuffie et al., 2018b; McDuffie et al., 2018a), but are commonly used to predict N₂O₅ uptake and ClNO₂ production on internally-mixed inorganic aerosol when N₂O₅ chemistry is included in global models (e.g. Sarwar et al., 2014; Shah et al., 2018).

12

Deleted: is

Deleted: most

Deleted: sources of uncertainty

Deleted: , and

Deleted: the

Moved up [1]: model-derived values of $k_{N_2O_5}$ are consistent with those derived from observations (discussed below).

Deleted: Figure 8

Deleted: observations

Deleted: Figure 8

Deleted: determinations

Deleted: based

Deleted: by

Results in Figure S5 show that the median $\gamma(N_2O_5)$ value predicted by the BT09 parameterization is within a factor of 2 of the box model median, but that this parameterization does not reproduce the observed variability (Figures 8). For $\phi(ClNO_2)$, the BT09 parameterization largely over-predicts model-derived values with a median of 0.66 relative to the model median of 0.22 (Figure S5). This over-prediction is consistent with all previous studies to compare parameterized and field-derived $\phi(ClNO_2)$

5   results (Wagner et al., 2013; Wang et al., 2017b; Ryder et al., 2015; Thornton et al., 2010; Riedel et al., 2013; Wang et al., 2017a; Tham et al., 2018; McDuffie et al., 2018a). These results also suggest that the parameterization would need to be reduced by 68% for agreement with the box model median, similar to the 74-85% reduction required for agreement of this parameterization with the WINTER campaign median (McDuffie et al., 2018a). The possible presence of additional, refractory-phase chloride (i.e. NaCl, CaCl$_2$, and KCl) in the accumulation mode would increase the predicted $\gamma(N_2O_5)$ and improve agreement with the box model but

10   would further degrade the agreement of $\phi(ClNO_2)$.

Lastly, the empirical $\gamma(N_2O_5)$ parameterization from McDuffie et al. (2018b) was applied to UWFPS data, though only an estimated range for the campaign median is presented due to uncertainties in the aerosol O:C ratio and aerosol organic density, both required for this calculation (discussed in Section S4.2). This parameterization models N_2O_5 uptake onto an aqueous inorganic particle with a resistive organic coating, with a thickness determined by the volume ratio of inorganic to total aerosol components

15   (McDuffie et al., 2018b; Riemer et al., 2009; Anttila et al., 2006). By estimating a range of O:C ratios using the improved-ambient O:C ratio method from Canagaratna et al. (2015) and AMS organic m/z 44 fraction (Figure 6, Franchin et al. (2018)), assuming an organic density of 1.3 g/cm^3 (e.g. Kuwata et al., 2012) to estimate the organic-associated volume, and applying additional constants described in Section S4.2, this parameterization estimated a median $\gamma(N_2O_5)$ between 60 and 85% lower than the box model. Though there are large uncertainties in the required parameters, these results suggest that during pollution events: 1) aerosol

20   organics are not surface active, 2) aerosol organics are not resistive toward N_2O_5, or 3) box model $\gamma(N_2O_5)$ values are over-predicted due to missing SA (e.g. fog, Section 3.3.2) or other simplifying assumptions (e.g. dilution) discussed above.

Despite disagreement between the box model and parameterizations, the $\gamma(N_2O_5)$ values predicted by all three methods are large enough, in combination with the large measured aerosol SA, to fall within the range where models of nighttime chemistry are insensitive to variation in uptake efficiency (e.g. Macintyre and Evans, 2010; Riemer et al., 2003; Wang et al., 2018). Under

25   these conditions, the NO$_2$ gas-phase oxidation rate (i.e. $P_{NO_3^-}$), rather than N_2O_5 uptake, becomes the limiting factor to HNO$_3$ formation. As further evidence of this limitation, the median lifetime of NO$_2$ with respect to O$_3$ ($\tau_{NO_2} = 1/(k_1[O_3])$) was 9-hours while the lifetime of N_2O_5 ($\tau_{N_2O_5} = 1/k_{N_2O_5}$) was just 14-minutes, resulting in low N_2O_5 mixing ratios (median = 0.03 ppbv) during the SLV pollution events (Figure S6). In addition, explicit box modeling of day and nighttime chemical processes during UWFPS by Womack et al. (2019) also showed that the production of O$_{x,total}$ (= NO$_2$ + O$_3$ + 2*NO$_3$ + 1.5*(HNO$_3$ +particulate nitrate) +

30   ClNO$_2$ + 3*N$_2$O$_5$ + others) was insensitive (<1.5%) to order-of-magnitude changes in $\gamma(N_2O_5)$. Short lifetimes of N_2O_5 relative to NO$_2$, as well as nitrate insensitivity to $\gamma(N_2O_5)$, both indicate that nocturnal heterogeneous chemistry contributes to NH$_4$NO$_3$ formation, but that absolute production is limited by gas-phase kinetics rather than aerosol composition and $\gamma(N_2O_5)$. This insensitivity to $\gamma(N_2O_5)$ provides confidence in the ability of the box model to predict the magnitude of nocturnal nitrate production in the SLV, regardless of uncertainties in $\gamma(N_2O_5)$.

3.3.3 Modeled Nocturnal Nitrate Production Rates and Contribution of Heterogeneous Chemistry to Total NH₄NO₃ Aerosol Accumulation Rates

As described in Section 2.2 and shown in Figure 3, the box model simulates the amount of total nitrate (HNO_3 + NO_3^-) produced from heterogeneous chemistry over the course of a single night. This amount of nitrate, in units of µg m⁻³ night⁻¹, is in addition to any nitrate present at sunset from the previous day (e.g. Figure 3). Figure 9 shows the distribution of nightly nitrate production predicted by base case simulations (N = 1033), ranging from ~0 to 31 µg m⁻³ nitrate night⁻¹, with a median of 9.9 µg m⁻³ nitrate night⁻¹.

In addition to evidence from the previous section, comparisons between the base case results and integrated $P_{NO_3^-,max}$ values from Section 3.3.1 also suggest that nocturnal nitrate production is limited by the rate of NO_2 oxidation rather than the efficiency of N_2O_5 aerosol uptake. Based on the calculations in Section 3.1, upper-limit $P_{NO_3^-,max}$ values, integrated over an average 14 hour night and reduced to account for a $\phi(ClNO_2)$ value of 0.2, ranged from < 0.5 to > 40 µg m⁻³ night⁻¹, with a median of 20.2 µg m⁻³ night⁻¹ (N = 21666). To more directly compare with box model results, the subset of points with simultaneous $\gamma(N_2O_5)$ determinations had a median of 10.6 µg m⁻³ night⁻¹, which is slightly larger, but agrees well with the box-model predicted median of 9.9 µg m⁻³ night⁻¹. As described in Section 3.3.1, the $P_{NO_3^-,max}$ calculation assumes efficient N_2O_5 uptake and only considers nitrate production to be limited by gas-phase kinetics. Observed agreement between the integrated $P_{NO_3^-,max}$ values and box model-predicted production rates, therefore suggests that nitrate production may be largely limited by gas-phase oxidation rather than multi-phase processes. As a result, the large variability in predicted nitrate production rates is reflective of the variability in the observed NO_3 radical production rates (Figure 6).

Uncertainties associated with base case production rates are discussed in Section 2.2.2 and shown as a time series in Figure S3. Air parcel dilution associated with the vertical entrainment of air from the free troposphere (Section S1.4.1) was the largest source of uncertainty (Table S4, Figure S3). This process was not included in base case simulations, though mixing / dilution has been observed and predicted in an analysis of WINTER nighttime flights (Kenagy et al., 2018; McDuffie et al., 2018b). Estimating the impact of dilution by including a single first order dilution rate constant ($k_{dilution}$) of 1.3×10^{-5} s⁻¹ reduced the median nocturnal nitrate production rate by 42% to 5.7 µg m⁻³ night⁻¹ and resulted in a smaller range of production rates (~0 to 16 µg m⁻³ night⁻¹) relative to base case simulations in Figure 9. As described in Womack et al. (2019) (and in Section S1.4.1), a single 1ˢᵗ-order dilution rate constant of 8×10^{-6} s⁻¹ was derived for pollution event #4 in the SLV by fitting a box model to best reproduce the day-to-day build-up of observed $O_{x,total}$ between 28 January and 1 February at the UU ground site. In the model described by Womack et al. (2019), this rate constant was then scaled up by 40% when simulating the nocturnal RL in order to maintain constant dilution and account for the reduced volume relative to the mixed daytime boundary layer. While dilution / entrainment rates may vary day to night, the method of Womack et al. (2019) represents the single number that would best represent the average rate. The same procedure is followed here with a resulting $k_{dilution}$ value of 1.3×10^{-5} s⁻¹, which is ~60% lower than $k_{dilution}$ from the WINTER campaign, derived from observations of NO_y (= NO + NO_2 + NO_3 + 2*N_2O_5 + $ClNO_2$ + $RONO_2$...) overnight in a single RL air parcel over the eastern U.S. coast (McDuffie et al., 2018b). As processes relevant to RL dilution were not directly measured during UWFPS, there are uncertainties associated with this $k_{dilution}$ estimation. For instance, based on the modeled surface albedo in Womack et al. (2019), $k_{dilution}$ could have reproduced observed $O_{x,total}$ mixing ratios with scaled values ranging between 1.2×10⁻

14

[5] and 2.5×10^{-5} s^{-1} (Figure S10, Womack et al., 2019). This particular range of loss rate constants predicts median nitrate production rates in the SLV between 3.6 and 6.1 µg m^{-3} night^{-1}.

Modeled nitrate production rates are further compared in Figure 10 to the average daily accumulation of surface-level nitrate aerosol during pollution event #4 at the HW ground site. This ground-based accumulation rate (red diamond in Figure 10a) was taken as the slope of the 24-hr average PM$_{2.5}$ observations at HW (scaled by 0.58; average NO$_3^-$ fraction from Figure 4) during the first six days of event #4, before it began to degrade on 1 February 2017 (Figure 10b). Only data from event #4 data are assessed here as this was the only PCAP sampled with the aircraft on multiple nights. Figure 10a shows this average, 24-hour surface accumulation rate of 4.6 µg m^{-3} day^{-1} (red diamond) compared to the 10th – 90th percentile distributions, medians, and averages of the nocturnal production rates predicted by base case box model simulations (gray) and simulations including the effects of 24-hour dilution (blue), described below.

Comparing modeled RL chemical nitrate production to the observed ground-based accumulation rate can provide an estimate for the fractional contribution of N$_2$O$_5$ uptake to total particulate nitrate production in the SLV. Direct comparison is difficult, however, as the 24-hour ground-based accumulation rate includes contributions from photochemistry and nocturnal formation in the RL and nocturnal boundary layer (NBL), and is impacted by dilution and mixing processes. For example, the amount of nocturnally produced nitrate at the surface will depend on mixing between the NBL and RL during morning boundary layer expansion (Figure 2). In Figure 10a, the median base case prediction without dilution or mixing (gray, 8.6 µg m^{-3} night^{-1}) was nearly twice as large as the 24-hour average accumulation rate observed at the surface during the same event (4.6 µg m^{-3} night^{-1}, red). Therefore, to more directly compare box model predictions and ground-based observations, Figure 10a also shows the results from two simulations that include upper- and lower-limit estimates of loss from nocturnal and daytime dilution. For both scenarios, the nighttime (0-14 hours) $k_{dilution}$ value of 1.3×10^{-5} s^{-1} (blue) was applied to all modeled species as described above. At sunrise, morning mixing between the NBL (taken as 40% by volume) and RL (taken as 60% by volume) was then estimated using the assumed volume ratio between the two layers and assuming either equivalent nocturnal nitrate production in both layers (upper limit) or no production in the NBL (lower limit). Nocturnal production in the NBL is expected to be suppressed relative to the RL due to O$_3$ titration (e.g. Figure 6 and Figure S6 in Womack et al. (2019), making the assumption of equivalence an upper limit estimate to nocturnally-produced nitrate at the surface after morning mixing. The upper limit case required no reduction of the model-predicted nitrate concentrations at sunrise (e.g. Figure 9), whereas these concentrations were instantaneously reduced by 40% for the lower limit case. To account for daytime dilution in the remaining ~10 hours, morning concentrations for both cases were further diluted with the daytime boundary dilution rate constant from Womack et al. (2019) (8×10^{-6} s^{-1}), described above and in Section S1.4.1. For a single 24-hour period, this resulted in a net median of 2.4 to 3.9 µg m^{-3} nitrate produced from nocturnal heterogeneous N$_2$O$_5$ uptake for the lower and upper-limit cases, respectively. When considering the entire possible range of dilution rate constants from Womack et al. (2019), the median values from both cases were between 1.1 and 4.2 µg m^{-3} day^{-1}, as shown in Figure S7.

Comparison of modeled rates to the observed surface build-up of 4.6 µg m^{-3} day^{-1} suggests that on average, nitrate produced from heterogenous chemistry can account for at least 50% of the nitrate accumulation observed at the surface. This result is qualitatively consistent with an observational analysis by Pusede et al. (2016), who determined that nocturnal heterogeneous chemistry was the main source of regional aerosol nitrate during wintertime pollution events in the San Joaquin Valley. The lower limit estimate, however, is also similar to a box model analysis of this same event by Womack et al. (2019), who found roughly

15

equal contributions between photochemical and nocturnal nitrate production pathways, highlighting that photochemical nitrate production is also occurring during these events. Therefore, while results in Figure 10a (including dilution) predict a median nocturnal fractional contribution of 52 - 86% (ranging between 24 and 91% (Figure S7)), confirmation and further quantification of this result will require additional, vertically resolved measurements of aerosol composition, gas-phase precursors, and physical parameters, as well as more sophisticated modeling of these multi-day pollution accumulation events with 3D-chemical transport models.

4 Summary and Conclusions

Aerosol and gas-phase measurements collected during the 2017 UWFPS campaign showed multiple pollution events that exceeded PM$_{2.5}$ standards in the SLV, the most populated region in the state of Utah. During these events, aerosol particles were largely composed of NH$_4$NO$_3$, which forms from the reaction between gas-phase NH$_3$ and HNO$_3$. While NH$_3$ is emitted from surface sources, HNO$_3$ is chemically formed from the oxidation of NO$_x$ emissions. This oxidation can occur through daytime reactions with the photochemical OH radical, or nocturnal heterogeneous reactions involving NO$_3$ and N$_2$O$_5$. The contribution of nocturnal chemistry to PM$_{2.5}$ formation in the SLV is dependent on whether NH$_4$NO$_3$ formation is NH$_3$- or HNO$_3$-limited, as well as the NO$_3$ production rate, N$_2$O$_5$ uptake efficiency, ClNO$_2$ and HNO$_3$ production yields, and loss processes such as air parcel dilution.

Vertically resolved measurements of gas and particulate phase oxidized and reduced nitrogen in the SLV showed that NH$_4$NO$_3$ formation during pollution events was nearly always HNO$_3$ limited, but that oxidized and reduced nitrogen approached equivalence as pollution events progressed. This reagent balance analysis is consistent with aerosol thermodynamic modeling presented in Franchin et al. (2018), which predicted that all three major valleys in Wasatch region were sensitive to nitrate reductions, and that the SLV was also sensitive to NH$_3$ reductions. Both observation and modeling-based analyses agreed that NH$_4$NO$_3$ formation in the RL was largely HNO$_3$-limited during pollution events, providing the possibility of a large contribution from nocturnal heterogeneous chemistry to HNO$_3$ and PM$_{2.5}$ mass.

Analysis of vertically-resolved, calculated nitrate production rates (an upper-limit estimate due to heterogeneous HNO$_3$ formation, $P_{NO_3^-,max}$) and results from an observationally-constrained chemical box model, suggest that nocturnal chemistry is an efficient mechanism for PM$_{2.5}$ production in the SLV during pollution events. Nitrate production rates had a median of 1.6 μg m^{-3} hr^{-1}, while values of γ(N$_2$O$_5$) and φ(ClNO$_2$) had medians of 0.076 and 0.220, respectively, during pollution events. Values of γ(N$_2$O$_5$) were larger than previous field-based determinations (e.g. McDuffie et al., 2018b) and those predicted from the Bertram and Thornton (2009) parameterization, but were in agreement with values derived using the N$_2$O$_5$ steady state approach. The median φ(ClNO$_2$) value was larger than that derived from aircraft observations over the eastern US coast, but was simultaneously overpredicted by 68% by the Bertram and Thornton (2009) parameterization, which uses measurements of aerosol chloride and aerosol water estimations.

While the box model has uncertainties associated with limited available measurements and model assumptions, the large measured aerosol SA, efficient N$_2$O$_5$ uptake coefficients, and moderate ClNO$_2$ yields resulted in nightly modeled nitrate production rates that were largely insensitive to specific values of derived parameters. Agreement between base case modeled nightly nitrate production (9.9 μg m^{-3} night^{-1}) and that calculated from $P_{NO_3^-,max}$ values (10.6 μg m^{-3} night^{-1}) alternatively suggests that nitrate production is more sensitive to gas-phase NO$_2$ oxidation rates than γ(N$_2$O$_5$), providing confidence in the model's predictions of nocturnal nitrate. Of the parameters tested, the model was most sensitive to loss through air parcel dilution, with a 42% reduction

16

Deleted: 42

Deleted: were

to 5.2 µg m^{-3} nitrate night^{-1} when including a nocturnal $k_{dilution}$ rate constant of $1.3×10^{-5}$ s^{-1}. When considering the possible effects of 24-hour dilution, model simulations predicted a reduced median of 2.4 - 3.9 µg m^{-3} nitrate day^{-1}, corresponding to 52 - 86% (median) of the net aerosol nitrate accumulation that was observed at a SLV ground site. Due to model uncertainties and sensitivities to dilution, further quantification of this result will require additional vertically-resolved measurements and photochemical / 3D modeling analyses. These results, however, highlight the importance of nocturnal chemistry in the formation of PM$_{2.5}$ in the SLV and can provide constraints for regulatory models of PM$_{2.5}$, used to assess control strategies in this populated non-attainment area.

Author Contributions

During the UWFPS campaign, EEM, CCW, DLF, and WPD were responsible for the CRD gas-phase measurements, AF and AM for the AMS particle measurements, LG, BHL, and JAT for the I$^-$TOF-CIMS measurements, and AM and JM for the NH$_3$ instrument. MB and SSB organized the UWFPS campaign with technical support from WPD. EEM developed the box model code and preformed the analyses with support from CCW and SSB. EEM prepared the manuscript with contributions from co-authors.

References

Anttila, T., Kiendler-Scharr, A., Tillmann, R., and Mentel, T. F.: On the reactive uptake of gaseous compounds by organic-coated aqueous aerosols: Theoretical analysis and application to the heterogeneous hydrolysis of N_2O_5, J. Phys. Chem. A, 110, 10435-10443, doi:10.1021/jp062403c, 2006.

Atkinson, R., and Arey, J.: Atmospheric degradation of volatile organic compounds, Chem. Rev., 103, 4605-4638, doi:10.1021/cr0206420, 2003.

Baasandorj, M., Hoch, S. W., Bares, R., Lin, J. C., Brown, S. S., Millet, D. B., Martin, R., Kelly, K., Zarzana, K. J., Whiteman, C. D., Dube, W. P., Tonnesen, G., Jaramillo, I. C., and Sohl, J.: Coupling between chemical and meteorological processes under persistent cold-air pool conditions: Evolution of wintertime $PM_{2.5}$ pollution events and N_2O_5 observations in Utah's Salt Lake Valley, Environ. Sci. Technol., 51, 5941-5950, doi:10.1021/acs.est.6b06603, 2017.

Badger, C. L., Griffiths, P. T., George, I., Abbatt, J. P. D., and Cox, R. A.: Reactive uptake of N_2O_5 by aerosol particles containing mixtures of humic acid and ammonium sulfate, J. Phys. Chem. A, 110, 6986-6994, doi:10.1021/jp0562678, 2006.

Bahreini, R., Ervens, B., Middlebrook, A. M., Warneke, C., de Gouw, J. A., DeCarlo, P. F., Jimenez, J. L., Brock, C. A., Neuman, J. A., Ryerson, T. B., Stark, H., Atlas, E., Brioude, J., Fried, A., Holloway, J. S., Peischl, J., Richter, D., Walega, J., Weibring, P., Wollny, A. G., and Fehsenfeld, F. C.: Organic aerosol formation in urban and industrial plumes near Houston and Dallas, Texas, J. Geophys. Res. Atmos., 114, doi:10.1029/2008JD011493, 2009.

Beard, J. D., Beck, C., Graham, R., Packham, S. C., Traphagan, M., Giles, R. T., and Morgan, J. G.: Winter temperature inversions and emergency department visits for asthma in Salt Lake County, Utah, 2003-2008, Environ. Health Persp., 120, 1385-1390, doi:10.1289/ehp.1104349, 2012.

Behera, S. N., Sharma, M., Aneja, V. P., and Balasubramanian, R.: Ammonia in the atmosphere: a review on emission sources, atmospheric chemistry and deposition on terrestrial bodies, Environ. Sci. Pollut. R., 20, 8092-8131, doi:10.1007/s11356-013-2051-9, 2013.

Behnke, W., George, C., Scheer, V., and Zetzsch, C.: Production and decay of $ClNO_2$ from the reaction of gaseous N_2O_5 with NaCl solution: Bulk and aerosol experiments, J. Geophys. Res. Atmos., 102, 3795-3804, doi:10.1029/96JD03057, 1997.

Bertram, T. H., and Thornton, J. A.: Toward a general parameterization of N_2O_5 reactivity on aqueous particles: the competing effects of particle liquid water, nitrate and chloride, Atmos. Chem. Phys., 9, 8351-8363, doi:10.5194/acp-9-8351-2009, 2009.

Bertram, T. H., Thornton, J. A., Riedel, T. P., Middlebrook, A. M., Bahreini, R., Bates, T. S., Quinn, P. K., and Coffman, D. J.: Direct observations of N_2O_5 reactivity on ambient aerosol particles, Geophys. Res. Lett., 36, L19803 doi:10.1029/2009GL040248, 2009.

Brock, C. A., Cozic, J., Bahreini, R., Froyd, K. D., Middlebrook, A. M., McComiskey, A., Brioude, J., Cooper, O. R., Stohl, A., Aikin, K. C., de Gouw, J. A., Fahey, D. W., Ferrare, R. A., Gao, R. S., Gore, W., Holloway, J. S., Hübler, G., Jefferson, A., Lack, D. A., Lance, S., Moore, R. H., Murphy, D. M., Nenes, A., Novelli, P. C., Nowak, J. B., Ogren, J. A., Peischl, J., Pierce, R. B., Pilewskie, P., Quinn, P. K., Ryerson, T. B., Schmidt, K. S., Schwarz, J. P., Sodemann, H., Spackman, J. R., Stark, H., Thomson, D. S., Thornberry, T., Veres, P., Watts, L. A., Warneke, C., and Wollny, A. G.: Characteristics, sources, and transport of aerosols measured in spring 2008 during the aerosol, radiation, and cloud processes affecting Arctic Climate (ARCPAC) Project, Atmos. Chem. Phys., 11, 2423-2453, doi:10.5194/acp-11-2423-2011, 2011.

Brock, C. A., Wagner, N. L., Anderson, B. E., Attwood, A. R., Beyersdorf, A., Campuzano-Jost, P., Carlton, A. G., Day, D. A., Diskin, G. S., Gordon, T. D., Jimenez, J. L., Lack, D. A., Liao, J., Markovic, M. Z., Middlebrook, A. M., Ng, N. L., Perring, A. E., Richardson, M. S., Schwarz, J. P., Washenfelder, R. A., Welti, A., Xu, L., Ziemba, L. D., and Murphy, D. M.: Aerosol optical properties in the southeastern United States in summer – Part 1: Hygroscopic growth, Atmos. Chem. Phys., 16, 4987-5007, doi:10.5194/acp-16-4987-2016, 2016.

18

Brown, S. G., Hyslop, N. P., Roberts, P. T., McCarthy, M. C., and Lurmann, F. W.: Wintertime Vertical Variations in Particulate Matter (PM) and Precursor Concentrations in the San Joaquin Valley during the California Regional Coarse PM/Fine PM Air Quality Study, J. Air Waste Manage., 56, 1267-1277, doi:10.1080/10473289.2006.10464583, 2006.

Brown, S. S., Stark, H., and Ravishankara, A. R.: Applicability of the steady state approximation to the interpretation of atmospheric observations of NO_3 and N_2O_5, J. Geophys. Res., 108, doi:10.1029/2003jd003407, 2003.

Brown, S. S., Dibb, J. E., Stark, H., Aldener, M., Vozella, M., Whitlow, S., Williams, E. J., Lerner, B. M., Jakoubek, R., Middlebrook, A. M., DeGouw, J. A., Warneke, C., Goldan, P. D., Kuster, W. C., Angevine, W. M., Sueper, D. T., Quinn, P. K., Bates, T. S., Meagher, J. F., Fehsenfeld, F. C., and Ravishankara, A. R.: Nighttime removal of NO_x in the summer marine boundary layer, Geophys. Res. Lett., 31, L07108, doi:10.1029/2004gl019412, 2004.

Brown, S. S., Osthoff, H. D., Stark, H., Dubé, W. P., Ryerson, T. B., Warneke, C., de Gouw, J. A., Wollny, A. G., Parrish, D. D., Fehsenfeld, F. C., and Ravishankara, A. R.: Aircraft observations of daytime NO_3 and N_2O_5 and their implications for tropospheric chemistry, J. Photoch. Photobio. A, 176, 270-278, doi:10.1016/j.jphotochem.2005.10.004, 2005.

Brown, S. S., Dubé, W. P., Osthoff, H. D., Stutz, J., Ryerson, T. B., Wollny, A. G., Brock, C. A., Warneke, C., de Gouw, J. A., Atlas, E., Neuman, J. A., Holloway, J. S., Lerner, B. M., Williams, E. J., Kuster, W. C., Goldan, P. D., Angevine, W. M., Trainer, M., Fehsenfeld, F. C., and Ravishankara, A. R.: Vertical profiles in NO_3 and N_2O_5 measured from an aircraft: Results from the NOAA P-3 and surface platforms during the New England Air Quality Study 2004, J. Geophys. Res., 112, doi:10.1029/2007jd008883, 2007.

Brown, S. S., Dubé, W. P., Fuchs, H., Ryerson, T. B., Wollny, A. G., Brock, C. A., Bahreini, R., Middlebrook, A. M., Neuman, J. A., Atlas, E., Roberts, J. M., Osthoff, H. D., Trainer, M., Fehsenfeld, F. C., and Ravishankara, A. R.: Reactive uptake coefficients for N_2O_5 determined from aircraft measurements during the Second Texas Air Quality Study: Comparison to current model parameterizations, J. Geophys. Res. Atmos., 114, D00F10, doi:10.1029/2008JD011679, 2009.

Brown, S. S., and Stutz, J.: Nighttime radical observations and chemistry, Chem. Soc. Rev., 41, 6405-6447, doi:10.1039/c2cs35181a, 2012.

Brown, S. S., Dubé, W. P., Tham, Y. J., Zha, Q., Xue, L., Poon, S., Wang, Z., Blake, D. R., Tsui, W., Parrish, D. D., and Wang, T.: Nighttime chemistry at a high altitude site above Hong Kong, J. Geophys. Res. Atmos., 121, 2457-2475, doi:10.1002/2015JD024566, 2016.

Canagaratna, M. R., Jimenez, J. L., Kroll, J. H., Chen, Q., Kessler, S. H., Massoli, P., Hildebrandt Ruiz, L., Fortner, E., Williams, L. R., Wilson, K. R., Surratt, J. D., Donahue, N. M., Jayne, J. T., and Worsnop, D. R.: Elemental ratio measurements of organic compounds using aerosol mass spectrometry: characterization, improved calibration, and implications, Atmos. Chem. Phys., 15, 253-272, doi:10.5194/acp-15-253-2015, 2015.

Cerully, K. M., Bougiatioti, A., Hite Jr, J. R., Guo, H., Xu, L., Ng, N. L., Weber, R., and Nenes, A.: On the link between hygroscopicity, volatility, and oxidation state of ambient and water-soluble aerosols in the southeastern United States, Atmos. Chem. Phys., 15, 8679-8694, doi:10.5194/acp-15-8679-2015, 2015.

Chen, L. W. A., Watson, J. G., Chow, J. C., Green, M. C., Inouye, D., and Dick, K.: Wintertime particulate pollution episodes in an urban valley of the Western US: a case study, Atmos. Chem. Phys., 12, 10051-10064, doi:10.5194/acp-12-10051-2012, 2012.

Cosman, L. M., Knopf, D. A., and Bertram, A. K.: N_2O_5 reactive uptake on aqueous sulfuric acid solutions coated with branched and straight-chain insoluble organic surfactants, J. Phys. Chem. A, 112, 2386-2396, doi:10.1021/jp710685r, 2008.

Ellis, R. A., Murphy, J. G., Pattey, E., van Haarlem, R., O'Brien, J. M., and Herndon, S. C.: Characterizing a Quantum Cascade Tunable Infrared Laser Differential Absorption Spectrometer (QC-TILDAS) for measurements of atmospheric ammonia, Atmos. Meas. Tech., 3, 397-406, doi:10.5194/amt-3-397-2010, 2010.

Environmental Protection Agency: Ambinet Monitoring Technology Information Center [Available at: https://www.epa.gov/amtic], 2018.

19

Folkers, M., Mentel, T. F., and Wahner, A.: Influence of an organic coating on the reactivity of aqueous aerosols probed by the heterogeneous hydrolysis of N_2O_5, Geophys. Res. Lett., 30, 1644, doi:10.1029/2003GL017168, 2003.

Franchin, A., Fibiger, D. L., Goldberger, L., McDuffie, E. E., Moravek, A., Womack, C. C., Crosman, E. T., Docherty, K. S., Dube, W. P., Hoch, S. W., Lee, B. H., Long, R., Murphy, J. G., Thornton, J. A., Brown, S. S., Baasandorj, M., and Middlebrook, A. M.: Airborne and ground-based observations of ammonium-nitrate-dominated aerosols in a shallow boundary layer during intense winter pollution episodes in northern Utah, Atmos. Chem. Phys., 18, 17259-17276, doi:10.5194/acp-18-17259-2018, 2018.

Fried, A., Henry, B. E., Calvert, J. G., and Mozurkewich, M.: The reaction probability of N_2O_5 with sulfuric acid aerosols at stratospheric temperatures and compositions, J. Geosphys. Res. Atmos., 99, 3517-3532, doi:10.1029/93JD01907, 1994.

Fuchs, H., Dube, W. P., Lerner, B. M., Wagner, N. L., Williams, E. J., and Brown, S. S.: A sensitive and versatile detector for atmospheric NO_2 and NO_x based on blue diode laser cavity ring-down spectroscopy, Environ. Sci. Technol., 43, 7831-7836, doi:10.1021/es902067h, 2009.

Gillies, R. R., Wang, S.-Y., and Booth, M. R.: Atmospheric Scale Interaction on Wintertime Intermountain West Low-Level Inversions, Weather Forecast., 25, 1196-1210, doi:10.1175/2010WAF2222380.1, 2010.

Green, M. C., Chow, J. C., Watson, J. G., Dick, K., and Inouye, D.: Effects of Snow Cover and Atmospheric Stability on Winter PM2.5 Concentrations in Western U.S. Valleys, J. Appl. Meteorol. Clim., 54, 1191-1201, doi:10.1175/JAMC-D-14-0191.1, 2015.

Griffiths, P. T., Badger, C. L., Cox, R. A., Folkers, M., Henk, H. H., and Mentel, T. F.: Reactive uptake of N_2O_5 by aerosols containing dicarboxylic acids. Effect of particle phase, composition, and nitrate content, J. Phys. Chem. A, 113, 5082-5090, doi:10.1021/jp8096814, 2009.

Hansen, J. C., Woolwine Iii, W. R., Bates, B. L., Clark, J. M., Kuprov, R. Y., Mukherjee, P., Murray, J. A., Simmons, M. A., Waite, M. F., Eatough, N. L., Eatough, D. J., Long, R., and Grover, B. D.: Semicontinuous $PM_{2.5}$ and PM_{10} Mass and Composition Measurements in Lindon, Utah, during Winter 2007, J. Air Waste Manage., 60, 346-355, doi:10.3155/1047-3289.60.3.346, 2010.

IUPAC: Data Sheet NOx28, [Avaialble at: http://iupac.pole-ether.fr/htdocs/datasheets/pdf/NOx28_NO2_O3.pdf], 2008.

Jimenez, J. L., Canagaratna, M. R., Donahue, N. M., Prevot, A. S. H., Zhang, Q., Kroll, J. H., DeCarlo, P. F., Allan, J. D., Coe, H., Ng, N. L., Aiken, A. C., Docherty, K. S., Ulbrich, I. M., Grieshop, A. P., Robinson, A. L., Duplissy, J., Smith, J. D., Wilson, K. R., Lanz, V. A., Hueglin, C., Sun, Y. L., Tian, J., Laaksonen, A., Raatikainen, T., Rautiainen, J., Vaattovaara, P., Ehn, M., Kulmala, M., Tomlinson, J. M., Collins, D. R., Cubison, M. J., Dunlea, J., Huffman, J. A., Onasch, T. B., Alfarra, M. R., Williams, P. I., Bower, K., Kondo, Y., Schneider, J., Drewnick, F., Borrmann, S., Weimer, S., Demerjian, K., Salcedo, D., Cottrell, L., Griffin, R., Takami, A., Miyoshi, T., Hatakeyama, S., Shimono, A., Sun, J. Y., Zhang, Y. M., Dzepina, K., Kimmel, J. R., Sueper, D., Jayne, J. T., Herndon, S. C., Trimborn, A. M., Williams, L. R., Wood, E. C., Middlebrook, A. M., Kolb, C. E., Baltensperger, U., and Worsnop, D. R.: Evolution of organic aerosols in the atmosphere, Science, 326, 1525, doi:10.1126/science.1180353, 2009.

Kelly, K. E., Kotchenruther, R., Kuprov, R., and Silcox, G. D.: Receptor model source attributions for Utah's Salt Lake City airshed and the impacts of wintertime secondary ammonium nitrate and ammonium chloride aerosol, J. Air Waste Manage., 63, 575-590, doi:10.1080/10962247.2013.774819, 2013.

Kenagy, H. S., Sparks, T. L., Ebben, C. J., Wooldridge, P. J., Lopez-Hilfiker, F. D., Lee, B. H., Thornton, J. A., McDuffie, E. E., Fibiger, D. L., Brown, S. S., Montzka, D. D., Weinheimer, A. J., Schroder, J. C., Campuzano-Jost, P., Day, D. A., Jimenez, J. L., Dibb Jack, E., Apel, E., Campos, T., Shah, V., Jaegle, L., and Cohen, R. C.: NO_x Lifetime and NO_y Partitioning During WINTER, J. Geosphys. Res. Atmos., 123, 9813-9827, doi:10.1029/2018JD028736, 2018.

Kuprov, R., Eatough, D. J., Cruickshank, T., Olson, N., Cropper, P. M., and Hansen, J. C.: Composition and secondary formation of fine particulate matter in the Salt Lake Valley: Winter 2009, J. Air Waste Manage., 64, 957-969, doi:10.1080/10962247.2014.903878, 2014.

Kuwata, M., Zorn, S. R., and Martin, S. T.: Using Elemental Ratios to Predict the Density of Organic Material Composed of Carbon, Hydrogen, and Oxygen, Environ. Sci. Technol., 46, 787-794, doi:10.1021/es202525q, 2012.

Lee, B. H., Lopez-Hilfiker, F. D., Mohr, C., Kurtén, T., Worsnop, D. R., and Thornton, J. A.: An iodide-adduct high-resolution time-of-flight chemical-ionization mass spectrometer: Application to atmospheric inorganic and organic compounds, Environ. Sci. Technol., 48, 6309-6317, doi:10.1021/es500362a, 2014.

Lee, B. H., Lopez-Hilfiker, F. D., Veres, P. R., McDuffie, E. E., Fibiger, D. L., Sparks, T. L., Ebben, C. J., Green, J. R., Schroder, J. C., Campuzano-Jost, P., Iyer, S., D'Ambro, E. L., Schobesberger, S., Brown, S. S., Wooldridge, P. J., Cohen, R. C., Fiddler, M. N., Bililign, S., Jimenez, J. L., Kurtén, T., Weinheimer, A. J., Jaegle, L., and Thornton, J. A.: Flight Deployment of a High-Resolution Time-of-Flight Chemical Ionization Mass Spectrometer: Observations of Reactive Halogen and Nitrogen Oxide Species, J. Geosphys. Res. Atmos., 123, 7670-7686, doi:10.1029/2017JD028082, 2018.

Lelieveld, J., and Crutzen, P. J.: Influences of cloud photochemical processes on tropospheric ozone, Nature, 227-233, 1990.

Livingston, C., Rieger, P., and Winer, A.: Ammonia emissions from a representative in-use fleet of light and medium-duty vehicles in the California South Coast Air Basin, Atmos. Environ., 43, 3326-3333, doi:10.1016/j.atmosenv.2009.04.009, 2009.

Long, R. W., Eatough, N. L., Mangelson, N. F., Thompson, W., Fiet, K., Smith, S., Smith, R., Eatough, D. J., Pope, C. A., and Wilson, W. E.: The measurement of $PM_{2.5}$, including semi-volatile components, in the EMPACT program: results from the Salt Lake City Study, Atmos. Environ., 37, 4407-4417, doi:10.1016/S1352-2310(03)00585-5, 2003.

Long, R. W., Eatough, N. L., Eatough, D. J., Meyer, M. B., and Wilson, W. E.: Continuous Determination of Fine Particulate Matter Mass in the Salt Lake City Environmental Monitoring Project: A Comparison of Real-Time and Conventional TEOM Monitor Results, J. Air Waste Manage., 55, 1782-1796, doi:10.1080/10473289.2005.10464776, 2005a.

Long, R. W., Modey, W. K., Smith, P. S., Smith, R., Merrill, C., Pratt, J., Stubbs, A., Eatough, N. L., Eatough, D. J., Malm, W. C., and Wilson, W. E.: One– and Three–Hour PM2.5 Characterization, Speciation, and Source Apportionment Using Continuous and Integrated Samplers, Aerosol Sci. Tech., 39, 238-248, doi:10.1080/027868290925633, 2005b.

Macintyre, H. L., and Evans, M. J.: Sensitivity of a global model to the uptake of N_2O_5 by tropospheric aerosol, Atmos. Chem. Phys., 10, 7409-7414, doi:10.5194/acp-10-7409-2010, 2010.

Malek, E., Davis, T., Martin, R. S., and Silva, P. J.: Meteorological and environmental aspects of one of the worst national air pollution episodes (January, 2004) in Logan, Cache Valley, Utah, USA, Atmos. Res., 79, 108-122, doi:10.1016/j.atmosres.2005.05.003, 2006.

Mangelson, N. F., Lewis, L., Joseph, J. M., Cui, W., Machir, J., Eatough, D. J., Rees, L. B., Wilkerson, T., and Jensen, D. T.: The contribution of sulfate and nitrate to atmospheric fine particles during winter inversion fogs in Cache Valley, Utah, J. Air Waste Manage., 47, 167-175, doi:10.1080/10473289.1997.10464429, 1997.

Martin, R.: Cache Valley Air Quality Studies [Available at http://citeseerx.ist.psu.edu/viewdoc/download?doi=10.1.1.127.8179&rep=rep1&type=pdf], 2006.

McDuffie, E. E., Fibiger, D. L., Dubé, W. P., Lopez Hilfiker, F., Lee, B. H., Jaeglé, L., Guo, H., Weber, R. J., Reeves, J. M., Weinheimer, A. J., Schroder, J. C., Campuzano-Jost, P., Jimenez, J. L., Dibb, J. E., Veres, P., Ebben, C., Sparks, T. L., Wooldridge, P. J., Cohen, R. C., Campos, T., Hall, S. R., Ullmann, K., Roberts, J. M., Thornton, J. A., and Brown, S. S.: $ClNO_2$ Yields From Aircraft Measurements During the 2015 WINTER Campaign and Critical Evaluation of the Current Parameterization, J. Geosphys. Res. Atmos., 123, 12,994-913,015, doi:10.1029/2018JD029358, 2018a.

McDuffie, E. E., Fibiger, D. L., Dubé, W. P., Lopez-Hilfiker, F., Lee, B. H., Thornton, J. A., Shah, V., Jaegle, L., Guo, H., Weber, R. J., Reeves, J. M., Weinheimer, A. J., Schroder, J. C., Campuzano-Jost, P., Jimenez, J. L., Dibb Jack, E., Veres, P., Ebben, C., Sparks, T. L., Wooldridge, P. J., Cohen, R. C., Hornbrook, R. S., Apel, E. C., Campos, T., Hall, S. R., Ullmann, K., and Brown, S. S.: Heterogeneous N_2O_5 uptake duirng winter: Aircraft measurements during the 2015 WINTER campaign and critical evaluation of current parameterizations, J. Geosphys. Res. Atmos., 123, 4345-4372, doi:10.1002/2018JD028336, 2018b.

McNeill, V. F., Patterson, J., Wolfe, G. M., and Thornton, J. A.: The effect of varying levels of surfactant on the reactive uptake of N_2O_5 to aqueous aerosol, Atmos. Chem. Phys., 6, 1635-1644, doi:10.5194/acp-6-1635-2006, 2006.

21

Mei, F., Hayes, P. L., Ortega, A., Taylor, J. W., Allan, J. D., Gilman, J., Kuster, W., de Gouw, J., Jimenez, J. L., and Wang, J.: Droplet activation properties of organic aerosols observed at an urban site during CalNex-LA, J. Geophys. Res. Atmos., 118, 2903-2917, doi:10.1002/jgrd.50285, 2013.

Mentel, T., F, Sohn, M., and Wahner, A.: Nitrate effect in the heterogeneous hydrolysis of dinitrogen pentoxide on aqueous
5   aerosols, Phys. Chem. Chem. Phys., 1, 5451-5457, doi:10.1039/A905338G, 1999.

Middlebrook, A. M., Bahreini, R., Jimenez, J. L., and Canagaratna, M. R.: Evaluation of Composition-Dependent Collection Efficiencies for the Aerodyne Aerosol Mass Spectrometer using Field Data, Aerosol Sci. Tech., 46, 258-271, doi:10.1080/02786826.2011.620041, 2012.

Mielke, L. H., Furgeson, A., and Osthoff, H. D.: Observation of $ClNO_2$ in a Mid-Continental Urban Environment, Environ. Sci.
10 Technol., 45, 8889-8896, doi:10.1021/es201955u, 2011.

Mielke, L. H., Stutz, J., Tsai, C., Hurlock, S. C., Roberts, J. M., Veres, P. R., Froyd, K. D., Hayes, P. L., Cubison, M. J., Jimenez, J. L., Washenfelder, R. A., Young, C. J., Gilman, J. B., de Gouw, J. A., Flynn, J. H., Grossberg, N., Lefer, B. L., Liu, J., Weber, R. J., and Osthoff, H. D.: Heterogeneous formation of nitryl chloride and its role as a nocturnal NO_x reservoir species during CalNex-LA 2010, J. Geophys. Res. Atmos., 118, 10,638-610,652, doi:10.1002/jgrd.50783, 2013.

15 Mielke, L. H., Furgeson, A., Odame-Ankrah, C. A., and Osthoff, H. D.: Ubiquity of $ClNO_2$ in the urban boundary layer of Calgary, Alberta, Canada, Can. J. Chem., 94, 414-423, doi:10.1139/cjc-2015-0426, 2016.

Moravek, A., Murphy, J. G., Hrdina, A., Lin, J. C., Pennell, C., Franchin, A., Middlebrook, A. M., Fibiger, D. L., Womack, C. C., McDuffie, E. E., Martin, R., Moore, K., Baasandorj, M., and Brown, S. S.: Wintertime Spatial Distribution of Ammonia and its Emission Sources in the Great Salt Lake Region, Atmos. Chem. Phys. Discuss., doi:10.5194/acp-2019-266, 2019.

20 Morgan, W. T., Ouyang, B., Allan, J. D., Aruffo, E., Di Carlo, P., Kennedy, O. J., Lowe, D., Flynn, M. J., Rosenberg, P. D., Williams, P. I., Jones, R., McFiggans, G. B., and Coe, H.: Influence of aerosol chemical composition on N_2O_5 uptake: airborne regional measurements in northwestern Europe, Atmos. Chem. Phys., 15, 973-990, doi:10.5194/acp-15-973-2015, 2015.

Mozurkewich, M.: The dissociation constant of ammonium nitrate and its dependence on temperature, relative humidity and particle size, Atmos. Environ. A Gen., 27, 261-270, doi:10.1016/0960-1686(93)90356-4, 1993.

25 Nowak, J. B., Neuman, J. A., Bahreini, R., Middlebrook, A. M., Holloway, J. S., McKeen, S. A., Parrish, D. D., Ryerson, T. B., and Trainer, M.: Ammonia sources in the California South Coast Air Basin and their impact on ammonium nitrate formation, Geophys. Res. Lett., 39, L07804, doi:10.1029/2012GL051197, 2012.

Osthoff, H. D., Roberts, J. M., Ravishankara, A. R., Williams, E. J., Lerner, B. M., Sommariva, R., Bates, T. S., Coffman, D., Quinn, P. K., Dibb, J. E., Stark, H., Burkholder, J. B., Talukdar, R. K., Meagher, J., Fehsenfeld, F. C., and Brown, S. S.: High
30 levels of nitryl chloride in the polluted subtropical marine boundary layer, Nat. Geosci., 1, 324-328, doi:10.1038/ngeo177, 2008.

Phillips, G. J., Thieser, J., Tang, M., Sobanski, N., Schuster, G., Fachinger, J., Drewnick, F., Borrmann, S., Bingemer, H., Lelieveld, J., and Crowley, J. N.: Estimating N_2O_5 uptake coefficients using ambient measurements of NO_3, N_2O_5, $ClNO_2$ and particle-phase nitrate, Atmos. Chem. Phys., 16, 13231-13249, doi:10.5194/acp-16-13231-2016, 2016.

Pope, C. A., Muhlestein, J. B., May, H. T., Renlund, D. G., Anderson, J. L., and Horne, B. D.: Ischemic Heart Disease Events
35 Triggered by Short-Term Exposure to Fine Particulate Air Pollution, Circulation, 114, 2443, 2006.

Pope, C. A., Muhlestein, J. B., Anderson, J. L., Cannon, J. B., Hales, N. M., Meredith, K. G., Le, V., and Horne, B. D.: Short-Term Exposure to Fine Particulate Matter Air Pollution Is Preferentially Associated With the Risk of ST-Segment Elevation Acute Coronary Events, J. Am. Heart Assoc., 4, 2015.

Prabhakar, G., Parworth, C. L., Zhang, X., Kim, H., Young, D. E., Beyersdorf, A. J., Ziemba, L. D., Nowak, J. B., Bertram, T. H.,
40 Faloona, I. C., Zhang, Q., and Cappa, C. D.: Observational assessment of the role of nocturnal residual-layer chemistry in determining daytime surface particulate nitrate concentrations, Atmos. Chem. Phys., 17, 14747-14770, doi:10.5194/acp-17-14747-2017, 2017.

Pusede, S. E., Duffey, K. C., Shusterman, A. A., Saleh, A., Laughner, J. L., Wooldridge, P. J., Zhang, Q., Parworth, C. L., Kim, H., Capps, S. L., Valin, L. C., Cappa, C. D., Fried, A., Walega, J., Nowak, J. B., Weinheimer, A. J., Hoff, R. M., Berkoff, T. A., Beyersdorf, A. J., Olson, J., Crawford, J. H., and Cohen, R. C.: On the effectiveness of nitrogen oxide reductions as a control over ammonium nitrate aerosol, Atmos. Chem. Phys., 16, 2575-2596, doi:10.5194/acp-16-2575-2016, 2016.

5 Reeves, H. D., and Stensrud, D. J.: Synoptic-Scale Flow and Valley Cold Pool Evolution in the Western United States, Weather Forecast., 24, 1625-1643, doi:10.1175/2009WAF2222234.1, 2009.

Riedel, T. P., Bertram, T. H., Ryder, O. S., Liu, S., Day, D. A., Russell, L. M., Gaston, C. J., Prather, K. A., and Thornton, J. A.: Direct N_2O_5 reactivity measurements at a polluted coastal site, Atmos. Chem. Phys., 12, 2959-2968, doi:10.5194/acp-12-2959-2012, 2012.

10 Riedel, T. P., Wagner, N. L., Dubé, W. P., Middlebrook, A. M., Young, C. J., Öztürk, F., Bahreini, R., VandenBoer, T. C., Wolfe, D. E., Williams, E. J., Roberts, J. M., Brown, S. S., and Thornton, J. A.: Chlorine activation within urban or power plant plumes: Vertically resolved $ClNO_2$ and Cl_2 measurements from a tall tower in a polluted continental setting, J. Geophys. Res. Atmos., 118, 8702-8715, doi:10.1002/jgrd.50637, 2013.

Riemer, N., Vogel, H., Vogel, B., Schell, B., Ackermann, I., Kessler, C., and Hass, H.: Impact of the heterogeneous hydrolysis of
15 N_2O_5 on chemistry and nitrate aerosol formation in the lower troposphere under photosmog conditions, J. Geophys. Res. Atmos., 108, 4144, doi:10.1029/2002JD002436, 2003.

Riemer, N., Vogel, H., Vogel, B., Anttila, T., Kiendler-Scharr, A., and Mentel, T. F.: Relative importance of organic coatings for the heterogeneous hydrolysis of N_2O_5 during summer in Europe, J. Geophys. Res. Atmos., 114, D17307, doi:10.1029/2008JD011369, 2009.

20 Ryder, O. S., Campbell, N. R., Shaloski, M., Al-Mashat, H., Nathanson, G. M., and Bertram, T. H.: Role of organics in regulating $ClNO_2$ production at the air–sea interface, J. Phys. Chem. A, 119, 8519-8526, doi:10.1021/jp5129673, 2015.

Sarwar, G., Simon, H., Xing, J., and Mathur, R.: Importance of tropospheric $ClNO_2$ chemistry across the Northern Hemisphere, Geophys. Res. Lett., 41, 4050-4058, doi:10.1002/2014gl059962, 2014.

Shah, V., Jaeglé, L., Thornton, J. A., Lopez-Hilfiker, F. D., Lee, B. H., Schroder, J. C., Campuzano-Jost, P., Jimenez, J. L., Guo,
25 H., Sullivan, A. P., Weber, R. J., Green, J. R., Fiddler, M. N., Bililign, S., Campos, T. L., Stell, M., Weinheimer, A. J., Montzka, D. D., and Brown, S. S.: Chemical feedbacks weaken the wintertime response of particulate sulfate and nitrate to emissions reductions over the eastern United States, P. Natl. Acad. Sci. USA, doi:10.1073/pnas.1803295115, 2018.

Shetter, R. E., and Müller, M.: Photolysis frequency measurements using actinic flux spectroradiometry during the PEM-Tropics mission: Instrumentation description and some results, J. Geophys. Res. Atmos., 104, 5647-5661, doi:10.1029/98JD01381, 1999.

30 Shingler, T., Crosbie, E., Ortega, A., Shiraiwa, M., Zuend, A., Beyersdorf, A., Ziemba, L., Anderson, B., Thornhill, L., Perring, A. E., Schwarz, J. P., Campazano-Jost, P., Day, D. A., Jimenez, J. L., Hair, J. W., Mikoviny, T., Wisthaler, A., and Sorooshian, A.: Airborne characterization of subsaturated aerosol hygroscopicity and dry refractive index from the surface to 6.5 km during the SEAC4RS campaign, J. Geophys. Res. Atmos., 121, 4188-4210, doi:10.1002/2015JD024498, 2016.

Silcox, G. D., Kelly, K. E., Crosman, E. T., Whiteman, C. D., and Allen, B. L.: Wintertime $PM_{2.5}$ concentrations during persistent,
35 multi-day cold-air pools in a mountain valley, Atmos. Environ., 46, 17-24, doi:10.1016/j.atmosenv.2011.10.041, 2012.

Silva, P. J., Vawdrey, E. L., Corbett, M., and Erupe, M.: Fine particle concentrations and composition during wintertime inversions in Logan, Utah, USA, Atmos. Environ., 41, 5410-5422, doi:10.1016/j.atmosenv.2007.02.016, 2007.

Stutz, J., Alicke, B., Ackermann, R., Geyer, A., White, A., and Williams, E.: Vertical profiles of NO_3, N_2O_5, O_3, and NO_x in the nocturnal boundary layer: 1. Observations during the Texas Air Quality Study 2000, J. Geophys. Res. Atmos., 109,
40 doi:10.1029/2003JD004209, 2004.

Tham, Y. J., Wang, Z., Li, Q., Wang, W., Wang, X., Lu, K., Ma, N., Yan, C., Kecorius, S., Wiedensohler, A., Zhang, Y., and Wang, T.: Heterogeneous N_2O_5 uptake coefficient and production yield of $ClNO_2$ in polluted northern China: Roles of aerosol water content and chemical composition, Atmos. Chem. Phys. Discuss., 2018, 1-27, doi:10.5194/acp-2018-313, 2018.

Thornton, J. A., Braban, C. F., and Abbatt, J. P. D.: N_2O_5 hydrolysis on sub-micron organic aerosols: the effect of relative humidity, particle phase, and particle size, Phys. Chem. Chem. Phys., 5, 4593-4603, doi:10.1039/B307498F, 2003.

Thornton, J. A., and Abbatt, J. P. D.: N_2O_5 reaction on submicron sea salt aerosol: Kinetics, products, and the effect of surface active organics, J. Phys. Chem. A, 109, 10004-10012, doi:10.1021/jp054183t, 2005.

Thornton, J. A., Kercher, J. P., Riedel, T. P., Wagner, N. L., Cozic, J., Holloway, J. S., Dube, W. P., Wolfe, G. M., Quinn, P. K., Middlebrook, A. M., Alexander, B., and Brown, S. S.: A large atomic chlorine source inferred from mid-continental reactive nitrogen chemistry, Nature, 464, 271-274, doi:10.1038/nature08905, 2010.

U.S. Census Bureau: Quickfacts [Available at: https://www.census.gov/quickfacts/], 2018.

Utah Department of Environmental Quality: Serious Area $PM_{2.5}$ State Implementaion Plan Development [Available at: https://deq.utah.gov/legacy/pollutants/p/particulate-matter/pm25/serious-area-state-implementation-plans/index.htm],

Utah Division of Air Quality: Utah State Implementation: Plan Control Measures for Area and Point Sources, Fine Particulate Matter, PM2.5 SIP for the Logan, UT Nonattainment Area 2014a.

Utah Division of Air Quality: Utah State Implementation: Plan Control Measures for Area and Point Sources, Fine Particulate Matter, PM2.5 SIP for the Provo, UT Nonattainment Area 2014b.

Utah Division of Air Quality: Utah State Implementation: Plan Control Measures for Area and Point Sources, Fine Particulate Matter, PM2.5 SIP for the Salt Lake City, UT Nonattainment Area [Available at: http://www.deq.utah.gov/Laws_Rules/daq/sip/docs/2014/12Dec/SIP%20IX.A.21_SLC_FINAL_Adopted%2012-3-14.pdf], 2014c.

UWFPS Science Team: 2017 Utah Winter Fine Particulate Study Final Report [Available at: https://deq.utah.gov/legacy/programs/air-quality/research/projects/northern-ut-air-polution/winter-fine-particulate-aircraft-study.htm]. 2018.

Vaughan, S., Canosa-Mas, C. E., Pfrang, C., Shallcross, D. E., Watson, L., and Wayne, R. P.: Kinetic studies of reactions of the nitrate radical (NO_3) with peroxy radicals (RO_2): an indirect source of OH at night?, Phys. Chem. Chem. Phys., 8, 3749-3760, doi:10.1039/B605569A, 2006.

Wagner, N. L., Dubé, W. P., Washenfelder, R. A., Young, C. J., Pollack, I. B., Ryerson, T. B., and Brown, S. S.: Diode laser-based cavity ring-down instrument for NO_3, N_2O_5, NO, NO_2 and O_3 from aircraft, Atmos. Meas. Tech., 4, 1227-1240, doi:10.5194/amt-4-1227-2011, 2011.

Wagner, N. L., Riedel, T. P., Roberts, J. M., Thornton, J. A., Angevine, W. M., Williams, E. J., Lerner, B. M., Vlasenko, A., Li, S. M., Dubé, W. P., Coffman, D. J., Bon, D. M., de Gouw, J. A., Kuster, W. C., Gilman, J. B., and Brown, S. S.: The sea breeze/land breeze circulation in Los Angeles and its influence on nitryl chloride production in this region, J. Geophys. Res. Atmos., 117, D00V24, doi:10.1029/2012JD017810, 2012.

Wagner, N. L., Riedel, T. P., Young, C. J., Bahreini, R., Brock, C. A., Dubé, W. P., Kim, S., Middlebrook, A. M., Öztürk, F., Roberts, J. M., Russo, R., Sive, B., Swarthout, R., Thornton, J. A., VandenBoer, T. C., Zhou, Y., and Brown, S. S.: N_2O_5 uptake coefficients and nocturnal NO_2 removal rates determined from ambient wintertime measurements, J. Geophys. Res. Atmos., 118, 9331-9350, doi:10.1002/jgrd.50653, 2013.

Wahner, A., Mentel, T. F., Sohn, M., and Stier, J.: Heterogeneous reaction of N_2O_5 on sodium nitrate aerosol, J. Geophys. Res. Atmos., 103, 31103-31112, doi:10.1029/1998JD100022, 1998.

24

Wang, H., Lu, K., Chen, X., Zhu, Q., Wu, Z., Wu, Y., and Sun, K.: Fast particulate nitrate formation via N2O5 uptake aloft in winter in Beijing, Atmos. Chem. Phys., 18, 10483-10495, doi:10.5194/acp-18-10483-2018, 2018.

Wang, S.-Y., Gillies, R. R., Martin, R., Davies, R. E., and Booth, M. R.: Connecting Subseasonal Movements of the Winter Mean Ridge in Western North America to Inversion Climatology in Cache Valley, Utah, J. Appl. Meteorol. Clim., 51, 617-627, doi:10.1175/JAMC-D-11-0101.1, 2012.

Wang, X., Wang, H., Xue, L., Wang, T., Wang, L., Gu, R., Wang, W., Tham, Y. J., Wang, Z., Yang, L., Chen, J., and Wang, W.: Observations of N_2O_5 and $ClNO_2$ at a polluted urban surface site in North China: High N_2O_5 uptake coefficients and low $ClNO_2$ product yields, Atmos. Environ., 156, 125-134, doi:10.1016/j.atmosenv.2017.02.035, 2017a.

Wang, Z., Wang, W., Tham, Y. J., Li, Q., Wang, H., Wen, L., Wang, X., and Wang, T.: Fast heterogeneous N_2O_5 uptake and $ClNO_2$ production in power plant and industrial plumes observed in the nocturnal residual layer over the North China Plain, Atmos. Chem. Phys., 17, 12361-12378, doi:10.5194/acp-17-12361-2017, 2017b.

Washenfelder, R. A., Wagner, N. L., Dube, W. P., and Brown, S. S.: Measurement of atmospheric ozone by cavity ring-down spectroscopy, Environ. Sci. Technol., 45, 2938-2944, doi:10.1021/es103340u, 2011.

Watson, J. G., and Chow, J. C.: A wintertime $PM_{2.5}$ episode at the Fresno, CA, supersite, Atmos. Environ., 36, 465-475, doi:10.1016/S1352-2310(01)00309-0, 2002.

Wexler, A. S., and Clegg, S. L.: Atmospheric aerosol models for systems including the ions H^+, NH_4^+, Na^+, SO_4^{2-}, NO_3^-, Cl^-, Br^-, and H_2O, J. Geosphys. Res. Atmos., 107, ACH 14-11-ACH 14-14, doi:10.1029/2001JD000451, 2002.

Whiteman, C. D., Hoch, S. W., Horel, J. D., and Charland, A.: Relationship between particulate air pollution and meteorological variables in Utah's Salt Lake Valley, Atmos. Environ., 94, 742-753, doi:10.1016/j.atmosenv.2014.06.012, 2014.

Wild, R. J., Edwards, P. M., Dube, W. P., Baumann, K., Edgerton, E. S., Quinn, P. K., Roberts, J. M., Rollins, A. W., Veres, P. R., Warneke, C., Williams, E. J., Yuan, B., and Brown, S. S.: A measurement of total reactive nitrogen, NO_y, together with NO_2, NO, and O_3 via cavity ring-down spectroscopy, Environ. Sci. Technol., 48, 9609-9615, doi:10.1021/es501896w, 2014.

Womack, C. C., McDuffie, E. E., Edwards, P. M., Bares, R., de Gouw, J. A., Docherty, K. S., Dube, W. P., Fibiger, D. L., Franchin, A., Gilman, J. B., Goldberger, L., Lee, B. H., Lin, J. C., Long, R., Middlebrook, A. M., Millet, D. B., Moravek, A., Murphy, J. G., Quinn, P. K., Riedel, T. P., Roberts, J. M., Thornton, J. A., Valin, L. C., Veres, P. R., Whitehill, A. R., Wild, R. J., Warneke, C., Yuan, B., Baasandorj, M., and Brown, S. S.: An odd oxygen framework for wintertime ammonium nitrate aerosol pollution in urban areas: NOx and VOC control as mitigation strategies, Geophys. Res. Lett., 0, doi:10.1029/2019GL082028, 2019.

Wood, E. C., Bertram, T. H., Wooldridge, P. J., and Cohen, R. C.: Measurements of N_2O_5, NO_2, and O_3 east of the San Francisco Bay, Atmos. Chem. Phys., 5, 483-491, doi:10.5194/acp-5-483-2005, 2005.

Zhang, L., Jacob, D. J., Knipping, E. M., Kumar, N., Munger, J. W., Carouge, C. C., van Donkelaar, A., Wang, Y. X., and Chen, D.: Nitrogen deposition to the United States: distribution, sources, and processes, Atmos. Chem. Phys., 12, 4539-4554, doi:10.5194/acp-12-4539-2012, 2012.
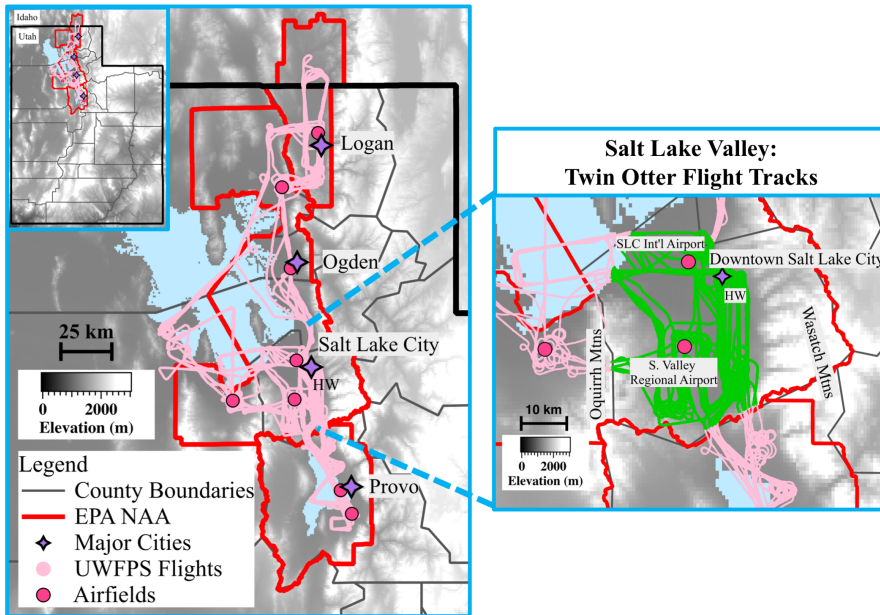
Figure 1. (Left) Elevation Map of Utah's Wasatch region (Utah State in insert), with the Great Salt Lake (north) and Utah Lake (south) shown in blue and county borders in black. U.S. EPA designated non-attainment areas (NAA) for PM$_{2.5}$ are shown by red boundaries. From north to south these NAAs include the Logan NAA: "Moderate" status, Salt Lake City NAA: "Serious" status, and Provo NAA: "Serious" status. UWFPS TO flight tracks are shown in pink. Purple markers indicate the locations of major cities, including Logan in the Cache Valley, Ogden and Salt Lake City in the SLV, and Provo in the Utah Valley. The location of missed approaches conducted with the aircraft are shown by dark pink circles. The Hawthorne (HW) measurement site in the SLV is labeled. (Right) Expanded view of the SLV, with analyzed flight tracks highlighted in green.
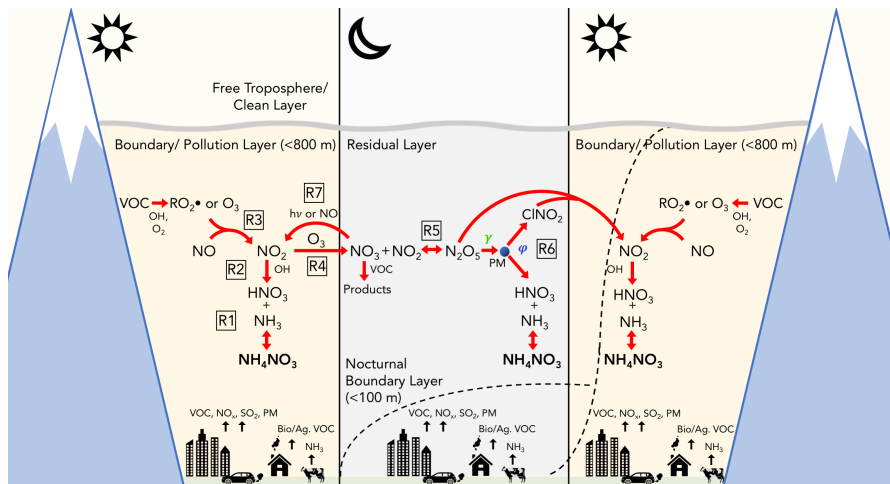
26

Figure 2. Illustration of the day-night dynamics and chemical cycles of reactive nitrogen oxides, O$_3$, and NH$_4$NO$_3$ during PCAP conditions in the SLV. The development of the nocturnal boundary layer and morning growth and mix-out are illustrated by the dashed lines. Figure is not to scale. (R6) represents the reaction: $N_2O_5 \xrightarrow{\gamma(N_2O_5),\ M} 2*(1-\varphi)*HNO_3 + \varphi*ClNO_2$.
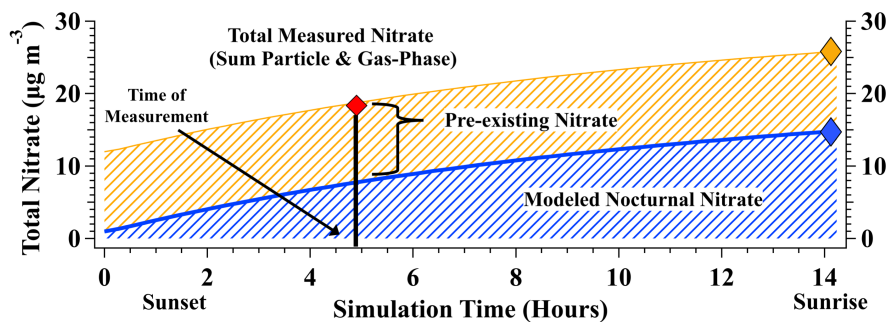

Figure 3. Example simulation of total nitrate production from sunset to sunrise for an air parcel sampled over the SLV on 28 January 2017. Model derived $\gamma(N_2O_5)$ and $\varphi(ClNO_2)$ values were 0.05 and 0.21, respectively. Modeled nocturnal nitrate (blue) is the total nitrate produced by heterogeneous chemistry in the box model, with the nocturnal production rate (μg m^{-3} night^{-1}) represented by the blue diamond. Pre-existing nitrate (yellow) represents the nitrate present at sunset and is calculated as the difference between total measured nitrate from the aircraft (red diamond) and the model-predicted nitrate at the time of aircraft measurement (vertical black line). Assuming pre-existing nitrate is constant overnight (i.e. no deposition or dilution) and constant values of $\gamma(N_2O_5)$ and $\varphi(ClNO_2)$, the fractional contribution of nitrate production from a single night to the total observed is calculated as the ratio of modeled nitrate (blue diamond) to total nitrate (gold diamond) at sunrise.
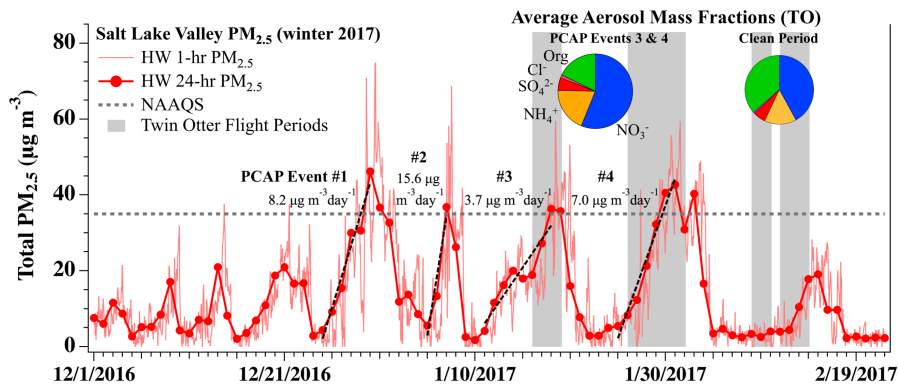
27

Figure 4. Time series of total PM$_{2.5}$ mass (μg m^{-3}) (1-hr and 24-hr averages) for the 2016-2017 winter, measured at the Hawthorne (HW) UDAQ site in the SLV. Dashed black lines are daily PM$_{2.5}$ accumulation rates (rates given in Figure). The 24-hour EPA national ambient air quality standard for PM$_{2.5}$ (35 μg m^{-3}) is shown by the dashed gray line. Gray shading indicates days when the TO aircraft was flying during UWFPS. Average aerosol mass fractions measured by the AMS aboard the TO are given in pie charts for polluted and clean conditions. Aerosol components are colored by nitrate (blue), ammonium (gold), sulfate (red), non-refractory chloride (pink), and organics (green).
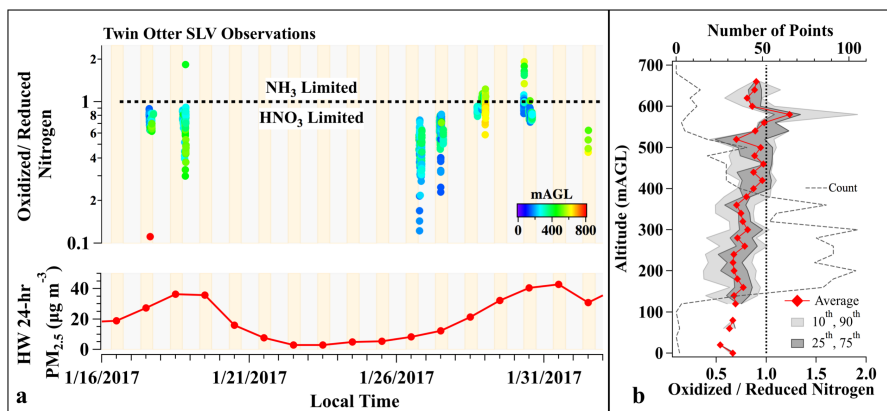

Figure 5. (a, top) Time series of ratio of total oxidized (HNO$_3$ + NO$_3^-$) to reduced (NH$_3$ + NH$_4^+$) nitrogen between 16 January and 1 February 2017 (10s averages), calculated from TO observations over the SLV. Individual nitrogen ratios are colored by aircraft altitude (mAGL). Yellow and gray shading indicate times of day and night, respectively. **(a, bottom)** PM$_{2.5}$ mass (24-hour average) measured at the HW ground-site (bottom). **(b)** Vertical profile of oxidized to reduced nitrogen ratios from panel (a). Diamonds represent the average values in each altitude bin and gray shading shows the 10th-90th (light gray) and 25th-75th (dark gray) percentiles. The number of points in each bin is shown by the gray dashed line. The vertical black line illustrates a nitrogen ratio of 1.
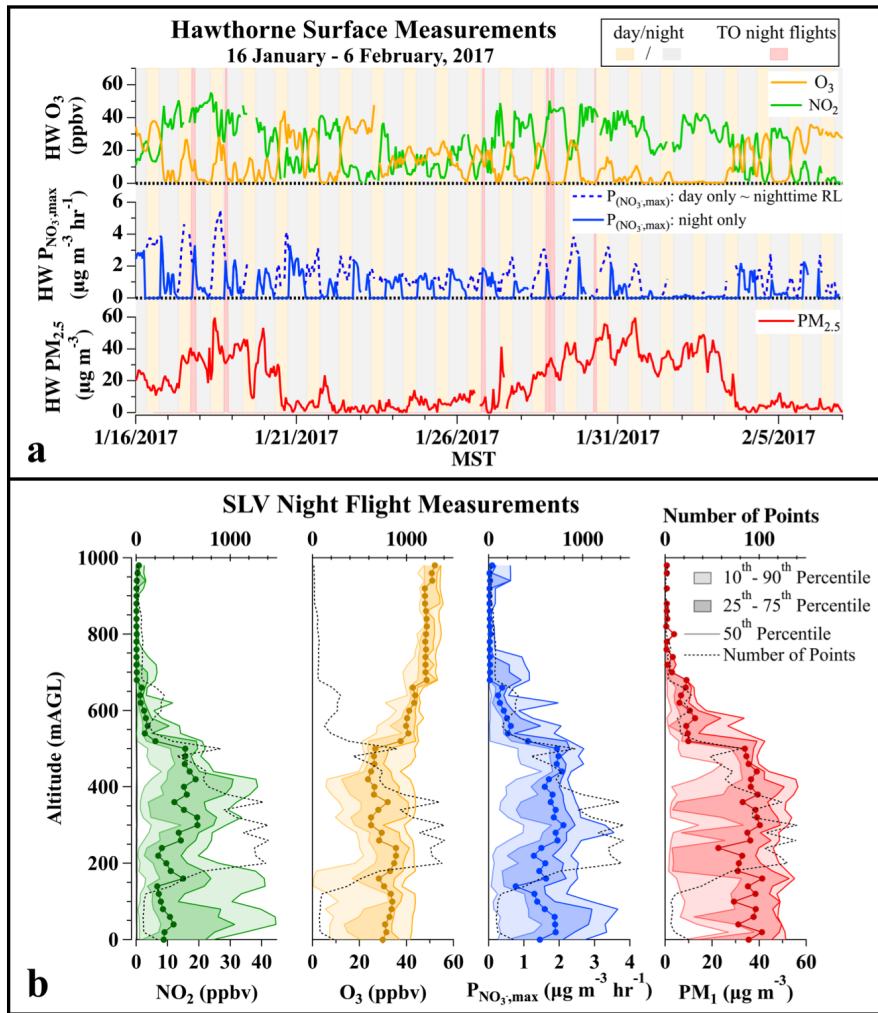
Hawthorne Surface Measurements
16 January - 6 February, 2017

day/night TO night flights

HW O$_3$ (ppbv) O$_3$ NO$_2$

HW P$_{(NO_3,max)}$ (µg m^{-3} hr^{-1}) P$_{(NO_3,max)}$: day only ~ nighttime RL P$_{(NO_3,max)}$: night only

HW PM$_{2.5}$ (µg m^{-3}) PM$_{2.5}$

1/16/2017 1/21/2017 1/26/2017 1/31/2017 2/5/2017
a MST

SLV Night Flight Measurements **Number of Points**

Altitude (mAGL)

10th- 90th Percentile
25th- 75th Percentile
50th Percentile
Number of Points

b NO$_2$ (ppbv) O$_3$ (ppbv) P$_{NO_3,max}$ (µg m^{-3} hr^{-1}) PM$_1$ (µg m^{-3})

Figure 6. (a) Time series of NO$_2$, O$_3$ (top), $P_{NO_3^-,max}$ (middle, see text for definition), and PM$_{2.5}$ (bottom) measured at the HW ground site during 16 January – 6 February 2017. O$_3$ data during the middle January pollution event were corrected to account for a 4.5 ppbv offset in the HW measurements, as shown in Figure S4. Aircraft flight times are shown by red shading. Dashed blue line shows the calculated $P_{NO_3^-,max}$ rates that would occur during the day if this mechanism were operative. Solid blue line assumes nitrate production from this mechanism during the day is zero. Late afternoon $P_{NO_3^-,max}$ at the surface (dashed line), is roughly equivalent to the $P_{NO_3^-,max}$ expected in the RL at night. (b) Vertical profiles of O$_3$, NO$_2$, $P_{NO_3^-,max}$ (1-second data) and PM$_1$ (10-second data) measured from the aircraft on all night flights over the SLV. In each panel, light shaded regions show the 10th-90th percentile ranges, dark shaded regions are the 25th-75th percentile ranges, and the solid lines are the 50th percentile. Dashed black lines show the number of points at each altitude.
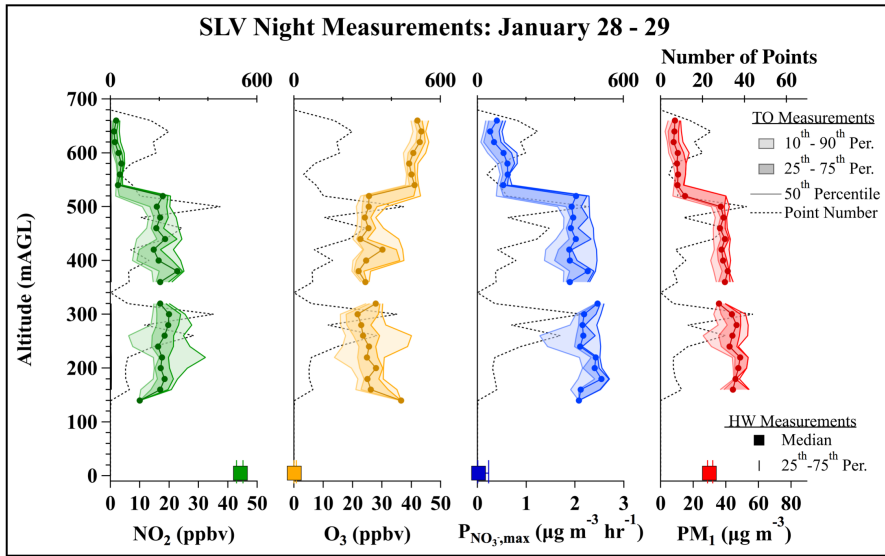
Deleted: ,

Figure 7. Vertical Profiles of NO$_2$, O$_3$, P$_{NO_3^-,max}$ (1-second data), and PM$_1$ (10-second data) measured from the TO aircraft during 5 box patterns, flown over the SLV urban core between 21:20 and 00:30 MST on 28 and 29 January. Percentiles and number of points at each altitude are shown as in Figure 6. Square markers and error bars represent the median and 25th-75th percentile range of NO$_2$, O$_3$, P$_{NO_3^-}$, and PM$_{2.5}$ measured concurrently at the HW ground site.
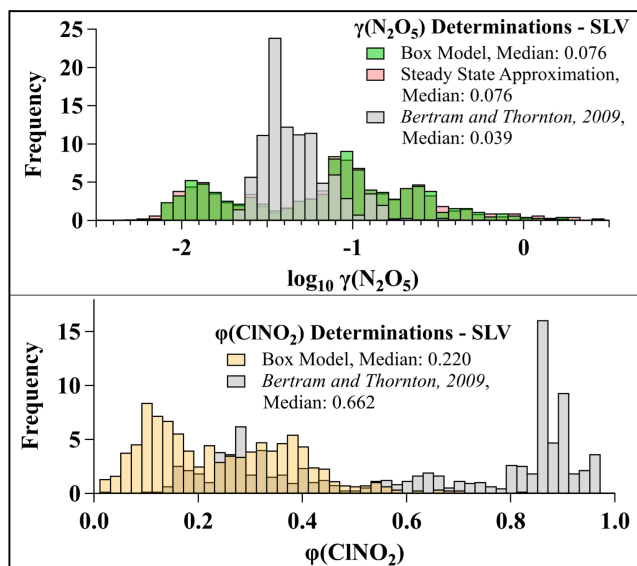
5

Figure 8. (Top) Histograms of $\gamma(N_2O_5)$ determinations from the SLV during pollution events, calculated with the box model (green), steady state approximation (pink), and parameterization from Bertram and Thornton (2009). (Bottom) Histograms of $\phi(ClNO_2)$ determinations from the SLV during pollution events calculated with the box model (gold) and parameterization from Bertram and Thornton (2009) (gray).

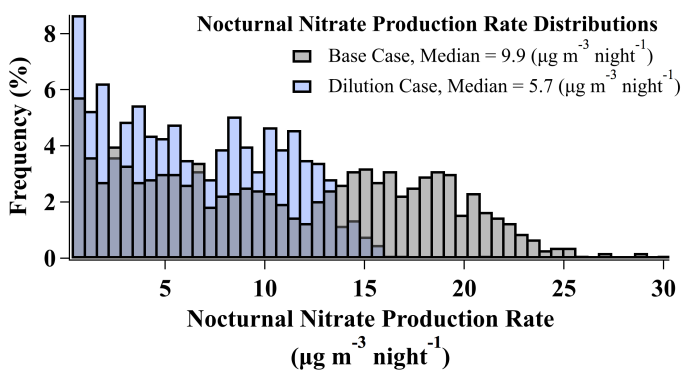Figure 9. Histograms of nocturnal nitrate production rates ($\mu g\ m^{-3}\ night^{-1}$) predicted by base case simulations and simulations incorporating a first-order dilution loss process with rate constant $k_{dilution} = 1.3 \times 10^{-5}\ s^{-1}$.

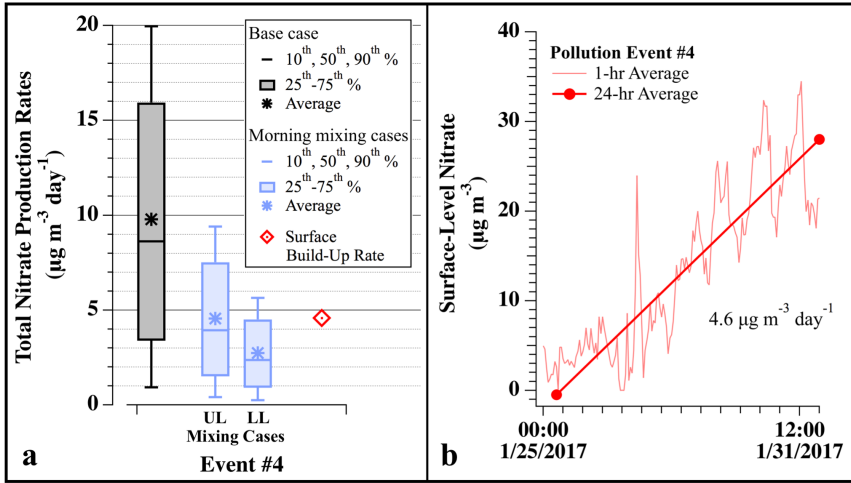**Figure 10. (a) For pollution event #4, comparison of model-predicted nocturnal nitrate production (μg m⁻³ day⁻¹) for base case simulations (gray), simulations with 24-hours of dilution (blue), and the average daily nitrate build-up observed at HW (red). Dilution cases are for simulations that incorporate nocturnal dilution rate constants of 1.2×10⁻⁵ (L), 1.3×10⁻⁵ (M), and 2.5 ×10⁻⁵ (H) s⁻¹, scaled by 60% during the day. Box and whisker plots show the 10th – 90th percentile distributions of each set.** Upper-limit (UL) values assume morning mixing between equivalent nitrate concentrations produced in the RL and NBL. Lower-limit (LL) values assume morning mixing with no nitrate production in the NBL **The red diamond shows the ground-based build-up rate, calculated from 24-hr averaged data at HW in panel b. (b) Observed concentrations and average daily build-up rate of nitrate aerosol mass (total mass * 0.58) at HW during event #4.**

Table 1. Aircraft measurements used in this analysis

Compound	Method / Instrument	Accuracy	Meas. Frequency	Location	Reference
Gas-Phase Species					
NO	CRDS[a]	5%	1s	Aircraft	(Fuchs et al., 2009; Wild et al., 2014)
NO_2	CRDS	5%	1s	Aircraft	(Fuchs et al., 2009; Wild et al., 2014)
O_3	CRDS	5%	1s	Aircraft	(Washenfelder et al., 2011; Wild et al., 2014)
NO_y	CRDS	12%	1s	Aircraft	(Wild et al., 2014)
N_2O_5	I⁻ToF-CIMS[c]	30%	1s	Aircraft	(Lee et al., 2014)
$ClNO_2$	I⁻ToF-CIMS	30%	1s	Aircraft	(Lee et al., 2014)
NH_3	QC-TILDAS[d]		1s	Aircraft	(Ellis et al., 2010)
Aerosol Measurements					
Aerosol (<1 μm) Composition	AMS[e]	20%	10s	Aircraft	(Bahreini et al., 2009; Middlebrook et al., 2012)
Dry Surface Area Density (<1 μm)	UHSAS[f]	34%[g]	3s	Aircraft	(Brock et al., 2011)

[a]NOAA, Cavity Ring down Spectrometer (CRDS, NOxCaRD)
[b]Hawthorne
[c]University of Washington I⁻Time of Flight Chemical Ionization Mass Spectrometer
[d]University of Toronto, Quantum Cascade Tunable Infrared Laser Differential Absorption Spectrometer
[e]NOAA, Aerosol Mass Spectrometer
[f]Droplet Measurement Techniques, Ultra-High Sensitivity Aerosol Spectrometer
[g]Estimated according to the performance of a different UHSAS in the WINTER campaign

5

Supplemental Information for:

On the contribution of nocturnal heterogeneous reactive nitrogen chemistry to particulate matter formation during wintertime pollution events in Northern Utah

Erin E. McDuffie[1,2,3ξ], Caroline Womack[1,2], Dorothy L. Fibiger[1,2†], William P. Dube[1,2], Alessandro Franchin[1,2], Ann Middlebrook[1], Lexie Goldberger[4‡], Ben H. Lee[4], Joel A. Thornton[4], Alexander Moravek[5], Jennifer Murphy[5], Munkhbayar Baasandorj[6§], Steven S. Brown[1,3]

[1]Chemical Sciences Division, National Oceanic and Atmospheric Administration, Boulder, CO, USA
[2]Cooperative Institute for Research in Environmental Sciences, University of Colorado, Boulder, CO, USA
[3]Department of Chemistry, University of Colorado, Boulder, CO, USA
[4]Department of Atmospheric Science, University of Washington, Seattle, WA, USA
[5]Department of Chemistry, University of Toronto, Toronto, Canada
[6]Department of Atmospheric Sciences, University of Utah, Salt Lake City, UT, USA

[5]Now at: Department of Physics and Atmospheric Science, Dalhousie University, Halifax, NS, Canada
†Now at: California Air Resources Board, Sacramento, CA, USA
‡Now at: ARM Aerial Facility, Pacific Northwest National Laboratory, Richland, WA, USA
§Now at: Chevron Corporation, Houston, TX, USA

Correspondence to: Steven S. Brown (steven.s.brown@noaa.gov)

Contents:

Pages: 13

Sections: S1-S6

Figures: S1- S7

Tables: S1-S4

| Deleted: 2 |
| Deleted: 4 |
| Deleted: 5 |

Section S1 Additional Model Details

S1.1 Model Chemical Mechanism

Table S1. Box Model Chemical Mechanism and Reactions used in Sensitivity Simulations

Reactants	Products	Rate Coefficient Expression	Reference/ Source
$NO_2 + O_3$	→ $NO_3 + O_2$	$k_1 = 1.4 \times 10^{-13} e^{(-2470/T)}$ [cm^3 molec.$^{-1}$ s^{-1}]	IUPAC 2008
$NO_3 + NO_2$	→ N_2O_5	$k_{2f} = (k0/k\infty)*F/(k0+k\infty)$ [cm^3 molec.$^{-1}$ s^{-1}] ^{a}	IUPAC 2012
N_2O_5	→ $NO_3 + NO_2$	$k_{2r} = (k0/k\infty)*F/(k0+k\infty)$ [cm^3 molec.$^{-1}$ s^{-1}] ^{b}	IUPAC 2012
N_2O_5 + aerosol	→ 2 HNO_3	$k_3 = k_{HNO_3}$ [s^{-1}]	Derived
N_2O_5 + aerosol	→ $HNO_3 + ClNO_2$	$k_4 = k_{ClNO_2}$ [s^{-1}]	Derived
NO_3 + VOC	→ $RONO_2$	$k_5 = k_{NO_3}$ [s^{-1}]	Calculated^c
$NO_3 + NO$	→ 2 NO_2	$k_6 = 1.80 \times 10^{-11} e^{(110/T)}$ [cm^3 molec.$^{-1}$ s^{-1}]	IUPAC 2008
$NO + O_3$	→ $NO_2 + O_2$	$k_7 = 2.07 \times 10^{-12} e^{(-1400/T)}$ [cm^3 molec.$^{-1}$ s^{-1}]	IUPAC 2013
O_3 + hv	→ $O + O_2$	$k_8 = j(O^1D)$	WINTER^c
NO_2 + hv	→ $NO + O$	$k_9 = j(NO_2)$	WINTER^c
NO_3 + hv	→ $NO_2 + O$	$k_{10} = j(NO_3)$	WINTER^c
N_2O_5 + hv	→ $NO_2 + NO_3$	$k_{11} = j(N_2O_5)$	WINTER^c
$ClNO_2$ + hv	→ $Cl + NO_2$	$k_{12} = j(ClNO_2)$	WINTER^c
Styrene + NO_3	→ $RONO_2$	$k_{NO_3} = 1.5 \times 10^{-12}$ [s^{-1}]	k_{NO_3} case^d
Σ(cis, trans-2-Butene) + NO_3	→ $RONO_2$	$k_{NO_3} = 3.7 \times 10^{-13}$ [s^{-1}]	k_{NO_3} case^d
Σ(cis, trans-2-Pentene) + NO_3	→ $RONO_2$	$k_{NO_3} = 3.7 \times 10^{-13}$ [s^{-1}]	k_{NO_3} case^d
Isoprene + NO_3	→ $RONO_2$	$k_{NO_3} = 3.15 \times 10^{-12} * exp^{(-450/T)}$ [s^{-1}]	k_{NO_3} case^d
N_2O_5	→	$k_{Dilution} = 1.3 \times 10^{-6}$ [s^{-1}]	$k_{Dilution}$ case^e
$ClNO_2$	→	$k_{Dilution} = 1.3 \times 10^{-6}$ [s^{-1}]	$k_{Dilution}$ case^e
NO_2	→	$k_{Dilution} = 1.3 \times 10^{-6}$ [s^{-1}]	$k_{Dilution}$ case^e
HNO_3	→	$k_{Dilution} = 1.3 \times 10^{-6}$ [s^{-1}]	$k_{Dilution}$ case^e
NO_3	→	$k_{Dilution} = 1.3 \times 10^{-6}$ [s^{-1}]	$k_{Dilution}$ case^e
NO	→	$k_{Dilution} = 1.3 \times 10^{-6}$ [s^{-1}]	$k_{Dilution}$ case^e
O_3	→	$k_{Dilution} = 1.3 \times 10^{-6}$ [s^{-1}]	$k_{Dilution}$ case^e
O_3 Bkg^f	→ O_3	$k_{Dilution} = 1.3 \times 10^{-6}$ [s^{-1}]	$k_{Dilution}$ case^e

^{a}$k0 = 3.6 \times 10^{-30}*M*(T/300)^{-4.1}$, $k_\infty = 1.9 \times 10^{-12}*(T/300)^{0.2}$, KR = $k0/k_\infty$ NC = 0.75-1.27*$\log_{10}(0.35)$, F = $10^{(\log10(0.35)/(1+\log10(KR)/NC)^2)}$, M = Pressure [mbar] $1 \times 10^{-4}/(k_b*T)$

^{b}$k0 = 1.3 \times 10^{-3}*M*(T/300)^{-3.5}e^{(-11000/T)}$, $k_\infty = 9.7 \times 10^{14}*(T/300)^{0.1}e^{(-11080/T)}$, KR = $k0/k_\infty$ NC = 0.75-1.27*$\log_{10}(0.35)$, F = $10^{(\log10(0.35)/(1+\log10(KR)/NC)^2)}$, M = Pressure [mbar] $1 \times 10^{-4}/(k_b*T)$

^{c}Described in Section S1.4.3, from the WINTER campaign

^{d}Described in Sections S1.2 and S1.4.5, used only to test the sensitivity to time-varying NO_3 reactivity; rate constants from Atkinson and Arey (2003)

^{e}Described in Section S1.4.1, used only in simulations that included air parcel dilution/vertical mixing

^{f}Background O_3 = 45 ppbv

S1.2 NO₃ Reactivity Calculation Details

The values of the k_{NO_3} reaction rate constants for simulations of each flight were calculated from multiple ground-based VOC measurements as described below.

As noted in the main text, a set of select (< 20) VOCs were measured by a PTR-MS with hourly time resolution during UWFPS at a ground site on the University of Utah campus (Table S2). During 2012-2014, a larger set of > 45 VOCs was collected with hourly time resolution at the HW ground site and analyzed with a Gas-Chromatography Flame Ionization Detector. For calculations of k_{NO_3} here, concentrations of VOCs during UWFPS were estimated by applying the average 2012-2014 VOC:benzene ratio (from December – March data) to PTR-MS benzene concentrations observed in 2017, as described in Text S1

of Womack et al. (2019). Benzene was chosen as both benzene and toluene were the least reactive of the five compounds that were reported in both the historical data set and during the 2017 campaign. The toluene:benzene ratio derived from historical data (Table S2) reproduced the 2017 toluene concentrations within 3%, but the benzene:toluene ratio could only reproduce the 2017 concentrations of benzene by 30%. Applying the historical VOC:benzene ratios, estimates of 2017 VOC concentrations were used in Eq. (S1) to calculate total k_{NO_3} for all the simulations of 2017 flights. A complete list of measured/estimated VOC concentrations, their reaction rate constants (k_{VOC}), average historical VOC:benzene ratios, and measurement years are provided in Table S2.

$$k_{NO_3} = \sum([\text{VOC}]_i * k_{VOC_i}) \tag{S1}$$

Table S2. NO$_3$ + VOC Reaction Rate Constants

VOC	A Factor (10^{14} cm^3 s^{-1})	B Factor (n)	Reference	VOC:benzene	Meas. Year
Alkanes					
CH$_4$	0.0001	0	(Atkinson & Arey, 2003)		2017
Ethane	0.0001	0	(Atkinson & Arey, 2003)	26.15	2012-2014
Propane	0.007	0	(Atkinson & Arey, 2003)	14.82	2012-2014
iso-Butane	305	3060	(Atkinson & Arey, 2003)	1.87	2012-2014
n-Butane	276	3279	(Atkinson & Arey, 2003)	5.48	2012-2014
2,2-Dimethylbutane	0.044	0	Estimated	0.03	2012-2014
2,3-Dimethylbutane	0.044	0	(Atkinson & Arey, 2003)	0.27	2012-2014
iso-Pentane	299	2927	(Atkinson & Arey, 2003)	2.41	2012-2014
n-Pentane	0.0087	0	(Atkinson & Arey, 2003)	2.17	2012-2014
2-Methyl Pentane	0.018	0	(Atkinson & Arey, 2003)	0.24	2012-2014
3-Methyl Pentane	0.022	0	(Atkinson & Arey, 2003)	0.01	2012-2014
n-Hexane	0.011	0	(Atkinson & Arey, 2003)	1.1	2012-2014
2-Methylhexane	0.015	0	Estimated	0.30	2012-2014
3-Methylhexane	0.015	0	Estimated	0.31	2012-2014
n-Heptane	0.015	0	(Atkinson & Arey, 2003)	0.49	2012-2014
n-Octane	0.019	0	(Atkinson & Arey, 2003)	0.11	2012-2014
n-Nonane	0.023	0	(Atkinson & Arey, 2003)	0.07	2012-2014
n-Decane	0.028	0	(Atkinson & Arey, 2003)	0.047	2012-2014
n-Undecane	0.032	0	Estimated	0.035	2012-2014
n-Dodecane	0.036	0	Estimated	0.02	2012-2014
Cyclohexane	0.014	0	(Atkinson & Arey, 2003)	0.40	2012-2014
Alkenes					
Ethene	0.000488	2282 (2)	(Atkinson & Arey, 2003)	9.35	2012-2014
Propene	4.59	1156	(Atkinson & Arey, 2003)	2.65	2012-2014
∑(*iso*, 1-Butene)	31.4[a]	938	(Atkinson & Arey, 2003)	0.31	2012-2014
cis-2-Butene	35.2	0	(Atkinson & Arey, 2003)	0.27	2012-2014
trans-2-Butene	0.000122	-382 (2)	(Atkinson & Arey, 2003)	0.22	2012-2014
cis-2-pentene	37	0	MCM	0.05	2012-2014
1-pentene	1.5	0	(Atkinson & Arey, 2003)	0.15	2012-2014
trans-2-pentene	37	0	MCM	0.09	2012-2014
1-Hexene	1.8	0	(Atkinson & Arey, 2003)	0.01	2012-2014
Alkynes					
Ethyne	0	0	MCM	7.58	2012-2014
Aromatics					
Benzene	0.003	0	(Atkinson & Arey, 2003)	1	2012-2014, 2017
Toluene	0.007	0	(Atkinson & Arey, 2003)	2.09	2012-2014, 2017
m-Ethyltoluene	0.045	0	MCM	0.11	2012-2014
o-Ethyltoluene	0.071	0	MCM	0.06	2012-2014
p-Ethyltoluene	0.086	0	MCM	0.05	2012-2014
Ethylbenzene	0.06	0	(Atkinson & Arey, 2003)	0.15	2012-2014
p-Xylene	0.050[b]	0	(Atkinson & Arey, 2003)	0.82	2012-2014, 2017

o-Xylene	0.041	0	(Atkinson & Arey, 2003)	0.25	2012-2014
m-Xylene	0.026	0	(Atkinson & Arey, 2003)	0.52	2012-2014
1,2,4-Trimethylbenzene	0.18	0	(Atkinson & Arey, 2003)	0.16	2012-2014, 2017
1,2,3-Trimethylbenzene	0.19	0	(Atkinson & Arey, 2003)	0.04	2012-2014
1,3,5-Trimethylbenzene	0.088	0	(Atkinson & Arey, 2003)	0.07	2012-2014
n-propylbenzene	0.014	0	MCM	0.03	2012-2014
iso-propylbenzene	0.014	0	MCM	0.01	2012-2014
Styrene	150	0	(Atkinson & Arey, 2003)	0.09	2012-2014
Biogenics					
Isoprene	315	450	(Atkinson & Arey, 2003)	0.02	2012-2014, 2017
MVK	0.06	0	(Atkinson & Arey, 2003)		2017
MACR	0.34	0	(Atkinson & Arey, 2003)		2017
Alcohols					
Methanol	94	2650	(Atkinson & Arey, 2003)		2017
Ketones					
Acetone	0.003	0	(Atkinson & Arey, 2003)		2017
MEK	0	0			2017
Pentanone	0	0			2017
Hexanone	0	0			2017
Aldehydes					
Acetaldehyde	140	1860	(Atkinson & Arey, 2003)		2017
Formaldehyde	0.056	0	(Atkinson & Arey, 2003)		2017

As the k_{NO_3} calculations in this analysis were based on ground-site measurements, k_{NO_3} values in each box model simulation were held constant at the 4pm value on each flight day (values in Table S3). Measured late afternoon concentrations at the ground within a mixed boundary layer are expected to be similar at night in the residual layer. For the flight on 18 January 2017, the PTR-MS was not measuring VOCs and the k_{NO_3} value was estimated by the growth rate of k_{NO_3} during the second PCAP event in Figure S1.

Table S3. Total k_{NO_3} values and initial VOC concentrations used model simulations

Flight Day	Total k_{NO_3} [s^{-1}]	Init. Conc. Styrene [molec. cm^{-3}]	Init. Conc. $\sum$(*cis, trans*-2-Butene) [molec. cm^{-3}]	Init. Conc. $\sum$(*cis, trans*-2-Pentene) [molec. cm^{-3}]	Init. Conc. Isoprene [molec. cm^{-3}]
18 Jan	9.5×10^{-3}	2.2×10^9	1.2×10^{10}	3.2×10^9	4.8×10^8
26 Jan	1.5×10^{-3}	3.5×10^8	1.8×10^9	5.1×10^8	7.6×10^7
28 Jan	4.4×10^{-3}	1.0×10^9	5.3×10^9	1.5×10^9	2.2×10^8
29 Jan	5.1×10^{-3}	1.2×10^9	6.3×10^9	1.7×10^9	2.6×10^8

One limitation of this method is that it does not allow the k_{NO_3} rate constant to vary with time, which is expected as VOCs are removed overnight in the RL by reaction with NO$_3$. To investigate the impact of time varying k_{NO_3} values on the model results, the top six contributing VOCs (Figure S1) (average 96% of the total reactivity) were represented semi-explicitly in the model using four additional reactions and second order rate constants given in Table S1. The *cis*- and *trans*-isomers of 2-butene and 2-pentene were lumped in this analysis with the rate constants averaged between the two isomers. The initial concentrations of each VOC were taken as the concentrations at 4pm on the day of each flight (values in Table S3). Allowing the VOC reactivity to be reduced overnight minimally impacted the model-derived nocturnal nitrate production rate (<0.1%), as shown discussed further in Section S1.4.
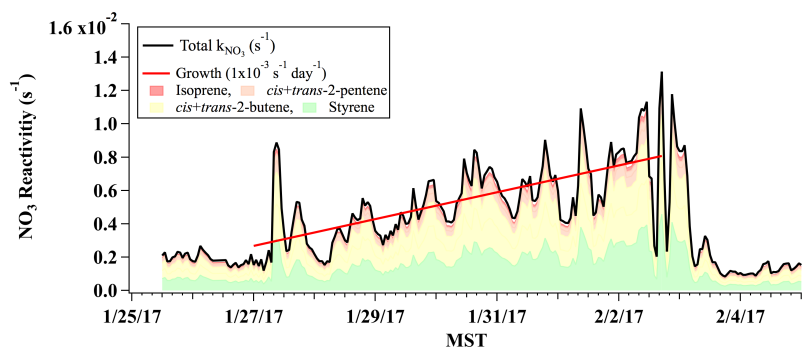
Figure S1. Time series of k_{NO_3} during the late January PCAP event (event #4) at the UU ground site in the SLV. Total calculated k_{NO_3} is shown in black. The fractional contributions from the largest six contributing VOCs are shown in color. The PCAP k_{NO_3} growth rate is shown by the red line.

comment: Deleted: HW

S1.3 Wet Surface Area Calculation

Total aerosol wet surface area (SA) density (m^2 m^{-3}) was used to calculate γ(N$_2$O$_5$) in Eq. (1) from the model-derived $k_{N_2O_5}$ loss rate constant. For the UWFPS campaign, the total wet SA (for particles < 1 μm in diameter) was estimated by applying a relative humidity-dependent, surface area hygroscopic growth curve to the dry PM$_1$ SA measured by the UHSAS aboard the TO. For base case simulations, the applied growth curve was calculated using the Extended-AIM Aerosol Thermodynamic Model (Wexler & Clegg, 2002), assuming no solid formation (i.e. metastable liquid particles) and pure NH$_4$NO$_3$ particles (Figure S2).

Alternatively, the growth factor for each point can be estimated from the aircraft AMS measurements, following supplemental Eqs. (S2) - (S5), as described further in McDuffie et al. (2018b). In these equations, V_{Dry} is the total dry aerosol volume measured by the UHSAS and V_{Total} is the sum of the dry and wet volume contributions. To assess the possible SA error associated with the assumption of pure NH$_4$NO$_3$ particles, V_{Wet} was calculated in (S3) from the mass of aerosol liquid water (M_{Wet}) and water density (ρ_{water}). M_{Wet} was calculated in (S4) as the sum of inorganic-associated water (calculated from ISORROPIA as described in Franchin et al. (2018)) and the organic-associated water, which was estimated in (S5) by the measured dry organic aerosol mass (M_{org}), organic density (ρ_{org}), water activity ($a_w = RH/100$), water density (ρ_{water}), and the organic hygroscopicity constant (κ_{Org}). While ρ_{org} and κ_{Org} have been shown to depend on multiple factors such as the aerosol O:C ratio (Cerully et al., 2015; Jimenez et al., 2009; Mei et al., 2013), ρ_{org} is set here to a constant value of 1.3 g/cm^3, typical of secondary organic aerosol (e.g. Kuwata et al., 2012) and κ_{Org} is set to 0.1 (Brock et al., 2016; Shingler et al., 2016).

Figure S2a shows the diameter growth curves (square root of the SA growth curves) as a function of RH for both the E-AIM and AMS estimates. As the aerosol in the SLV are primarily composed of NH$_4$NO$_3$ during pollution events (Figure 4), the organic-associated water content has a small impact on the growth curve and total wet aerosol SA. The insert in Figure S2a shows that the wet SA only increases by ~ 3% when the organic-associated water is included in the growth factor calculation. Due to the small impact and large uncertainties associated with the calculation of organic-associated water, total wet SA and volume densities used in the main text include inorganic-associated aerosol water only. Figure S2b shows the distribution of measured dry and calculated wet aerosol surface area densities for points where γ(N$_2$O$_5$) and φ(ClNO$_2$) values were derived from the box model.

comment: Deleted: Figure S2 (multiple), (S2, (S5, (S3, (S4, (S5

5

$$Aerosol\ SA\ Growth\ Factor = \left(\frac{V_{Total}}{V_{dry}}\right)^{\frac{2}{3}} \qquad (S2)$$

$$V_{Total} = M_{Wet}/\rho_{water} + V_{dry} \qquad (S3)$$

$$M_{Wet} = M_{Inorg.\ water} + M_{Org.\ Water} \qquad (S4)$$

$$M_{Org.\ Water} = \left(\frac{a_w}{1-a_w}\right) * \kappa_{Org} * \left(\frac{M_{org}}{\rho_{org}}\right) * \rho_{water} \qquad (S5)$$
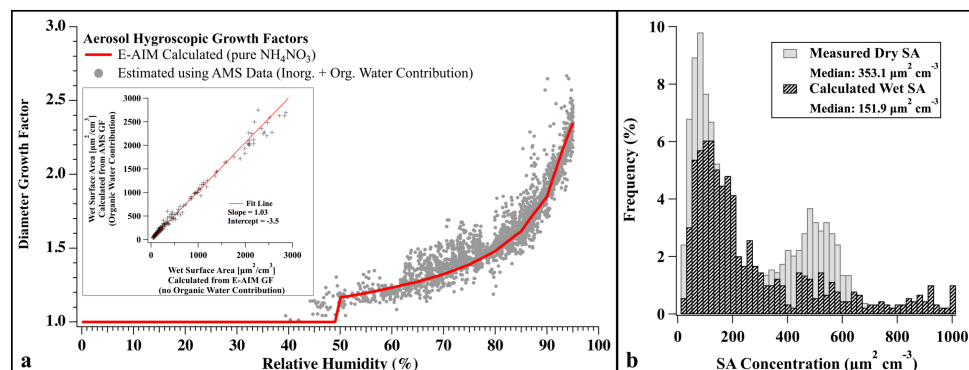
Figure S2. (a) Hygroscopic Diameter Growth Factors for <1μm diameter aerosol. (Red line) derived using E-AIM, assuming pure NH$_4$NO$_3$ aerosol and used for base case γ(N$_2$O$_5$) calculations, (gray circles) derived from Eqs. (S2) - (S5), using AMS data, including organic and inorganic-associated water. (Insert) Comparison of total wet SA during UWFPS, calculated using AMS and E-AIM growth factors. (b) Distributions of measured (dry) and calculated (wet) aerosol SA, with medians provided in figure caption. All data shown are from observation times with derived values of γ(N$_2$O$_5$) and φ(ClNO$_2$) (N = 1031).

S1.4 Sensitivity Studies and Model Uncertainties

This section describes results of 17 additional simulations that were conducted to test the sensitivity of the model predicted nocturnal nitrate production rate (μg m^{-3} night^{-1}) to uncertainties in the box model inputs, constraints, and parameters. Results are summarized in Table S4 and Figure S3. Table S4 shows the percent change in the median nocturnal nitrate production rate and the number of points in each comparison. The number of points are different in each test as the model cannot always converge to a solution ($k_{N_2O_5} < 1\times10^{-7}$ s^{-1} or $k_{ClNO_2} > k_{N_2O_5}$), as described in McDuffie et al. (2018b) and McDuffie et al. (2018a). Non-converging points have been removed from this analysis. Figure S3 shows a time series of the nitrate produced overnight in base case simulations (black points), and the uncertainty associated with each point (shading). The uncertainty for each point was calculated from the quadrature addition of the percent changes associated with each of the sensitivity tests summarized in Table S4. The total absolute uncertainty is shown by the dark blue shading and the fraction of uncertainty associated with the incorporation of dilution is highlighted by light blue. An expanded view of data from 28 January is also shown for illustrative purposes. Individual sensitivity tests and results are described in further details in Sections S1.4.1– S1.4.2, discussed in decreasing order of model sensitivity.

Table S4. Median sensitivity of simulated nitrate to changes in model parameters.

Parameter	Base Case Value	Value Adjustment	ΔMedian Nocturnal Nitrate Production Rate (%)[a]	N
Dilution	n/a	$k_{dilution} = 1.3 \times 10^{-5}$ s^{-1}[b]	-42.4	1027
Deposition	n/a	$k_{dep} = 2.6 \times 10^{-6}$ s^{-1}[c]	+7.7	1027
NO$_2$	CRDS	+5%, -5%[d]	+5.7, -5.8	1021
O$_3$	CRDS	+5%, -5%[d]	+4.8, -4.8	1025
ClNO$_2$	I$^-$-ToF-CIMS	+30%, -30%[d]	-3.9, +4.3	1025
Photolysis Rates	WINTER values[e]	+40%, -40%	-1.4, +2.8	1809
N$_2$O$_5$	I$^-$-ToF-CIMS	+30%, -30%[d]	-1.0, +1.2	1021
Pre-Sunset Time	1.3 hours[f]	0 hrs, 2 hrs	-0.3, +0.2	505
Constant k_{NO_3}	Calculated[g]	+50%, -50%	-0.2, +0.2	1027
Varying k_{NO_3}	Constant k_{NO_3}	Varying k_{NO_3} [g]	<0.1	1027

[a]Defined as (base case value – sensitivity test value)/base case value *100
[b]See Section S1.4.1
[c]See Section S1.4.2
[d]Reported instrument measurement accuracies
[e]See Section S1.4.3
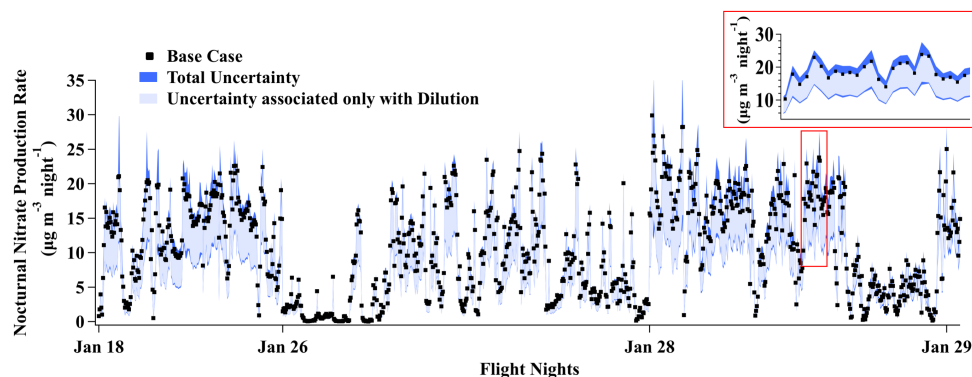[f]See Section S1.4.4
[g]See Section S1.4.5

Figure S3. Time series of simulated nitrate production rate. Base case simulations are shown by black dots. The total uncertainty in each simulated point is given by the dark blue shading. Light blue shading shows the absolute uncertainty associated with the presence of dilution/mixing only ($k_{dilution} = 1.3 \times 10^{-5}$ s^{-1}). The insert shows a larger view of the region inside the red box.

S1.4.1 Dilution/Vertical Mixing

To test the box model sensitivity to the presence of vertical mixing/horizontal dilution, a first order loss rate constant of 1.3×10^{-5} s^{-1} was implemented into the chemical mechanism, as shown in Table S1. In addition to the first order loss of all simulated species, a constant 45 ppbv of background O$_3$ (average mixing ratio above the boundary layer during UWFPS) was added to the model with the same dilution rate constant to simulate the entrainment of O$_3$ into the RL from the free troposphere. The dilution rate constant was derived by Womack et al. (2019) as the rate constant that, in combination with the derived surface albedo, allowed an observationally-constrained box model to best reproduce the build-up of total O$_x$ (= NO$_2$ + O$_3$ + 1.5*(HNO$_3$ + pNO$_3^-$) + 3*N$_2$O$_5$ + ClNO$_2$ + PANs + OH + 2*alkyl nitrates) observed between 28 and 31 January, 2017 at the UU ground site. Womack et al. (2019)

Deleted:

Deleted: (scaled up by 40% to represent the RL only),

Deleted: diurnal profile

Deleted: , that was

Deleted: HW

7

derived a $k_{dilution}$ value of 8×10^{-6} s^{-1} for the boundary layer following this approach. Due to the reduced volume of the nocturnal RL relative to the boundary layer, this rate constant was scaled up at night by 40% to maintain constant dilution over the entire pollution build-up period. The same approach was applied to our analysis, which resulted in a $k_{dilution}$ value of 1.3×10^{-5} s^{-1} for the RL. The box model-predicted nocturnal nitrate production rate was most sensitive to this parameter, with a 42.2% reduction in the median predicted rate when including an overnight dilution rate of 1.3×10^{-5} s^{-1}. Based on Figure S10 in Womack et al. (2019), the RL dilution rate constant could have reasonably ranged between 1.2 and 2.5×10^{-5} s^{-1} (0.7 -1.5×10^{-5} s^{-1} / 0.6), depending on the albedo. Results incorporating this range of estimated dilution rate constants are discussed further in Section 3.3.3 of the main text and below in Figure S7.

S1.4.2 Deposition

To estimate the effect of deposition on the amount of nocturnal nitrate produced by the model, an extra reaction was added to the mechanism where modeled nitrate (HNO$_3$) was lost with a first order rate constant of 2.6×10^{-6} s^{-1}. This rate constant was calculated assuming a gas-phase nitric acid deposition velocity of 2.7 cm s^{-1} (Zhang et al., 2012) and an average boundary layer height of 800m (determined from measured NO$_y$ and PM vertical profiles). This deposition rate constant of 3.3×10^{-5} s^{-1} was reduced by 92% to account for the gas-particle partitioning of HNO$_3$ and particulate nitrate, modeled using the AMS and I$^-$ToF-CIMS data from the Twin Otter (Franchin et al., 2018). The presence of this small loss of gas-phase HNO$_3$ had a much smaller impact than dilution, with an increase in the median nocturnal nitrate production rate of 7.7%.

S1.4.3 Photolysis Rates

As described in the following section, each simulation was started 1.3 hours prior to sunset (as calculated from the solar zenith angle). In this analysis, photolysis rates during the 1.3 hours prior to sunset were calculated as a function of time prior to sunset from measurements of j(NO$_2$), j(O^{1}D), j(N$_2$O$_5$), j(ClNO$_2$), and j(NO$_3$) during the 2015 WINTER aircraft campaign. During WINTER, photolysis rates were calculated from actinic flux measurements from the National Center for Atmospheric Research, High-performance Instrumented Airborne Platform for Environmental Research (HAIPER) Airborne Radiation Package – Actinic Flux (HARP-AF) HARP-AF instrument (Shetter & Müller, 1999). These radiative measurements have an increased uncertainty of up to 40% near sunset at large solar zenith angles, which exacerbate the optical angular response biases. Accounting for this source of uncertainty, the nocturnal nitrate production rate over the SLV during the UWFPS campaign changed by -1.4/+2.8% for +/-40% changes in photolysis rates.

S1.4.4 Pre-Sunset Time

Simulations were set to begin before sunrise to account for the observed build-up of N$_2$O$_5$ and ClNO$_2$ at large solar zenith angles. The value of 1.3 hours was derived from the 2015 WINTER campaign as the time when ambient observations of N$_2$O$_5$ deviated from the values predicted by the daytime steady state approximation of N$_2$O$_5$ (Brown et al., 2005) (Eqs. (S6) and (S7)). This value could not be recalculated for the UWFPS campaign as it requires measurements of j(NO$_3$). During the WINTER campaign, this "pre sunset" time was found to vary between 0.8 to 1.8 hours. In this analysis, the box model was tested by changing the start time of each simulation to 0 and 2 hours prior to sunset. Of the points that converged, the median nocturnal nitrate production rate changed by < 0.3% for both tests.

$$[NO_3]_{\text{daytime ss}} = \frac{k_1[O_3][NO_2]}{k_7[NO] + j(NO_3)} \tag{S6}$$

$$[N_2O_5]_{\text{daytime ss}} = \frac{k_{2f}}{k_{2r}}[NO_2][NO_3]_{\text{daytime ss}} \tag{S7}$$

S1.4.5 NO$_3$ Reactivity, k_{NO_3}

In the base case simulations, first order reaction rate constants were held constant for the NO$_3$ + VOC reaction. As described in Sections 2.2.2 and S1.2, values of k_{NO_3} were held constant throughout each simulation at values equivalent to the concentrations calculated for 4pm at the JJU ground site (Figure S1). Due to uncertainties in the VOC measurements, the possible presence of non-measured VOCs and/or HO$_2$ or RO$_2$ radicals, and lack of measurements in the residual layer, sensitivity studies were conducted with k_{NO_3} values scaled by $\pm$ 50%. The median model predicted nocturnal nitrate production rate changed by 0.2% with $\pm$ 50% changes in constant k_{NO_3}.

As mentioned in Section S1.2, applying a constant k_{NO_3} does not allow for the potential decrease of k_{NO_3} overnight as VOCs are consumed by reaction with NO$_3$. To test the model sensitivity to this variable process, the six largest contributing VOCs to k_{NO_3} (average 96% of the total reactivity) were represented semi-explicitly in model simulations, as shown in Table S1. These six VOCs were styrene, *cis*-, *trans*-2-butene, *cis*-, *trans*-2-pentene, and isoprene. The average of *cis* and *trans* isomers were used to minimize the number of additional reactions in the model mechanism. Initial concentrations of each VOC for each flight are listed in Table S3 and were taken from the 4pm values on each flight day. Allowing the total k_{NO_3} to vary overnight changed the median nocturnal nitrate production rate by <0.1%.

Section S2 $P_{NO_3^-,max}$ Calculation Details

The instantaneous nitrate production rate ($P_{NO_3^-,max}$) is calculated as two times the production rate of the NO$_3$ radical (P_{NO_3}) (assumed equivalent to the N$_2$O$_5$ production rate). P_{NO_3} is calculated from the first order reaction of O$_3$ + NO$_2$, which is the rate limiting step in the formation of NO$_3$. P_{NO_3} is calculated in units of molec. cm^{-3} s^{-1} but is frequently reported in units of ppbv hr^{-1} after it is converted using the ambient air number density (ND) and the conversion between seconds and hours (3600) and mixing ratio to ppbv. In Section 3.3.1 of this analysis, P_{NO_3} is further converted to units of μg m^{-3} hr^{-1}, shown below in Eq. (S8), in order for $P_{NO_3^-,max}$ to have consistent units with the aerosol concentration measurements and box model results.

$$P_{NO_3^-,max}[\mu\text{g m}^{-3}\text{ hr}^{-1}] \tag{S8}$$
$$= 2 * P_{NO_3} [\text{ppbv hr}^{-1}] * 1 \times 10^{-9} * ND [\text{molec. cm}^{-3}] * \frac{1}{6.022 \times 10^{23} [\text{molec. mol}^{-1}]}$$
$$* 62 [\text{g mol}^{-1}] \, NO_3 * 1 \times 10^{12} [\mu\text{g cm}^3 \text{ g}^{-1}\text{m}^{-3}]$$

Deleted: HW

Deleted: Figure S1

Formatted: Normal, Indent: First line: 0.5"

Deleted: Table S1

Deleted: Table S3

Deleted: N$_2$O$_5$

Deleted: $P_{N_2O_5}$

Deleted: $P_{N_2O_5}$

Deleted: sometimes reported as P_{NO_3}

Deleted:

Formatted: Not Superscript/ Subscript

Deleted: , which forms an equilibrium with N$_2$O$_5$ at night.

Deleted: $P_{N_2O_5}$

Deleted: in

Deleted: $P_{N_2O_5}$

Formatted: Font: 10 pt

Formatted: Font: 10 pt

Formatted: Font: 10 pt

Formatted: Font: 10 pt

Formatted: Font: 10 pt

Deleted: $P_{N_2O_5}$

Formatted: Font: 10 pt

Formatted: Font: 10 pt

Formatted: Font: 10 pt

Deleted: $P_{N_2O_5}$

Section S3 Additional Figures

As noted in the main text, O_3 measurements at the HW ground site were corrected for an apparent offset in the data prior to a 2-hour data gap on 23 January 2017. As shown in Figure S4, the O_3 at HW becomes fully titrated during pollution episodes after the 23rd. Prior to 23 January, the O_3 data have the same apparent titration during pollution events but reach a minimum of ~ 4.5 ppbv. The O_3 data during this time were therefore reduced by a constant 4.5 ppbv to bring these data into agreement with 0 ppbv during pollution episodes. No adjustments were made to the data span during either time period.
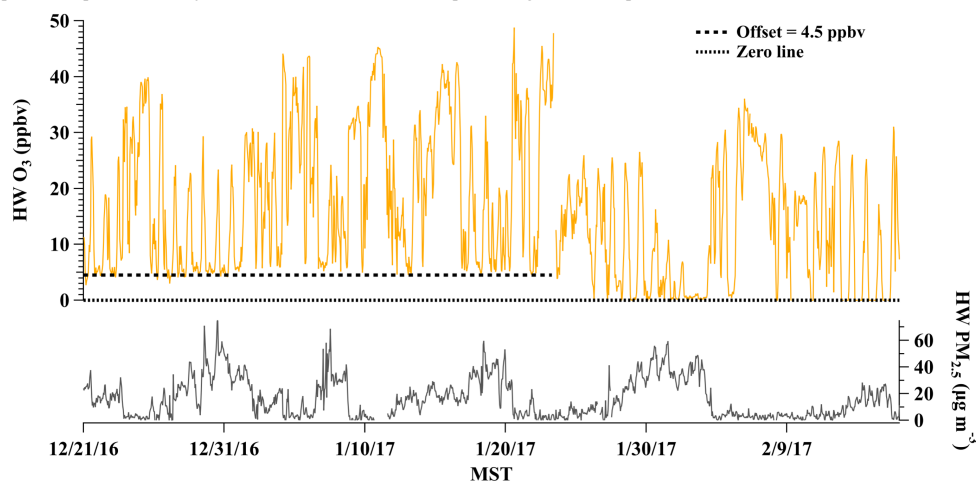

Figure S4. Time series of measured HW PM$_{2.5}$ (bottom) and O_3 (top), highlighting the O_3 offset correction of 4.5 ppbv

Section S4 $\gamma(N_2O_5)$ and $\phi(ClNO_2)$ Derivation Method Details

S4.1 Steady State Approximation for $\gamma(N_2O_5)$

The nocturnal steady state lifetime of N_2O_5 ($\tau_{ss}(N_2O_5)$) has been previously defined by Brown et al. (2003) and is shown in Eq. (S9) as a steady state between N_2O_5 production and nocturnal destruction pathways. Substituting the expression in Eq. (1) for $k_{N_2O_5}$, Eq. (S9) can be rearranged into to Eq. (S10) to solve for the steady state approximation of N_2O_5 uptake ($\gamma_{ss}(N_2O_5)$). This method for estimating the N_2O_5 uptake coefficient is simple relative to the box model but can fail under cold temperatures, high NO_2 concentrations, and small sinks for both N_2O_5 and NO_3 (Brown et al., 2003). Figure S5 shows that agreement between the box model and steady state approximation was within 19% (2-sided slope) over the SLV during the UWFPS campaign.

$$\tau_{ss}(N_2O_5)^{-1} = \frac{k_1[NO_2][O_3]}{[N_2O_5]} \approx (k_{N_2O_5}) + \frac{k_{NO_3}}{K_{eq}[NO_2]} \tag{S9}$$

$$\gamma_{ss}(N_2O_5)0.25cSA = \frac{k_1[NO_2][O_3]}{[N_2O_5]} - \frac{k_{NO_3}}{K_{eq}[NO_2]} \tag{S10}$$

Deleted: Figure S4

Deleted: (S9

Deleted: (S9

Deleted: (S10

Deleted: Figure S5

S4.2 $\gamma(N_2O_5)$ and $\phi(ClNO_2)$ Parameterizations

Box model values were also compared to $\gamma(N_2O_5)$ and $\phi(ClNO_2)$ values predicted from the parameterizations presented by Bertram and Thornton (2009), provided in Eqs. (S11) and (S12).

$$\gamma(N_2O_5) = \frac{4}{c}\frac{V}{SA}K_H * \beta * (1 - e^{(-\delta[H_2O(l)])}) \left(1 - \frac{1}{\left(\frac{0.06[H_2O(l)]}{[NO_3^-]}\right) + 1 + \left(\frac{29[Cl^-]}{[NO_3^-]}\right)}\right) \tag{S11}$$

$$\phi(ClNO_2) = \frac{1}{\left(1 + \frac{[H_2O(l)]}{483[Cl^-]}\right)} \tag{S12}$$

Here, c (m s^{-1}) is the mean molecular speed, SA is the total wet aerosol SA (discussed in Section S1.3), and V is the total wet aerosol volume (m^3 m^{-3}). Here, V was calculated using the UHSAS-measured dry aerosol volume density and the inorganic-associated aerosol water mass (discussed above in Section S1.3). The constants β (1.15 ×10^6 [s^{-1}]), δ (0.13 [M^{-1}]), 0.06, and 29, and 483 were derived from fits to laboratory results presented by Bertram and Thornton (2009). K_H is the unitless Henry's Law Coefficient of 51, taken from Fried et al. (1994). Aerosol water molarity was calculated using ISORROPIA-predicted aerosol water mass and V. This estimate does not include aerosol mass associated with organic-associated aerosol water, which is estimated to be a relatively small fraction of total aerosol water (3-17%) due to the small dry mass fraction of aerosol organics (~20%, Figure 4). Aerosol chloride and nitrate molarities were calculated from AMS nitrate and chloride mass measurements and V. Comparisons of these parameterizations to the box model results are shown in Figure S5, and discussed in the main text.
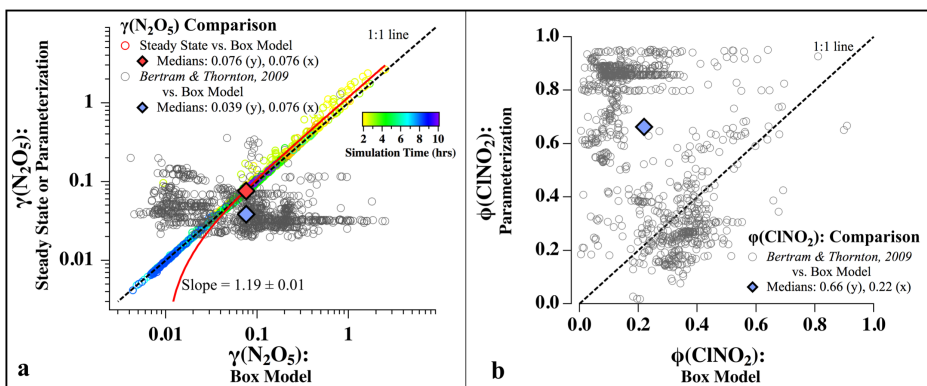

Figure S5. Methods comparison for $\gamma(N_2O_5)$ and $\phi(ClNO_2)$ values during pollution events in the SLV. (Left) Colored circles show the comparison between steady state (y-axis) and box model (x-axis) derived $\gamma(N_2O_5)$ values, colored by model simulation duration (i.e. time since sunset). The 2-sided fit produces a slope of 1.19 ± 0.01, shown by the red line. (Left & Right) Gray circles show the comparison between parametrized values (from Bertram and Thornton (2009)) (y-axis) and box model (x-axis) results. Dashed lines show the 1:1 line. Medians of each derivation are shown by diamonds and labeled accordingly.

As mentioned in the main text, the median $\gamma(N_2O_5)$ was also predicted by an empirical parameterization (S13) (McDuffie et al., 2018b). Details of this parameterization can be found in McDuffie et al. (2018b). For estimations here, the O:C ratio was calculated using the improved-ambient O:C ratio method from Canagaratna et al. (2015), shown in (S14). The AMS organic mass fragment at m/z 44 (f_{44}) ranged between 0.05 and 0.25 during UWFPS (Figure 6, Franchin et al. (2018)), corresponding to an O:C ratio

between ~0.3 and 1.16. Additional parameters include R_p, R_c, and ℓ, which are the total particle radius, radius of the inorganic core, and thickness of the organic coating, respectively. Here R_p was take as the effective aerosol radius, while R_c was calculated from the inorganic/(organic + inorganic) volume fraction following the equations presented in Table S8 of McDuffie et al. (2018b), based on Riemer et al. (2009). The organic volume required for this calculation was estimated using a constant organic density of 1.3 g/cm^3. In addition to the same variables as described above, R is the ideal gas constant, T is the ambient temperature and H_{aq} (5000 mol m^{-3} atm^{-1}) (Anttila et al., 2006) and D_{aq} (1x10^{-9} m^2 s^{-1}) (Riemer et al., 2009) are the aqueous N$_2$O$_5$ solubility and diffusion rate constants, respectively. With the assumptions described here, the median uptake coefficient predicted by this parameterization was estimated to be between 60 and 85% lower than the box model for O:C ratios between 0.05 and 1.16. As this parameterization treats the presence of organics as a coating that is resistive to uptake, the under-estimation of γ(N$_2$O$_5$) relative to the box model may indicate: 1) aerosol organics during pollution events are not surface active, 2) organics are not resistive toward N$_2$O$_5$, or 3) box model γ(N$_2$O$_5$) values are over-predicted due to missing SA (Section 3.3.2, e.g. fog) or simplifying assumptions discussed in Sections 2.2.2 and 3.3.2 (e.g. dilution). Due to uncertainties, these results are not assessed further.

$$\frac{1}{\gamma} = \frac{1}{\frac{4}{c}\frac{V}{SA}K_H * 2.14 \times 10^5 * [\mathrm{H_2O}_{(l)}]\left(1 - \frac{1}{\left(\frac{0.04[\mathrm{H_2O}_{(l)}]}{[\mathrm{NO_3^-}]}\right)+1}\right)} + \frac{1}{\frac{4RT(0.15*O{:}C + 0.0016*RH)*H_{aq}D_{aq}R_c}{c\ell R_p}} \tag{S13}$$

$$\text{Aerosol } O{:}C = 0.079 + 4.31 * f_{44} \tag{S14}$$

Section S5 Vertical Profiles

The vertical profiles of measured N$_2$O$_5$ and ClNO$_2$ and box model-derived γ(N$_2$O$_5$) and ϕ(ClNO$_2$) values are shown in Figure S6.
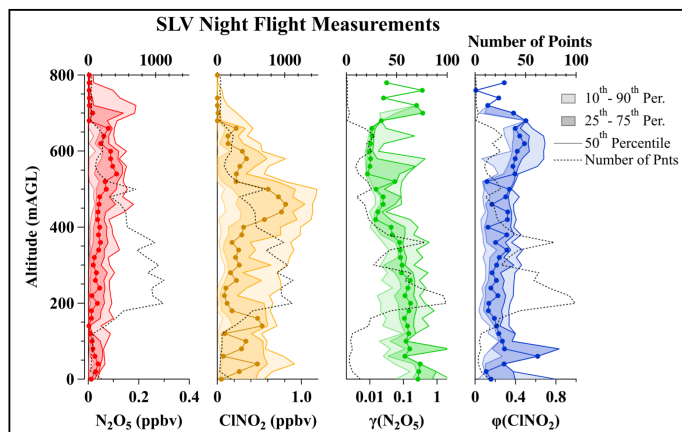

Figure S6. Vertical profiles of N$_2$O$_5$, ClNO$_2$ (1-second measurements), and box-model derived γ(N$_2$O$_5$) and ϕ(ClNO$_2$) values from all night flights over the SLV. In each panel, light shaded regions show the 10th-90th percentile ranges, dark shaded regions are the 25th-75th percentile ranges, and the solid lines are the 50th percentile. Dashed black lines show the number of points at each altitude.

Section S6 Additional Dilution Results

As described in Section S1.4.1, Womack et al. (2019) derived a range of rate constants between 0.7×10^{-5} and 1.5×10^{-5} s^{-1} (depending on surface albedo) that could best reproduce the build-up of $O_{x,total}$ observed during pollution event #4. To compare the box model results to the observed ground-based nitrate accumulation rate during the same event, and to assess the role of dilution, Figure 10 from the main text is reproduced here (M), with additional results using nocturnal $k_{dilution}$ rate constants of 1.2×10^{-5} s^{-1} (L) and 2.5×10^{-5} s^{-1} (H) (0.7×10^{-5} and 1.5×10^{-5} s^{-1} during the day).
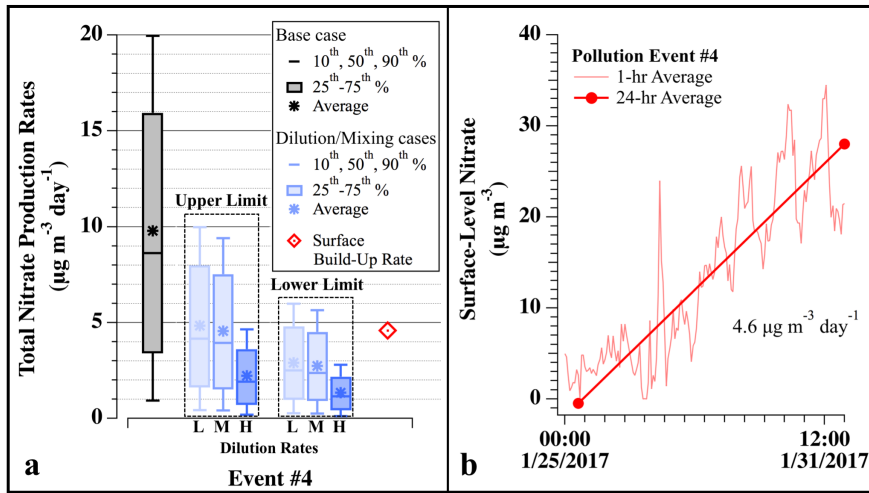

Figure S7. (a) For pollution event #4, comparison of model-predicted nocturnal nitrate production (μg m^{-3} day^{-1}) for base case simulations (gray), simulations with 24-hours of dilution (blue), and the average daily nitrate build-up observed at HW (red). Dilution cases are for simulations that incorporate nocturnal dilution rate constants of 1.2×10^{-5} (L), 1.3×10^{-5} (M), and 2.5×10^{-5} s^{-1} (H), scaled by 60% during the day. Box and whisker plots show the 10th – 90th percentile distributions of each set. The red diamond shows the ground-based build-up rate, calculated from 24-hr averaged data at HW in panel b. Upper-limit values assume morning mixing between equivalent nitrate concentrations produced in the RL and NBL. Lower-limit values assume morning mixing with no nitrate production in the NBL (b) Observed concentrations and average daily build-up rate of nitrate aerosol mass (total mass * 0.58) at HW during event #4.

13